Department of Mathematics
Technische Universität München

# A Mathematical Model Describing the Effects of Anti-PD-1 Immunotherapy on Tumor Growth and Behavior in Metastatic Melanoma

**Master's Thesis by Florian Karl**

| | |
|---|---|
| Examiner: | Prof. Dr. Christina Kuttler |
| Advisor: | Prof. Dr. Christina Kuttler |
| Submission Date: | November 01, 2018 |

I hereby confirm that this is my own work, and that I used only the cited sources and materials.

München, November 01, 2018

_____

Florian Karl

## Abstract

Through this thesis we provide a mathematical modeling approach to describe tumor growth and behavior in metastatic melanoma under immunotherapy treatment via PD-1 blockade (specifically treatment with *Pembrolizumab*). We impart needed basics in biological, medicinal and mathematical contexts and move on to explore two modeling approaches. A system of Ordinary Differential Equations models the interaction between cancer cells and the patient's immune response under PD-1 blockade. A system of Partial Differential Equations expands on these dynamics and includes vascular cells, introduces several classes of cancer cells and examines the spatial behavior of a tumor over time. Both models are simulated and compared to clinical data of three patients and display good fit as well as the ability to emulate characteristic tumor behavior such as response, stable disease and progress. The results offer evidence, that *Pembrolizumab* treatment can even have a significant effect on tumors displaying low PD-L1 expression levels. They further indicate the importance of synergy effects with adjuvant treatments to immunotherapy as well as the possibility of acquired resistance to treatment through modified tumor structure.

## Zusammenfassung

Im Rahmen dieser Arbeit werden mathematische Modellierungsansätze entwickelt, die Tumorwachstum und -verhalten des metastasierten Melanoms unter Einfluss von Immuntherapie durch PD-1 Immun-Checkpoint-Inhibitoren (explizit durch das Medikament *Pembrolizumab*) beschreiben. Es werden die nötigen biologischen, medizinischen und mathematischen Grundlagen vermittelt und anschließend zwei Modellierungsansätze behandelt. Ein System Gewöhnlicher Differentialgleichungen beschreibt die Interaktionen zwischen Krebszellen und der Immunantwort des Patienten unter Einfluss von PD-1 Immun-Checkpoint-Inhibitoren. Ein System Partieller Differentialgleichungen erweitert diese Dynamik durch Inklusion vaskulärer Zellen und verschiedener Typen von Krebszellen, um das räumliche Verhalten von Tumoren im Verlauf der Zeit zu untersuchen. Beide Modelle werden anschließend simuliert und mit Messdaten von drei Patienten verglichen. Die Modelle passen gut zu den Datensätzen und konnten charakteristisches Verhalten eines Tumors wie Progress, Remission oder "Stable Disease" reproduzieren. Die Ergebnisse unterstützen die Hypothese, dass Behandlung mit *Pembrolizumab* auch signifikante Auswirkungen auf Tumore mit geringer Proteinexpression von PD-L1 haben kann. Außerdem weisen sie daraufhin, dass Synergieeffekte mit adjuvanten Therapien großen Einfluss haben können und der Tumor (durch eine veränderte Struktur) Resistenz gegenüber der Behandlung entwickeln kann.

# Contents

# Chapter 1

# Introduction

Over the past decades cancer has ascended as one of the leading causes of death in many nations worldwide and it is abundantly clear that the threat of cancerous cell mutations is one that might occupy research capacities for years to come and rightfully so. Research regarding several aspects from evolutionary cancer dynamics [86] to long-term behavior along with deep examination of various treatment options has been prevalent in the scientific community since the emergence of oncology in the 19th century [48]. To further emphasize the importance of cancer research it shall be mentioned, that the *2018 Nobel Prize in Physiology or Medicine* was awarded for the development of revolutionary cancer treatment options in the field of immunotherapy.

While often times associated solely with medicine as a scientific field, cancer research has been conducted in various disciplines. Mathematics has long outgrown its supporting role in the statistical evaluation of clinical trials. Medicinal oncology and mathematics have been two sides of the same coin for a while now, striving to produce a comprehensive explanation of cancer, treatment options and all defining dynamics involved.

The mathematics concerned when it comes to modeling the behavior of cancers can roughly be divided in probabilistic, allowing for some measurement of randomness through stochastics, and deterministic approaches. An example for the former is the modeling of evolutionary processes that lead to cancerous mutations in the first place. As we will examine the growth behavior of tumors, we opt for the latter approach as (in theory) the number of cells involved simply eliminates the need for probabilistic elements. Specifically, we will examine the effects of anti-PD-1 treatment, an immunotherapy medication, on tumor growth in metastatic melanoma. This treatment method is based upon the research that was awarded this year's Nobel prize and is one of the most promising treatment options currently available [71].

Chapters 2 and 3 serve to provide the biological foundation for cancer and treatment options and Chapter 4 will convey some mathematical basics. After presentation and discussion of the data utilized later on (Chapter 5), we start by employing a spatially homogeneous modeling approach through Ordinary Differential Equations to emulate the

dynamics between cancer, immune system and anti-PD-1 medication in Chapter 6. In an attempt to better understand the precise structure of tumors, we employ a spatially heterogeneous modeling approach involving Partial Differential Equations in Chapter 7. For this we introduce several classes of cancer cells, depending on oxygen saturation and include the local vasculature - angiogenesis-induced by the tumor and preexisting. We will conclude this thesis with a summarizing conclusion and provide an outlook on possible extensions of the research at hand.

# Chapter 2

# Cancer - The Scourge of our Time

## 2.1 A Brief History of Cancer

The first recorded diagnosis of cancer dates back to around 2625 BC, when the Egyptian physician *Imhotep* observed "bulging masses" in a patient [80]. Because of its current prominence, cancer is often though of as a modern disease, but diagnosis of various cancer types and the overwhelming feeling of impotence in curing it date back to ancient Egypt and are found throughout a number of time periods [103]. The first recorded course of treatment was removing the tumors. This remained the main course of action for a long time - throughout the ancient Greek civilization (as recorded by Herodotus in 440 BC [80]) as well as later on, albeit more refined [103]. While these records are certainly quite indicative of and believed to be cases of cancer, concrete evidence was furthermore procured from several excavations in Peru and Egypt (the latter dating back to about 400 AD) in the form of preserved cancer tissue [80].

As medicine took a decline throughout the middle ages, so did the understanding and treatment of cancer. In the 16th to 18th century, surgery prospered and with it its impact on cancer treatment [61]. Finally, in the 19th century the field of scientific oncolgy emerged when new research options presented themselves. In particular the first written description of melanoma was recorded by *René Laennec*, the inventor of the stethoscope [34]. Today cancer is one of the leading causes of death in many industrial nations and for example, only second to heart disease in the United States of America (U.S.) [103], [35]. Projections such as in the works of *Weir et al.* ([113]) propose that cancer might even overtake heart disease as the number one cause of death in the U.S. as soon as 2020.

## 2.2 Cancer and its Causes

As old as the disease are the attempts to explain and ultimately cure it. While for a long time and all throughout the middle ages cancer was believed to be an imbalance in the four humors (i.e. body fluids) as defined by Hippocrates, nowadays we can explain the disease much better [103] - yet many aspects still remain a mystery [80]. The term "cancer" itself is merely an umbrella term for over one hundred genetical conditions that

cause cells to grow and proliferate uncontrollably [102]. The mutated genes that lead to cancer are generally believed to fall into one of two groups: Oncogenes and Tumor Suppressor Genes [22]. Oncogenes take a more active role and "*encode proteins that control cell proliferation, apoptosis, or both*" [22]; their products (categorized in six groups as per [22]) act as cancer inducing through their manipulation of cellular growth and/or proliferation [86]. Tumor Suppressor Genes on the other hand impose a negative effect on the cell cycle [11] and if mutation causes loss of function for these genes, it can lead to abnormal cell development. Further research shows a vast number of interactions between genes classified in these categories, making the categorization somewhat arbitrary [11].

An important role in the development and growth of cancer is attributed to vascular structures inside the tumor, the creation of which is known as *angiogenesis* [38]. While cancer starts with one mutated cell and continues to grow through the induced proliferation, when the tumor reaches a certain size, the needed supply of nutrients and oxygen grows to levels too high to support from the outside. To support further growth, angiogenesis sets in at tumors of about $1\,\mathrm{mm} - 2\,\mathrm{mm}$ in diameter [38].

Lastly, when talking about tumors, we need to differentiate between malignant tumors (i.e. cancer) and benign tumors. Where a tumor in general is a local accumulation of cells displaying abnormal behavior (such as enhanced growth), a benign tumor will not invade blood vessels, attack surrounding tissue or indeed undergo metastasis (see Figure 2.1). Cancers are then classified as either Sarcoma (originating from connective
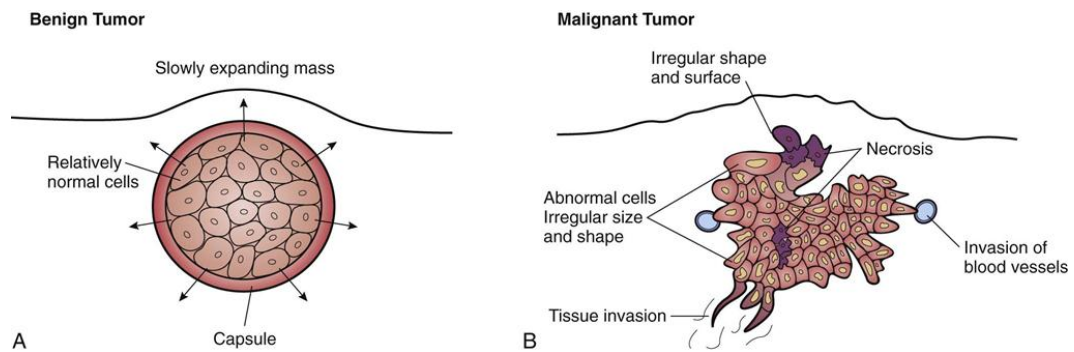


**Figure 2.1:** Rough comparison of pathology and behavior of benign and malignant tumors. Source: [84]

tissue), Leukemia/Lymphoma (blood or blood-forming tissue), Myeloma (bone marrow) or Carcinoma (epithelial tissue); Melanoma along with 90 % of diagnosed cancers belongs to the latter group [83]. For a more detailed classification see [83].

## 2.3 Malignant Melanoma

Skin cancer is the most common type of cancer and incidence is increasing worldwide. However, the largest proportion is made of cases of Basal-cell carcinoma, which is unlikely to metastasize and has very low mortality rates [30]. We focus on malignant melanoma in this discourse, which is rarer, but displays significantly higher risk of spreading and mortality rates if left untreated [73], [30].

The risk of metastasis increases with tumor depth ( [108] and is quite low in the early stages [29], making early prevention measures crucial [95]. The majority risk factor for the development of primary cutaneous melanoma has been shown to be ultraviolet radiation. Genetics can also play a key role in melanoma risk, as several genes increase risk and susceptibility to melanoma [7]. Of course, further risk factors (such as gender, age etc.) can be identified. One standard of cutaneous melanoma classification is to differentiate four stages [29]:

- *Stage I & II - Localized melanoma:*
  In these stages the tumor depth can already be up to 4 mm and ulceration may or may not occur. Most importantly the melanoma is restricted to one locality, i.e. no spread has occurred yet. While the prognosis is generally quite good for diagnosed Stage I/II melanoma, a significant decrease in survival rates with increasing primary tumor thickness has been observed [29]. Ulceration, the lack of intact dermis over the primary tumor, is also considered a strong independent predictor of survival along with tumor depth: Chance of survival is significantly lower for patients with ulcerated melanoma compared to those without.

- *Stage III - Local Spread:*
  Patients in this category display regional metastasis (regional lymph node, satellite, in-transit metastasis) making this group a very heterogeneous one. Ulceration may or may not occur in this category, but presence generally lowers 5-year-survival rates by several percentage points. The regional lymph nodes are most commonly affected first and thus make the best predictor. Early on, size of nodes containing metastasis was used as a criterion, whereas eventually the number of affected nodes proved to be more effective. The heterogeneity of patients with metastasis in regional lymph nodes in Stage III reflects in the wide spread of 5-year-survival rates, ranging from 29% to 82% depending on the number of nodal micrometastases, nodal macrometastases [1] and ulceration.

---

[1]Microscopic disease refers to metastatic deposits detected on histological analysis following elective lymph node dissection, or more commonly, SLN biopsy. Macroscopic disease refers to nodal metastases that are clinically or radiographically apparent and pathologically confirmed [29].

- *Stage IV - Distant Spread:*
  Once metastasis to distant locations such as organs or even other skin locations is diagnosed, patients are determined to be in the Stage IV category. 5-year survival rates are significantly lower and tend to fall under 10 - 30 % (see Figure 2.2). This of course is dependent on several factors, such as the location of metastasis: Patients displaying metastasis to distant skin locations, for example, have twice the survival rate (62%) of those with non-pulmonary visceral metastasis. One other factor that can impact survival rates heavily, is serum lactate dehydrogenase (LDH) level (see Figure 2.2 B).
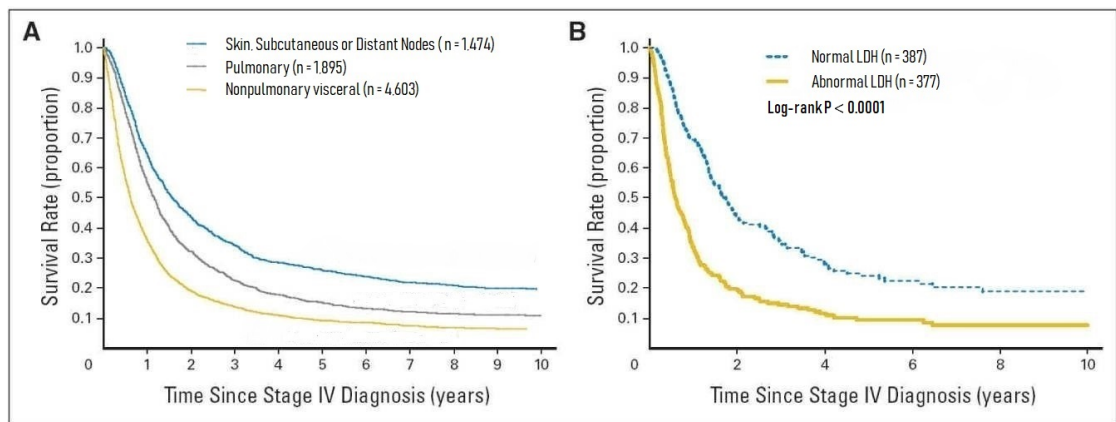


**Figure 2.2:** Survival of 7635 Stage IV melanoma patients in years grouped by site of metastasis in (A) and by serum lactate dehydrogenase (LDH) levels in (B) where data is available. Source: [29]

Another widely acknowledged option is to discard the four stages introduced above for *TNM Staging* (used for many different cancers), looking at three distinct characteristics: **T**umor depth (in combination with ulceration), the spread to nearby lymph **N**odes and the **M**etastasis to distant sites. These basically are the same characteristics as above in stages I-IV, so the two systems are somewhat interchangeable (indeed every category from *TNM Staging* can be attributed to one stage). An in-depth overview over both staging systems and how conversion from one to the other is possible can be found in Appendix A. Appendix A also offers a brief distinction between clinical staging and pathological staging, which is not hugely relevant for our purposes.

In addition to the *TNM* characteristics it has been proposed to examine primary tumor mitotic rate as an independent predictor, since increasing mitotic rate was shown to be associated with decreased survival (see [29]). The models proposed in later sections of this thesis are aimed at filiae of metastatic melanoma, i.e. Stage IV melanoma.

## 2.4 Immune Response to Cancer

The immune system is closely linked with cancer: The immune system can be weakened by cancer through spread into the bone marrow. Certain therapy options, such as chemo- or targeted therapy, can weaken the immune system as well by attacking the neutrophil count (white blood cells involved in the immune response to bacteria, viruses and fungi). Critically however, the immune system can help fight the disease by attacking cancerous cells. When examining the immune system, we need to differentiate between two closely related cascades: innate immunity and acquired immunity [2]. Innate immunity comprises of several different mechanisms such as inflammation and recruiting of certain leukocytes to specific sites.

A number of different cells contribute to the innate immune strategies, e.g. epithelial cells, innate leukocytes (such as Natural Killer Cells (NKC) or Eosinophils) among many others [27]. Acquired (adaptive) immunity includes genetic modification of two types of leukocytes: B lymphocytes and T lymphocytes [17]. While other cells, such as dendritic cells are involved in the adaptive immune response, B and T lymphocytes essentially define it. T cells express T cell receptors and B cells express antibodies on their surface. These in turn can bind to corresponding antigens, which are expressed on the surface of pathogens or through major histocompatibility complex (MHC) classes I and II [17]. T cells involved are $CD4^+$ and $CD8^+$ T cells, starting out as naive T cells and activated through binding of the T cell receptor to an antigen. They then move on to destroy cells expressing the same antigen or support the immune response by interacting with macrophages or B cells. On the other hand, B cells, upon recognizing an antigen will process it and then present the antigen to a $CD4^+$ T cell via MHC class II in order to activate the T cell. B cells can then become memory B cells or plasma cells creating corresponding antibodies to the processed antigen. Antibodies will react directly with the antigen (neutralization) or induce complement effects, e.g. by coating the antigen (opsonization) to promote phagocytosis or lysis [2]. The complex structures of inter-cell communication are further aided by cytokines. We don't want to go too deep into the general workings of the immune system (interested readers shall be referred to [2] for a comprehensive introduction that was written to complement the understanding of the immune system's interactions with cancerous cells).

The adaptive response of the immune system to cancer works in the outlined way aided by dendritic cells and cytokines. Specifically, dendritic cells are activated through necrosis of cancer cells and start producing the cytokine IL-12, which supports the activation of $CD4^+$ and $CD8^+$ T cells, that will start attacking cancer cells (as outlined above). $CD4^+$ T cells additionally enact the role of helper T cells and e.g. exert the cytokine IL-2, which induces further proliferation of effector T cells. While this describes interactions on a micro level, the dynamics on a macro scale (the entire tumor in this case) are interesting

also.

Penetration of the tumor by (especially $CD8^+$) T cells is a good prognostic tool for survival [14], but it is not fully understood what induces a high infiltration. Even in malignant melanoma, which is generally known as an immunogenic tumor and most susceptible to immunotherapy, 40% of tumors show only sparse infiltration. Especially the movement of the different T cell species is still a point of contention as the migration of T cells appears to be influenced by a number of factors, such as antigen expression, necrosis and the presence of collagen fibers or blood vessels; the velocities at which T cells move are also quite heterogeneous. The density of tumor infiltrating T cells increases, if the corresponding antigen is expressed on tumor cells, but the infiltration is believed to be affected by other factors, such as the interaction with tumor-associated macrophages [92].

Another hypothesis states, that the mutational load is a key factor with increasing number of mutations leading to increased T cell infiltration of the tumor [46]. This is
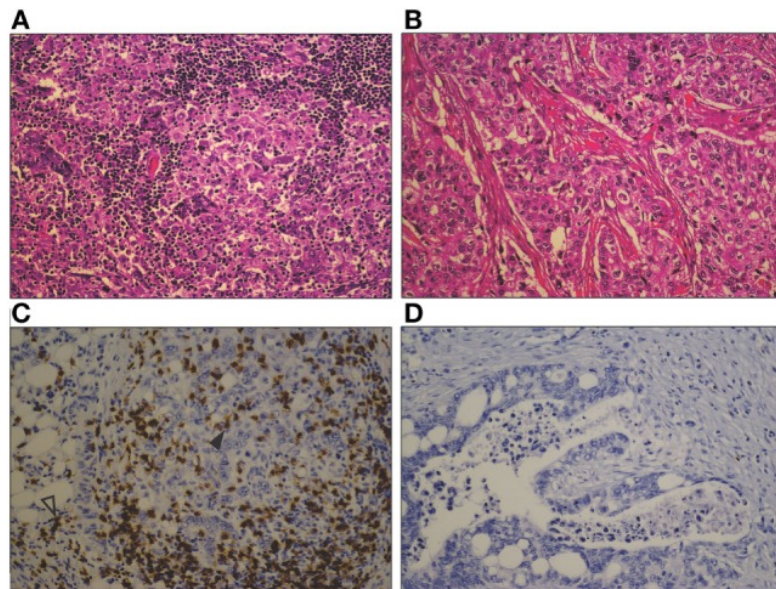


**Figure 2.3:** Comparison of heavy lymphocytic infiltration in a basal phenotype breast carcinoma (A), with a sparse infiltration in a different basal phenotype breast carcinoma (B). Similar comparison between a marked $CD8^+$ T cell infiltrate in a mismatch repair-deficient colon cancer (C), and the sparse infiltrate in a mismatch repair-proficient colon cancer (D). $CD8^+$ T cells are seen both within the tumor epithelium (closed arrowhead) and in the tumor stroma (open arrowhead) (original magnification by a factor of 200). Source: [46].

supported by the fact, that most cancers, that react well to immunotherapy (malignant

melanoma among others) display a high mutational load [46]. A further factor might be the role of tumor vasculature not permitting the entry of T cells into the microenvironment [46]. In conclusion, additionally to the complex processes of the immune system in terms of activation and proliferation, the migration and movement of T cells can pose further challenges in understanding the intricate workings of the immune response to cancer. A good visualization of how heavy infiltration vs sparse infiltration can present in the same type of tumor can be found in Figure 2.3. Figure 2.3 also hints at the heterogeneous patterns of T cell movement and local accumulations of effector cells.

# Chapter 3

# Cancer Treatment

## 3.1 An Overview over Treatment Options

This Section shall offer a quick study in the treatment options for cancer and their role in melanoma treatment. Other therapies of course exist (such as hormonal therapy e.g.), but will not be covered here.

### Surgery

As seen in Chapter 2, surgery has a long history when it comes to cancer treatment. While the main aim is generally to excise all cancerous cells, surgery has a multitude of purposes in the treatment of cancers today. It can additionally serve diagnostical (through biopsy) or prevention purposes and even be a help in palliative treatment [15]. Even today, it remains one of the, if not the most effective [94] modality of cancer treatment when it comes to curing. While this is critically dependent on the exact circumstances, if the cancer is contained in one locality and shows no sign of metastasis, surgery might be sufficient to cure the cancer completely.

Importantly, over the last decades, cancer surgery has evolved to be much more conservative and thus it is easier to retain organs completely and employ the invasive procedures with minimal damage to body structures [94]. In case of melanoma (and indeed all skin cancers) surgery is the preferred method of treatment as the excision imposes extremely low risk in comparison to other cancers due to the location [73]. Up to and including Stage I, surgery may be enough to cure the melanoma in its entirety [43].

For later stages, especially when the patient displays heavy metastatic burden, surgery will often be used in conjunction with other kinds of treatments, such as chemotherapy, radiotherapy or immunotherapy. While these other treatments will attack cancerous cells everywhere, surgery may be used to excise the primary tumor or (parts of) bigger metastases. This approach is of course not limited to malignant melanoma, but widely used in the treatments of various kinds of cancer (and benign tumors). Another option, especially for melanoma, is the removal of local lymph nodes through surgery, as they

are the first targets for the metastasis of melanoma (see Section 2.3).

Overall, while surgery remains vastly important today, the general hope is, that in the future, surgery will become somewhat superfluous as a treatment option and be reduced to the role of diagnosis through biopsy, as time will give rise to better methods for curing cancer.

### Chemotherapy

Chemotherapy utilizes drugs to destroy cancer cells via insertion locally (directly into the tumor) or into the blood stream, from where the drugs can reach any place in the body [64]. While the specific drug depends on the type of cancer, stage etc., chemotherapy generally aims to eliminate cancer cells, prevent further metastasis or preempt a relapse. As chemotherapy attacks and slows the growth and proliferation of cancer cells, it is known to have similar effects on healthy cells, as the drugs do not differentiate. Especially cells with a high proliferation rate, such as e.g. hair follicles, are at risk [64]. This limits the use of chemotherapy, so as not to overexert the capacities of healthy cells and leads to a treatment via cycles, in which the drugs are administered.

The uses of chemotherapy when it comes to cutaneous malignancies is unfortunately limited [73]. In the specific case of melanoma, chemotherapy has had a major role over the last decades, despite the known resistance of melanoma to conventional chemotherapy [96]. Dacarbazine and temozolomide, two alkylating agents, are generally the treatment of choice, though some debate exists if a multiple-agent regime might be more beneficial [96]. Lastly, biochemotherapy, the combination of chemotherapy agents with certain immune-based therapies, is another option showing good results as compared to conventional chemotherapy, albeit being extremely toxic [96]. Studies are not fully conclusive concerning biochemotherapy, but indicate an improved response rate without a significant impact on survival rates.

### Radiation Therapy

Radiation therapy equates to using high-energy rays to destroy cancer cells. The use of crude radium as a source for radiation, marking the onset of radiation therapy, has now given way to a number of more refined and sophisticated techniques [73]. Ionizing, high frequency radiation has become a standard and is a legitimate choice for the destruction of living tissue. The exact workings of radiation therapy are an extensive research subject involving a good understanding of physics and we will not delve into the subject too deeply. It shall be noted, that a technique, allowing higher frequencies, is to utilize radiation from several angles with the beams crossing at the tumor site. This produces a higher radiation level at the tumor, while not exposing any healthy tissue to the same

level of stress [53]. Radiation therapy often serves as an adjuvant therapy option, as for example in melanoma[2] (see below and Figure 3.1).

In the treatment of cutaneous malignancies and skin cancer in general, surgery and radiation may be used somewhat interchangeably [73] when attacking the primary tumor. For malignant melanoma, which had been believed to be quite radio-resistant in the past, surgery is usually preferred in this respect. However, in recent research [96] this was disproved and nowadays melanoma cells are considered responsive to radiation therapy. In addition to primary radiation, this includes the above-mentioned adjuvant therapy through radiation. It can be used to aid surgery by post-operatively treating the tumor site (including the regional lymph nodes) and kill residual cancer cells. All in all however, even adjuvant radiotherapy is not the norm and relegated to specific cases, but can certainly be relevant to the treatment of patients displaying macrometastases under certain circumstances.

**Targeted Therapy**

The term *targeted therapy* is a little more vague than previous terminology, which is ironic as the aim of targeted cancer therapy is that of maximal specificity. One of the big drawbacks to chemotherapy is the undesired effect on healthy cells; targeted therapy tries to avoid this while still employing a drug-oriented approach. It aims to utilize specific drugs whose effects are limited to tumorous cells through characteristic genes or proteins [26], [90]. Targeted therapy attempts to regulate the cell cycle, block proliferation or induce apoptosis in cancerous cells, but minimize off-target effects. We will further explain the idea of targeted therapy through an example of melanoma treatment: BRAF inhibition.

Rapidly Accelerated Fibrosarcoma (RAF) is a kinase involved in the RAS-RAF-MEK-ERK signal transduction cascade, a pathway regulating cell proliferation [13]. Three variations exist, but crucial for the treatment of melanoma is BRAF [13]. Since BRAF is ultimately inducing cell proliferation, we can categorize it as a proto-oncogene and an oncogene post mutation per Section 2.2. The pathway in question starts with the activation of RAS through a signal meant to induce cell proliferation, differentiation and growth. RAS in turn activates (B)RAF, which leads to the activation of MEK and ultimately ERK. This then sends a signal to the nucleus producing the desired effect [13]. Under normal conditions, this cascade is only triggered if the respective growth factors are present to activate RAS in the first place [96]. Melanoma cells can evolve

---

[2]Though some may argue, that radiation indeed is the primary therapy. Often the term "adjuvant therapy" refers to additional measures to surgery in the context of melanoma [96]. In the end, this terminology is of secondary interest to the effect of said therapy and the roles of primary and adjuvant therapy depend on the specific treatment case.

a so-called BRAF mutation, which leads to constant triggering of the cascade through BRAF (without the previous signals) and thus to a continuous sending of signals to the nucleus which ultimately leads to the characteristic and unnatural behavior of cancer cells [13].

The treatment of choice is then so called BRAF inhibition preventing or mitigating the constant activation of this pathway. A similar method is employed for MEK inhibition. A combination therapy of both BRAF and MEK inhibition is generally administered, offering practically no disadvantages over single agent therapy [104]. Unfortunately, in many cases BRAF inhibition only offers a temporary effect with a majority of patients showing relapse after some time [96].

**Immunotherapy**

Immunotherapy is an umbrella term for treatment options that aid the body's immune system in combating cancer as it is meant to be (see Section 2.4). This can range from actively supporting the immune system to battling mutations that help cancerous cells avoid normal immune reactions. Immunotherapies include, but are not limited to the administration of monoclonal antibodies, dendritic cells, T cells or even vaccines. Immunotherapy has proven to be an immense success and maybe most importantly displayed long-term survival benefits for patients responding to treatment [96].

Immunotherapy is often aided by a certain combination of adjuvant therapies. It can also be used alongside other therapy options as adjuvant therapy to surgery. An overview over adjuvant options to surgery for Stage III melanoma patients can be seen in Figure 3.1. This gives an impression of the complexity and heterogeneity of treatments - with new immunotherapy options emerging further choices become available constantly.

Since the first time the role of the immune system in tumor suppression was proposed to be an important one by Paul Ehrlich in 1909, researchers were set on exploiting this fact. Several drugs have been approved by the *U. S. Food and Drug Administration (FDA)* since then, starting in 1975 [96] and even resulting in the *Nobel Prize 2018 in Physiology or Medicine* to *Tasuku Honjo* and *James P. Allison* for their (separate) work and "their discovery of cancer therapy by inhibition of negative immune regulation" [107]. Honjo in particular was credited with discovering PD-1 and PD-L1 signaling pathways and first proposing the treatment method of PD-1 blockade. We will in this thesis focus on this revolutionary method of cancer treatment.

An overview concerning relevant, FDA-approved drugs used for the treatment of melanoma can be found in Appendix B.
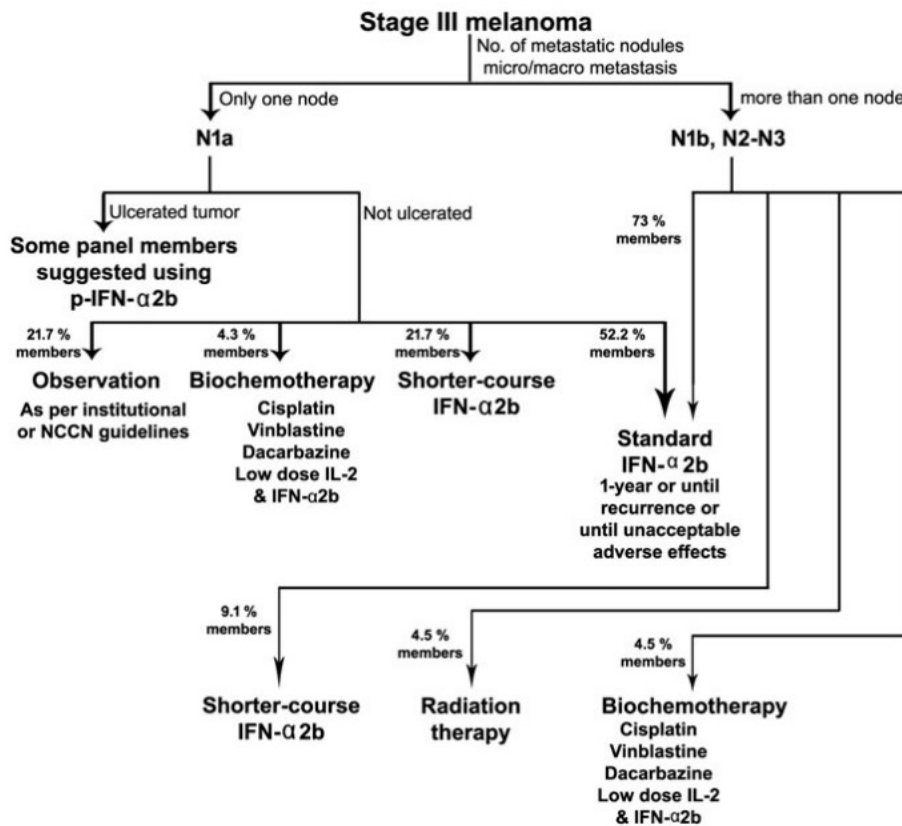
**Figure 3.1:** Recommendations of the *Society for Immunotherapy of Cancer* on adjuvant therapy in the treatment of Stage III melanoma patients, visualized in a flow diagram. Source [96].

## 3.2 Immunotherapy Approach via PD-1 and PD-L1 Inhibition

*Programmed cell death ligand-1 (PD-L1)* is normally expressed on cells involved in the immune response such as T cells, B cells or Natural Killer Cells [50]. Together with the checkpoint molecule *programmed cell death protein-1 (PD-1)*, expressed on activated T cells, it can form a pathway inhibiting immune response. From a physiological stand point, the PD-1/PD-L1 pathway evolved to limit inflammation when an antigen is expressed, so healthy tissue is exempted from harm. Thus the pathway is a mechanism set in place, so the immune system does not work uncontrollably [74].

Some cancers evolve a mutation abusing this signaling pathway to evade immunoediting. They overexpress PD-L1 to ultimately suppress anti-cancer immune response. Specifically

in tumor immune response, certain antigens are expressed on the tumorous cells, which would normally lead to T cells killing those cancer cells after detection of the antigen. The same antigen was previously presented through MHC molecules in order to activate the T cell. If, in addition to detecting the tumor specific antigen through T cell receptors, a PD-1-PD-L1 complex is formed, this will lead to immune tolerance even though the actionable antigen is present [4]. As the PD-1-PD-L1 complex emerges, this leads to dysfunction and/or exhaustion of the T cell. The presence of complexes inhibits further T cell activation and proliferation [60], [4]. A visual representation of this can be found in Figure 3.2 A.
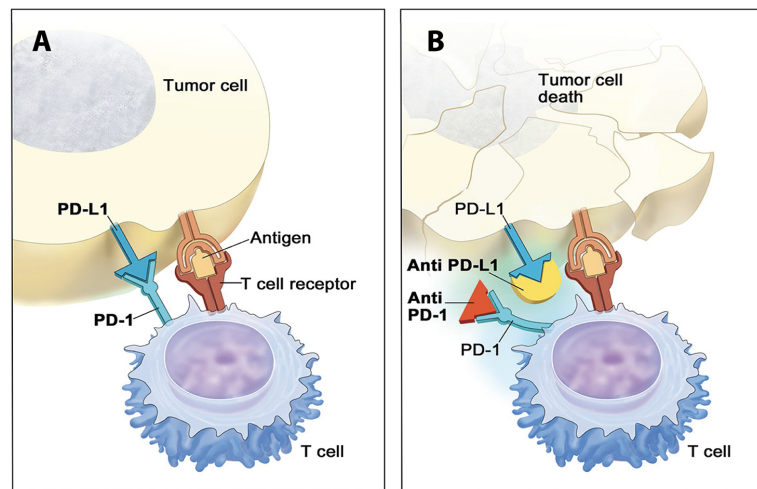


**Figure 3.2:** Rough sketch of the proteins and pathways involved in tumor immune evasion through PD-L1 expression (A) and the impact of PD-1 or PD-L1 blockade on those dynamics. Source: [119].

This is where PD-1 (and PD-L1) inhibition tries to interfere. It has shown great results, especially in later stage melanoma treatment, compared to other therapies and even other immunotherapy approaches, exhibiting greatly improved survival rates in several studies [71], [98]. We will in this thesis examine the effects of a medication called *Pembrolizumab*, which has shown greatly improved survival rates and success over similar treatment options, such as e.g. *Ipilimumab*, a monoclonal antibody aimed at the protein CTLA-4. For exact and extensive trial results see [98], [42] for example. *Pembrolizumab* is currently considered to be the most effective single agent immunotherapy against melanoma [115].

The PD-1 inhibiting substance (anti PD-1 for short) binds to PD-1 expressed on active T cells and thus prevents the creation of PD-1-PD-L1 complexes, and therefore undermining the evading mechanisms of the cancer [3] as is roughly seen in Figure 3.2

---

[3]PD-L1 inhibition works in a similar way, but instead binding to PD-L1, which also prevents the

B. While even today, PD-1 inhibition is largely associated with melanoma treatment, it has also shown good results in other cancers, such as non-small cell lung carcinoma or bladder cancer. PD-L1 expression was confirmed to be correlated with overall survival and response to PD-1 inhibition in lung cancer treatment by *Zhang et al.* in [118].

When it comes to melanoma, the situation is further complicated, as currently the usefulness of PD-L1 expression on tumors as an indicator for treatment success is extremely controversial [115]. *Wilmott et al.* in [115] concluded that even in a single patient receiving anti-PD-1 treatment some tumors respond, while others show resistance to the treatment and the extent of local PD-L1 expression gives no indication as to responsiveness versus resistance. They refer to other results indicating the improved response in tumors expressing PD-L1, but the data they present indicates no correlation. They introduce some uncertainty in these results and hypothesize the timing of biopsies may be a reason for their findings, as initially responding metastases may have acquired resistance [115]. *Wilmott et al.* propose a similarity to targeted BRAF and MEK inhibitors, where "epigenetic changes and tumor microenvironment factors are known to confer resistance". Specifically, they noticed a significantly upregulated expression of the laminin-3 subunit (LAMA3) in tumors resistant to anti-PD-1 treatment.

*Gong et al.* in [44] propose that there is enough evidence in support of the hypothesis that a high mutational load correlates positively with the benefits from immune checkpoint inhibition (in various tumor types). Overall, reliable indicators for response to anti-PD-1 treatment remain an area of interest as current results are sparse and controversial. We hope, that the mathematical models proposed later in this thesis may contribute a small part in understanding the intricate workings of PD-1 inhibition.

---

creation of PD-1-PD-L1 complexes

# Chapter 4

# Mathematical Foundation

## 4.1 Ordinary Differential Equations

The theory of Ordinary Differential is extensive and finds application in numerous fields. This brief introduction is not intended to give a comprehensive overview, but only impart some basics to support a better understanding of the following sections. More on Ordinary Differential Equations in the context of various fields can be found in many works, such as [32], [20], [106]. An Ordinary Differential Equation, simply speaking is a statement connecting the values of a function to its derivative:

**Definition 4.1**
Let $\Omega \subset \mathbb{R}^{n+2}$ an open subset with $n \in \mathbb{N}$. Let $f : \Omega \to \mathbb{R}$ a continuous function. Then $f\left[t, x(t), x^{(1)}(t), \cdots, x^{(n)}(t)\right] = 0$ is called an *Ordinary Differential Equation* of order $n$ (the degree of the highest derivative, that appears in the equation).

Linear equations are of the special form

$$a_0 x^{(n)} + a_1 x^{(n-1)} + \cdots + a_{n-1} x^{(1)} + a_n y = h(t),$$

where no multiples or other nonlinearities in $x$ or the derivatives of $x$ are included. Solutions to an Ordinary Differential Equation are n-times differentiable functions $x$ (which can be a vector of state variables), that satisfy the Differential Equation on an open set. $x$ is the so called dependent variable and depends only on $t$, the independent variable. In terms of biological context, the entries of $x$ can be thought of as concentrations, population numbers or similar and their state is dependent on time $t$.

In our case, we will look at the concentration of certain cell populations (such as T cells or cancerous cells) in a local tumor microenvironment or a larger area. When supplementing the Differential Equation with initial values (values a solution is required take at the starting time $t = t_0$), thus imposing further restrictions on possible solutions, this leads to a so called *Initial Value Problem*. Applying again biological context, this means we know the exact concentration/population size at time $t_0$ and look for a solution, that describes the concentration/population over time and satisfies the Differential

Equation as well as the values taken at $t_0$.

We are interested in first order Ordinary Differential Equations,

$$\frac{dx}{dt} = f(x, t), \tag{4.1}$$

as this helps us understand how the system (cell concentrations) behaves dependent on its current state. Other notations for the derivative include $x_t$, $\dot{x}(t)$ or $x'(t)$.

Of special interest tend to be states, where the system will remain as time progresses, so called *steady states* [32]:

**Definition 4.2**

A value $x^*$ for the state variables $x$ is called *steady state* or *equilibrium* of a first order Ordinary Differential Equation (4.1), if it holds

$$\frac{dx}{dt} = f(x^*, t) = 0, \qquad \text{for all } t \in \mathbb{R}.$$

Finally, for Ordinary Differential Equations and systems, such as will be introduced in Chapter 6, the *Picard–Lindelöf Theorem* can be of use in determining existence and uniqueness of a solution [20].

***Theorem 4.3 (Picard–Lindelöf Theorem)***

*Let $U \subset \mathbb{R} \times \mathbb{R}^n$ and $f : U \to \mathbb{R}$ a continuous function that satisfies a local Lipschitz condition, then there exists a value $\epsilon > 0$, so that there exists a unique solution $\hat{y}(t)$ on $[t_0 - \epsilon, t_0 + \epsilon]$ to the Initial Value Problem $x' = f(t, y)$,    $x(t_0) = x_0$.*

More specialized tools that will be relevant for the analysis of systems of Ordinary Differential Equations in later chapters will be provided in appropriate spots.

## Quasi-Steady-State Theory

We have introduced basic steady-state theory above as the existence of states in which the system does not change over time. Quasi-steady-state assumptions are - in simple terms - a helpful approximation to simplify a system by focusing on its "bottle-necks" [32]. Imagine for example an interaction between two substances where Substance A is always produced/available in extremely high concentrations. There is always enough present of Substance A to enable the interaction and thus we can basically discard the changes in concentration of Substance A.

Another example is from reaction kinetics: Assume a chemical reaction that produces intermediate complexes on the way from reactants to products. These generally are very short-lived and therefore these intermediates react very quickly. The actual conversion from reactants to products happens on a much slower timescale and thus we could assume

the intermediate complexes to be at steady state (thus the name *quasi-steady-state assumption*), which simplifies things [32]. Mathematically, we e.g. have a 2-dimensional system of Ordinary Differential Equations

$$\frac{dx_1}{dt} = f(x_1, x_2)$$
$$\epsilon \frac{dx_2}{dt} = g(x_1, x_2),$$

where $\epsilon$ very small. It is generally recommended to convert the system to a dimensionless form, when the exact relations between timescales, concentrations etc. are unclear. Thus, the small value for $\epsilon$ may e.g. result from one concentration's reference frame being much larger than another or from different timescales on which the two state variables operate. We can now assume

$$0 \approx g(x_1, x_2) \tag{4.2}$$

as $\epsilon$ very small, thus imposing our quasi-steady-state assumption on the system. Having one fewer state variable to solve for, makes things easier and often, further information can be extracted from the resulting equation (4.2). While this technique appears attractive to simplify complex systems, one should be certain that it is an appropriate approximation. The execution should always be handled with care [32].

## 4.2 Partial Differential Equations

In some instances we might not only be interested in the overall development of state variables over time, but dependent on another variable. For example, thinking back to cell concentrations, we could ask what the concentration was at a given time at a certain point in space. Thus, we are looking at a state variable dependent on space and time. Or we could be interested in the concentration of a substance or temperature in a point of a two dimensional or even three-dimensional area, thus facing the necessity of examining a function dependent on spatial coordinates $(x, y)$ or $(x, y, z)$.

This leads us to consider Partial Differential Equations; as before for Ordinary Differential Equations, this section is merely intended to offer a brief introduction into the topic (for further reference see [21], [32]). For this thesis we will concentrate on Partial Differential Equations involving time ($t$) and one dimension of space ($x$) as variables. Thus, Partial Differential Equations, such as used here and indeed often in physical or biological applications, are of the form:

$$F\left(x, t, u(x,t), \frac{\partial u}{\partial x}, \frac{\partial u}{\partial t}, \cdots, \frac{\partial^k u}{\partial^{k_1} \partial^{k-k_1}}\right) = 0,$$

where $\frac{\partial u}{\partial x}, \frac{\partial u}{\partial t}$ are the partial derivatives. The order of the Partial Differential Equation is that of the derivative of the highest order [21]. Partial derivatives are derivatives with

respect to only one of the independent variables and express the change of the function when moving in the direction of that variable. The partial derivative is technically the limit as the move shrinks to an infinitesimal size, i.e.

$$\frac{\partial u}{\partial x} = \lim_{\Delta x} \frac{u(x + \Delta x, t) - u(x, t)}{\Delta x}, \quad \text{for the spatial derivative}$$

$$\frac{\partial u}{\partial t} = \lim_{\Delta t} \frac{u(x, t + \Delta t) - u(x, t)}{\Delta t}, \quad \text{for the time derivative.}$$

The definition of a linear Partial Differential Equation functions similar to that of a linear Ordinary Differential Equation. A new term can be introduced in quasilinearity, however. A Partial Differential Equation is quasilinear, if it is linear in all the highest order derivatives; they offer some advantages in several applications [62]. Similar to Initial Value Problems in the Ordinary Differential Equation case, we can supplement a Partial Differential Equations with so called *boundary conditions.* If we for example examine a Partial Differential Equation on a bounded spatial domain $\Omega \in \mathbb{R}^n$, additionally to initial conditions, we need to characterize the behavior on the boundary $\partial\Omega$. Typical examples include

- *Dirichlet boundary conditions*
  Dirichlet boundary conditions specify the value of the function on the boundary of the domain, i.e.
  $$u = b(x, t) \qquad for \quad x \in \partial\Omega, \quad t > 0$$
  Should $b = 0$ everywhere, we call the Dirichlet boundary conditions homogeneous.

- *Neumann boundary conditions*
  Neumann boundary conditions on the other hand set a value to the normal of the function on the boundary of the domain, i.e.
  $$\nabla u \cdot n = b(x, t) \qquad for \quad x \in \partial\Omega, \quad t > 0,$$
  where $n$ is the outer normal to $\Omega$ at $x \in \partial\Omega$ and $\nabla$ is the gradient (in the one dimensional case this simplifies to $\frac{\partial u}{\partial x}$). The homogeneous case is again for $b = 0$ and corresponds to the well-known *zero-flux condition.*

- *Mixed boundary conditions*
  Mixed boundary conditions are fairly self-explanatory through their name; they mix Dirichlet and Neumann boundary conditions, i.e.
  $$\alpha(x, t)u + \beta(x, t)\nabla u \cdot n = b(x, t) \qquad for \quad x \in \partial\Omega, \quad t > 0,$$

We will primarily operate under Neumann boundary conditions.
While Partial Differential Equations offer a vast superiority in modeling options over

Ordinary Differential Equations, it should be noted, that analytical solutions are generally much harder to find - even numerical analysis is significantly more complicated. Whereas Theorem 4.3 offers an elegant solution for existence and uniqueness of solutions to a certain class of Ordinary Differential Equation problems, similar results for the field of Partial Differential Equations are few and far between. While some specific and well-known Partial Differential Equations are extensively researched and analyzed, in general, the analysis of (systems of) Partial Differential Equations proves extremely complex.

## 4.3 Reaction Diffusion Equations

Reaction Diffusion Equations are a special subset of Partial Differential Equations and generally take the form [59]:

$$\frac{\partial u}{\partial t} = \overbrace{D\Delta u}^{\text{diffusion term}} + \underbrace{f(x, u, \nabla u)}_{\text{reaction term}}, \tag{4.3}$$

where $u(x,t)$ is again a state variable and generally describes the density/concentration of a substance or a population (in our case concentration of a certain cell type) for a certain position $x \in \Omega \subset \mathbb{R}^n$ at a given time $t$. $\nabla$ again describes the gradient and $\Delta$ is the Laplace operator. The right-hand side of equation (4.3) can be partitioned as follows: The first term denotes the so called diffusion, i.e. random migratory dispersal, with the diffusion coefficient $D$ regulating the speed and manner of said dispersal. The second part, the reaction term, describes factual change through processes such as birth, death or proliferation among others. Effects such as chemotaxis, which can describe migration as well, are here included in the reaction term.

The derivation of the general Diffusion Equation (equation (4.3) without reaction term), which might seem very abstract to an unfamiliar reader, is a very intuitive one. It can either be derived from *Fick's Law* (as seen in [78] or [59]) or through the *Random Walk (Brownian Motion)*, which is nicely illustrated in [59] and can also be found in [117], [32]. When looking for existence and uniqueness results regarding Reaction Diffusion Equations, we can turn to the theory of weak solutions. As this would involve extensive theory on Sobolev spaces and weak derivatives, the interested reader shall be referred to [59], which also provides a comprehensive introduction to Reaction Diffusion Equations.

# Chapter 5

# Patient Data and Associated Challenges

For numerical analysis and parameter fitting, we employ a data set kindly provided by *Prof. Dr. Edgar Dippel* from *Klinikum der Stadt Ludwigshafen (am Rhein gemeinnützige GmbH)*. Overall, data from three patients treated with the PD-1 inhibition medication *Pembrolizumab* was provided and will be utilized in later chapters. Four further patient histories were supplied, but could not be utilized in a sensible manner due to the employment of different immunotherapies and/or duration of treatment. We need to be cautious when comparing between different immunotherapy treatments as the mechanisms involved are very specific. In terms of treatment duration, we are looking to have at least three separate measurements relevant to effect of *Pembrolizumab* treatment.

## 5.1 Relativization of Data

The benefits of adjuvant therapy to immunotherapy were briefly discussed in Section 3.1 and thus it is not surprising to encounter uses of various adjuvant measures in patient files. In addition, as *Pembrolizumab* is a fairly new medication, several patients had previously undergone other primary treatments (see below). This leads to a potentially vast number of interactions and implications concerning the mechanisms of PD-1 blockade, which will be examined fairly isolated in the mathematical models in Chapters 6 - 7. As metastases appear at different times this implies that even the comparison of different tumors in the same patient for growth and responsiveness to anti-PD-1 might present some challenges.

This is supported by the findings of *Wilmott et al.* in [115], who observed varying degrees of response in different metastases in the same patient. Additionally, data "blind spots" can occur through timing of imaging and therapy. When e.g. *Pembrolizumab* therapy is started in between two imaging dates (generally three to six months apart) it is hard to identify proper initial conditions, so to speak. Previously (last image *pre-Pembrolizumab*), the old therapy may still have had some effect and by the time the first images are available, *Pembrolizumab* already had some time to influence progression of disease. This also occurs in general when switching therapies, as especially in the early stages of *Pembrolizumab* administration, residual effects of the previous treatment or involuntary combination therapy effects (negative or positive) may occur. These factors

can make the data somewhat unreliable, as we will explicitly avoid the number of possible interactions between anti-PD-1 and other effects in our models; we try to emphasize the key interactions of anti-PD-1 treatment and purposefully avoid overloading the model.

## 5.2 Data Used In This Thesis

### Patient 1 (P1)

P1 had a melanoma excised, which was presumed to be the primary tumor for metastatic melanoma diagnosed roughly five years post-surgery. A local metastasis was removed shortly after diagnosis and treatment with *Ipilimumab* (monoclonal CTLA-4 antibody) initiated (*Pembrolizumab* at this point hadn't even been FDA-approved) and stopped after four cycles. Shortly after this, a targeted therapy with Dabrafenib was started and two months later supplemented by treatment through Trametinib.

Two years later aggressive progress with a large number of new metastases (76 visible metastases) was registered and thus treatment was switched to *Pembrolizumab*. These metastases were all located in the brain of the patient; the visible tumor burden in the rest of the body had reduced to zero at that point. Some images to display the impact of the newly emerged metastases can be found in Figure 5.1. The treatment continued through to end of our data set and minimal adjuvant therapy was conducted during this time (one general radiation of the brain).

### Patient 2 (P2)

P2 developed metastatic melanoma from an unidentified primary tumor and was diagnosed with several tumors which turned out to be malignant melanoma. An Interferon therapy was initiated and supported by excision of additional lymph node metastases as well as adjuvant radiation therapy. Due to further progress of the disease the therapy was switched to *Ipilimumab* 5 months after initial diagnosis. Continuing during the *Ipilumumab* treatment period were occurrences of radiation therapy.

After ten months the metastases had reduced in number, but two metastases showed progression in growth and thus the patient was ultimately switched to *Pembrolizumab*. The *Pembrolizumab* treatment continued through to end of our data set; still some radiation therapy occurred. The data on radiation (location, time) was partly missing and could not be transmitted in its entirety, which creates the necessity to handle this data set with care. Additionally, only two metastases are available for measurement during *Pembrolizumab* treatment and respecting the possible differences in tumors in a single patient (see [115]), the small data set may put some restrictions on significance of P2 data.
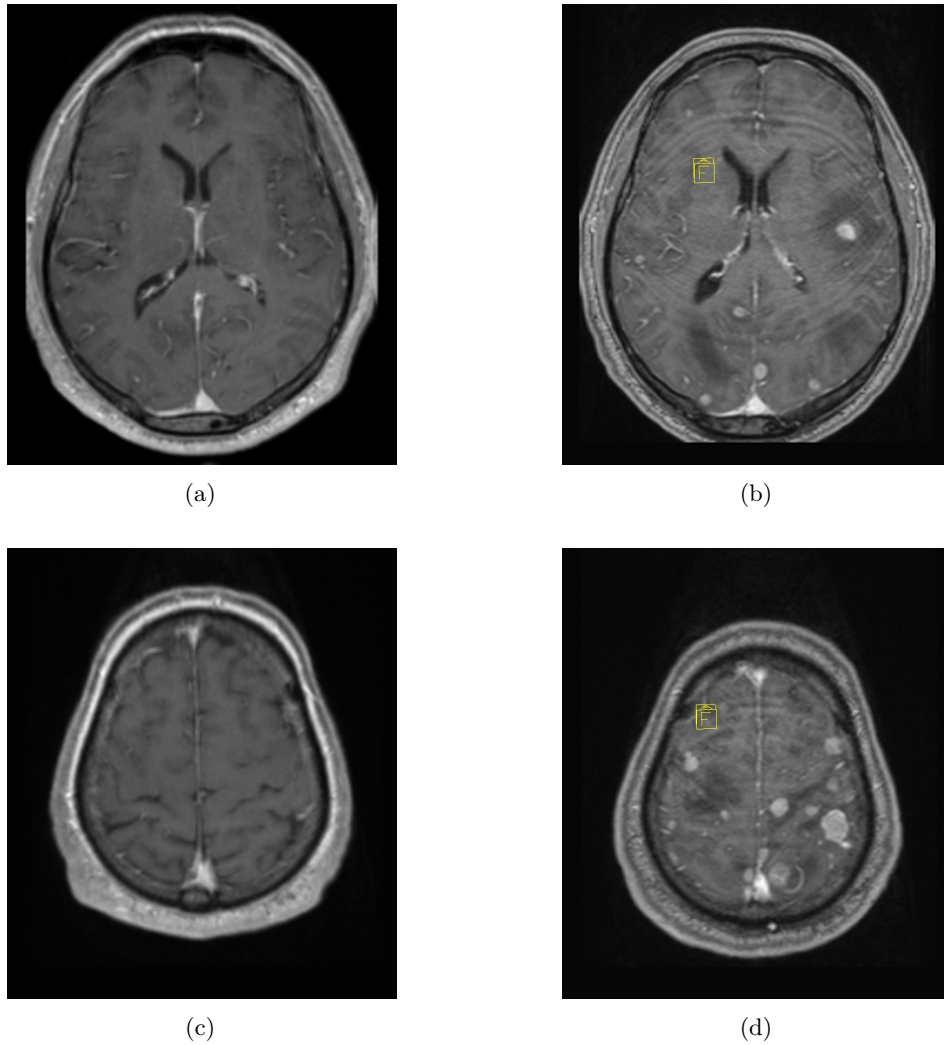
**Figure 5.1:** Comparison of tumor burden in P1, where (a) and (b) as well as (c) and (d) represent the same slice at different timepoints: At $t = 0$ (for(a),(c)), shortly before treatment with *Pembrolizumab* was started, and at $t = 63$ (for (b),(d)), the first image after treatment was started, where $t$ is measured in days. Source: Data provided by *E. Dippel*

**Patient 3 (P3)**

After excision of the primary melanoma tumor for P3, four local metastases were identified and immediately fully excised through surgery. Incidentally, a benign tumor was also diagnosed independently. Treatment with *Ipilimumab* was initiated and after further progress of disease changed to another immunotherapy. After continued progress, roughly a year after initial diagnosis, the method of treatment was switched to chemotherapy, which did not display the desired effects. Ultimately, a few months later, the patient was switched to *Pembrolizumab*. The treatment with *Pembrolizumab* continued through to end of our data set; during this interval several pulmonary tumors were partly resected, as this became necessary to sustain core bodily functions and relieve stress on vital organs.

From this first introduction to our patient data, we can already see the special status of data set P1. Some of the limitations mentioned above do not apply as strongly: The extremely aggressive nature of the cancer let's us reasonably exclude effects from previous medication. This assumption is further supported by the fact that the metastases occur only just before *Pembrolizumab* treatment. In comparison - the metastases we observe in P2,P3 had existed for a longer time and underwent previous treatments that may have had an effect on e.g. structure of the tumor.

Data set P1 is purer in a way and additionally we have a large number of metastases, that are all in the same tissue and environment. P1 is therefore best suited to evaluate our quantitative models in Chapters 6 and 7. We will briefly touch upon specific benefits to the model at hand when conducting numerical simulations that will be compared to data set P1.

### 5.2.1 On Methods of Measurement for Tumor Size

A standard measurement methodology in radiology and oncology sees physicians measuring only in one of the three main body planes: Transverse (Axial), coronal or sagittal plane [87]. It is a common procedure to identify the longest 1D extension (this goes for solid tumors as well as lymph nodes) and then use this measurement in conjunction with the longest (corresponding) perpendicular 1D extension in that plane [87] for classification or volume calculation through assuming the tumor shape as spheroid (ellipsoid of revolution), i.e. a spheroid with two identical semi-diameters [99]. The two measurements needed for this can be seen on an exemplary metastasis in Figure 5.2. We will refer to this method as the *Spheroidal Method* from here on.

The Response Evaluation Criteria in Solid Tumors (RECIST) is an international standard in classification of tumors and determining progress over stable disease or remission [100]. In RECIST, contrary to the method outlined above, only a single 1D measurement
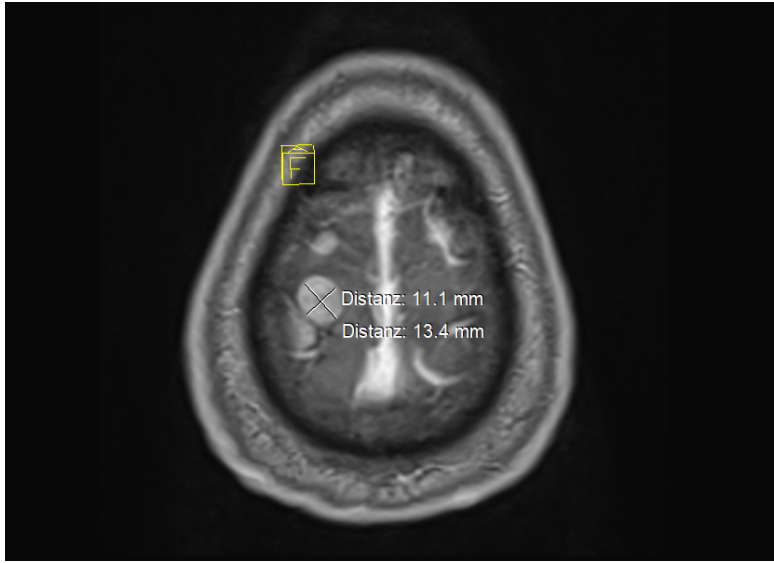
**Figure 5.2:** Two measurements in the transverse plane of a brain metastasis: The longest 1D extension and the corresponding longest, perpendicular 1D extension. Source: Data provided by *E. Dippel.*

is collected: that of the shorter extension for lymph nodes and the longest diameter for other lesions (see [87], [100] for further information). While it shall not be disputed here that this measurement is sufficient to judge over progress and treatment decisions in most instances, it may be careless to simply carry over such methods when it comes to mathematical modeling, as we are employing a more quantitative approach. As the question for exact volumes of three-dimensional masses in a body is of interest quite often, models were developed to better calculate the precise volume from 1D measurements of parallel (de facto) 2D slices even before the widespread ascent of 3D imaging software [77]. One such algorithm is presented in [77] and shall be referred to here as the *McKenney Algorithm.*

Even more preferred to get an accurate measurement are advanced imaging techniques and indeed, today we have access to several software options delivering great results when it comes to recreating 3D tumor models from MRI or CT imaging. A good example for this is the software *3D Slicer* [1]; we will be using it for the purposes of this thesis when it comes to imaging/measurement software. Should proper images not be available or not compatible with the software (through poor quality or incomplete information) algorithms such as the *McKenney Algorithm* can still produce more accurate results as compared to the *Spheroidal Method.* We will briefly demonstrate the differences that can occur due to use of the *Spheroidal Method* in five exemplary metastases from data set P1

at the first date of imaging after anti-PD-1 treatment initiation. These five metastases are the five biggest metastases at peak tumor burden ($t = 63$) and will be used later for numerical analysis:

| Metastasis | Spheroid method | 3D imaging through *3D Slicer* | $\Delta$ |
|:---:|:---:|:---:|:---:|
| M1 | $887\,\text{mm}^3$ | $1569\,\text{mm}^3$ | $-43\%$ |
| M2 | $733\,\text{mm}^3$ | $1553\,\text{mm}^3$ | $-53\%$ |
| M3 | $1239\,\text{mm}^3$ | $1618\,\text{mm}^3$ | $-23\%$ |
| M4 | $824\,\text{mm}^3$ | $1527\,\text{mm}^3$ | $-46\%$ |
| M5 | $509\,\text{mm}^3$ | $940\,\text{mm}^3$ | $-46\%$ |

**Table 5.1:** Comparison of measurement methodologies (*Spheroid Method*, 3D imaging through *3D Slicer*) on an exemplary set of metastases M1-M5 from P1. Source: Own work in conjunction with data provided by *E. Dippel.*

The reasons become evident through Figure 5.3. While M2 is assigned a significantly smaller volume than M3 through the *Spheroidal Method*, it is, in reality, almost equal in volume. The extension of M2 in the transverse plane appears to be indeed the smallest of all planes and the growth is restricted in lateral direction (as can be seen in Figure 5.3 a). Thus, the orientation of M2 is unfortunate, should we choose the *Spheroidal Method*, taking measurements only from the transverse plane. The extension perpendicular to the transverse plane of M2 is comparatively large, as seen in Figure 5.3b, which accounts for the volume of M2. This is somewhat fitting with the fact, that M1 and M2 are visible at $t = 0$, whereas M3-M5 are not. While not all metastases behave the same way and the measurement of small metastases can be critical due to the fact that slices are several $mm$ apart, it still would seem odd, that a metastasis (M2) of $733\,\text{mm}^3$ at $t = 63$ would be visible in earlier imaging, whereas a metastasis (M3) of $1239\,\text{mm}^3$ at $t = 63$ is not. In reality they are the same size at $t = 63$, which is more agreeable with these observations.

In conclusion, one needs to be extremely careful when evaluating single metastases - this will become even more evident in later sections. In addition to the individuality of treatment circumstances and different responses of single tumors in the same patient, measurements can become inaccurate. As long as image quality allows (and this is not always the case - especially for smaller metastases), it makes sense to employ a more accurate method of measurement when it comes to data intended for quantitative use.

### 5.2.2 Tumor Measurements For Patients

We present the obtained measurements for P1 in Table 5.2. In a similar fashion an equal presentation for the measurements P2,P3 can be found for in Appendix C. We introduce
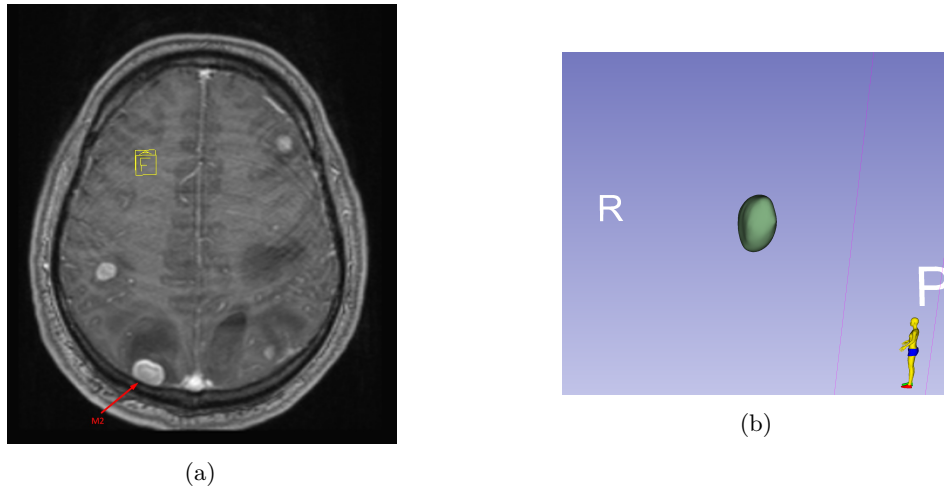
**Figure 5.3:** Comparison of MRI examining M2 of P1 in the transverse plane (indicated through red arrow) (a) and a 3D model of M2 created through *Slicer 3D* displaying the large extension perpendicular to the transverse plane (b). Source: Own work and data provided by *E. Dippel.*

a timeline, where one time unit is equal to one day. The beginning $t = 0$ for each patient is set to be the last date images were taken before *Pembrolizumab* treatment initiation. The timeline (values for $t$) for each patient combines both measurements and treatment dates; in the case of P1 e.g. Tables 5.2 and 5.3 utilize the same timeline. Similarly for the values found in Appendices C and D.

### 5.2.3 Time and Amount of Medication and Adjuvant Treatment

Here we outline the treatments that P1 underwent during the examined time interval in Table 5.3 (in similar form for P2,P3 in Appendix D). As outlined above, we don't know the exact dates and other specifics on some of the adjuvant methods. While some surgeries can at least be linked to a certain window of time as e.g. in the case of P3, other therapy schedules (e.g. radiation therapy for P2) could not be reconstructed. The *Pembrolizumab* treatment schedule was well documented and could be reconstructed in its entirety for all three patients. In terms of dose administered, the treatment employed the optimal dose as currently recommended and justified in scientific literature [91], [37]. We will reconsider the issue of optimal dosage, when it comes to quantifying the increase of concentrations in crucial locations in Chapter 6. For P1, we have fairly complete data, as there was minimal adjuvant treatment and it is well documented. This again emphasizes the special status of the data set P1, as Table 5.3 displays the treatment regime of P1 in its entirety (for the time interval we examine).

| Time | M1 | M2 | M3 | M4 | M5 | Full Tumor Burden |
|---|---|---|---|---|---|---|
| $t = 0$ | $14\,\mathrm{mm}^3$ | $14\,\mathrm{mm}^3$ | $0\,\mathrm{mm}^3$ | $0\,\mathrm{mm}^3$ | $0\,\mathrm{mm}^3$ | $398\,\mathrm{mm}^3$ |
| $t = 63$ | $1569\,\mathrm{mm}^3$ | $1553\,\mathrm{mm}^3$ | $1618\,\mathrm{mm}^3$ | $1527\,\mathrm{mm}^3$ | $940\,\mathrm{mm}^3$ | $23\,735\,\mathrm{mm}^3$ |
| $t = 124$ | $474\,\mathrm{mm}^3$ | $1053\,\mathrm{mm}^3$ | $614\,\mathrm{mm}^3$ | $658\,\mathrm{mm}^3$ | $1198\,\mathrm{mm}^3$ | $13\,512\,\mathrm{mm}^3$ |
| $t = 223$ | $498\,\mathrm{mm}^3$ | $418\,\mathrm{mm}^3$ | $510\,\mathrm{mm}^3$ | $408\,\mathrm{mm}^3$ | $772\,\mathrm{mm}^3$ | $9436\,\mathrm{mm}^3$ |
| $t = 285$ | $1248\,\mathrm{mm}^3$ | $284\,\mathrm{mm}^3$ | $260\,\mathrm{mm}^3$ | $290\,\mathrm{mm}^3$ | $1084\,\mathrm{mm}^3$ | $11\,630\,\mathrm{mm}^3$ |
| $t = 333$ | $1759\,\mathrm{mm}^3$ | $587\,\mathrm{mm}^3$ | $879\,\mathrm{mm}^3$ | $1363\,\mathrm{mm}^3$ | $1149\,\mathrm{mm}^3$ | $13\,712\,\mathrm{mm}^3$ |

**Table 5.2:** Measurement data of metastases of P1, including time of measurement and size of metastases. The five biggest metastases (M1 - M5) at $t = 63$ (heaviest overall tumor burden) were selected for an individual examination. They are presented alongside the overall tumor burden of the brain. Source: Own work building on data provided by *E. Dippel.*

| Time of Administration | Cycle, Medication and Amount |
|---|---|
| $t = 14$ | 1.) Cycle *Pembrolizumab* ($2\,\mathrm{mg/kg}$) |
| $t = 35$ | 2.) Cycle *Pembrolizumab* ($2\,\mathrm{mg/kg}$) |
| $t = 55$ | 3.) Cycle *Pembrolizumab* ($2\,\mathrm{mg/kg}$) |
| $t = 68$ | Radiation therapy on entire brain |
| $t = 88$ | 4.) Cycle *Pembrolizumab* ($2\,\mathrm{mg/kg}$) |
| $t = 109$ | 5.) Cycle *Pembrolizumab* ($2\,\mathrm{mg/kg}$) |
| $t = 129$ | 6.) Cycle *Pembrolizumab* ($2\,\mathrm{mg/kg}$) |
| $t = 151$ | 7.) Cycle *Pembrolizumab* ($2\,\mathrm{mg/kg}$) |
| $t = 172$ | 8.) Cycle *Pembrolizumab* ($2\,\mathrm{mg/kg}$) |
| $t = 193$ | 9.) Cycle *Pembrolizumab* ($2\,\mathrm{mg/kg}$) |
| $t = 213$ | 10.) Cycle *Pembrolizumab* ($2\,\mathrm{mg/kg}$) |
| $t = 234$ | 11.) Cycle *Pembrolizumab* ($2\,\mathrm{mg/kg}$) |
| $t = 255$ | 12.) Cycle *Pembrolizumab* ($2\,\mathrm{mg/kg}$) |
| $t = 276$ | 13.) Cycle *Pembrolizumab* ($2\,\mathrm{mg/kg}$) |
| $t = 297$ | 14.) Cycle *Pembrolizumab* ($2\,\mathrm{mg/kg}$) |
| $t = 319$ | 15.) Cycle *Pembrolizumab* ($2\,\mathrm{mg/kg}$) |

**Table 5.3:** Treatment data of P1, including time of treatment, medication administered and amount of medication for each treatment cycle if applicable. Source: Data provided by *E. Dippel.*

# Chapter 6

# A Spatially Homogeneous Ordinary Differential Equation Approach

## 6.1 The Model

As a first approach we try to concentrate on the dynamic between T cells, tumor cells and anti-PD-1 in a spatially homogenous model. We attempt to isolate this dynamic from the combination therapy model as presented in [60]. The comprehensive approach by *Lai and Friedman* chooses to include spatial dynamics and several factors in the complex process of immune response. In order to simplify these extensive pathways and processes we reduce the number of populations involved, inspired by the approach taken in [85].

We assume, that there are no other effects, especially including, but not limited to other treatments and adjuvant measures unless otherwise stated. We make special mention of the BRAF mutation (see Section 3.1), as it occurs in a number of melanoma patients. We assume, that, once it occurs, the patient is treated with appropriately targeted medication and thus the effect of the mutation on system behavior is nullified. This assumption allows us to exclude BRAF mutation effects from our model. Let $C$ be the concentration of cancer cells, $T$ the concentration of (activated, relevant) T cells, $A$ the concentration of anti-PD-1 immunotherapy medication and $D$ the concentration of free (i.e. not bound by anti-PD-1) PD-1 expressed on relevant T cells, all in $\frac{g}{cm^3}$ (see also Table 6.1.

It is of interest how much of the expressed PD-1 is completely free and how much is bound to PD-L1. For this we introduce the additional populations $Q$, the concentration of complexes formed between PD-1 and PD-L1; and $L$ the concentration of free PD-L1 (both in $\frac{g}{cm^3}$). Assuming $\alpha_{DL}$ as the rate of association and $d_Q$ as the rate of disassociation [4] the dynamic of these complexes can be written as

$$\frac{dQ}{d\tau} = \alpha_{DL}D(\tau)L(\tau) - d_Q Q(\tau) \tag{6.1}$$

---

[4]At this point we want to note, that - unless otherwise noted - all introduced parameters are constant and non-negative to ensure biological meaningfulness.

| State Variable | Meaning |
|:---:|:---:|
| $C$ | Concentration of cancerous cells in $g/cm^3$ |
| $T$ | Concentration of activated T cells in $g/cm^3$ |
| $A$ | Concentration of anti-PD-1 in $g/cm^3$ |
| $D$ | Concentration of free PD-1 expressed on T cells in $g/cm^3$ |
| $L$ | Concentration of PD-L1 expressed on T and cancer cells in $g/cm^3$ |
| $Q$ | Concentration of PD-1-PD-L1 complexes in $g/cm^3$ |

**Table 6.1:** List of variables involved in the system of Ordinary Differential Equations (6.3) - (6.6).

The half-life of a human PD-1-PD-L1 complex is less than one second [76]. The model (6.3) - (6.6) introduced below operates on a vastly different time scale; it is therefore a reasonable simplification to impose a quasi-steady-state assumption on this dynamic. Assume e.g. that the dynamic (6.1) is meaningful on a time scale where one unit represents one tenth of a second. Now, rescaling (6.1) to fit the timescale of the remaining system of Differential Equations, which operates with days as a standard time unit, assume $t = \tau \cdot 10 \cdot 3600 \cdot 24$. Therefore

$$\frac{d}{dt}\hat{Q}(t) = \frac{d}{d\tau}Q(\tau) \cdot \frac{d\tau}{dt} = \frac{1}{\epsilon} \cdot [\alpha_{DL}\hat{D}(t)\hat{L}(t) - d_Q\hat{Q}].$$

with $\epsilon = \frac{1}{10 \cdot 3600 \cdot 24}$. Dropping the hats in this notation leads to

$$Q \approx \frac{\alpha_{DL}}{d_Q}DL. \tag{6.2}$$

A comprehensive introduction to the rescaling of systems and the theory of quasi steady states can be found in various literature, such as [58]. With this important dynamic (6.2) taken care of, we formulate the system of Ordinary Differential Equations:

$$\frac{dC}{dt} = \lambda_C C(1 - \frac{C}{C_M}) - \eta CT \tag{6.3}$$

$$\frac{dT}{dt} = (\lambda_{I_{12}}T_0\frac{I_{12}}{K_{I_{12}} + I_{12}} + \lambda_{I_2}T\frac{I_2}{K_{I_2} + I_2}) \cdot F(Q) - d_T T \tag{6.4}$$

$$\frac{dA}{dt} = -\mu_{PA}DA - d_A A \tag{6.5}$$

$$\frac{dD}{dt} = \rho_{PD} \cdot (\lambda_{I_{12}}T_0\frac{I_{12}}{K_{I_{12}} + I_{12}} + \lambda_{I_2}T\frac{I_2}{K_{I_2} + I_2}) \cdot F(Q) - d_T D - \mu_{PA}DA. \tag{6.6}$$

We assume that all cells of one population behave the exact same way, experience the exact same conditions and that the system is well mixed at all times. We impose logistic

growth for the cancer cells through the growth function $G(C) = \lambda_C C(1 - \frac{C}{C_M})$. While this is somewhat arbitrary and not the main focus of the model, it has been proposed in a similar situation by *Lai et al.* in [60]. Logistic growth is also suggested to be a good choice over Gompertz growth in models involving effector cells in [54]. Without significantly changing the results in a qualitative manner, it is possible to use another growth function (growth law); Table 6.2 gives an overview over commonly used dynamics for tumor growth [5].

| Growth Law | Differential Equation |
|---|---|
| Power (Mendelsohn) | $\frac{dC}{dt} = aC^b$ |
| Logistic | $\frac{dC}{dt} = aC(1 - bC)$ |
| Gompertz | $\frac{dC}{dt} = aC ln(\frac{1}{bC})$ |
| von Bertalanffy | $\frac{dC}{dt} = aC[(bC)^c - 1]$ |

**Table 6.2:** Overview over commonly used growth functions for tumor growth dynamics in the context of mathematical modeling through Differential Equations. Source: [82].

The tumor burden grows at rate $\lambda_C$ up to a maximum carrying capacity $C_M$ of the tissue as in [60]. In turn, $\eta$ represents the killing rate of cancer cells by relevant T cells. Natural cell death and other means of expunging tumor cells from the system are neglected to realistically emulate the unnatural behavior of cancerous cells [6] [33]. T cells leave the system at rate $d_T$. The accumulation of T cells can be divided in two terms:

- $\lambda_{I_{12}} T_0 \frac{I_{12}}{K_{I_{12}} + I_{12}}$ represents the activation of naive T cells via IL-12 ($I_{12}$),

- $\lambda_{I_2} T \frac{I_2}{K_{I_2} + I_2}$ the proliferation of already activated T cells in the microenvironment, induced by IL-2($I_2$).

Lai and Friedman in [60] opt to include additional, time dependent populations into the system, where we decide to simplify by choosing constant values for $I_{12}, I_2$ instead. We set these to the steady states obtained from the control case in their paper [60]. We lose some effectiveness of the Michaelis-Menten form chosen in equations (6.4), (6.6) to regulate saturated effects of the immune response. In contrast to e.g. Kirschner et al. in [54] our model relies on the inhibition term $F(Q)$ in combination with a constant death

---

[5]Further possibilities for growth functions can be found in [82].

[6]As long as we do not include spatial dynamics or different cancer cell populations the inclusion of additional, natural death terms for cancer cells serves no purpose in our model.

rate $d_T$ to regulate immune response and ultimately impose saturation mechanics. Both the activation and proliferation are therefore inhibited by the presence of PD-1-PD-L1 complexes ($Q$) through the function

$$F(Q) = \frac{1}{1 + Q/K_{TQ}},$$

with $Q$ solely dependent on $D, L$ per our quasi steady state assumption (6.2). From [60] and the assumptions on PD-L1 from our model we can express the concentration $L(t)$ as follows:

$$L = \rho_L(T + \epsilon C).$$

This makes sense as we assume there is no way for PD-L1 to leave the microenvironment other than the death of T cells and cancer cells. There is no anti PD-L1 medication or anything similar present, that could bind to and deplete the PD-L1 available. We can simplify $\frac{1}{1 + Q/K_{TQ}}$ further to reduce the number of parameters involved. Due to (6.2):

$$\frac{1}{1 + Q/K_{TQ}} = \frac{1}{1 + (\frac{\alpha_{DL}}{d_Q}DL)/K_{TQ}} = \frac{1}{1 + (DL)/\hat{K}_{TQ}},$$

with $\hat{K}_{TQ} = \frac{\alpha_{DL}}{d_Q}/K_{TQ}$. Looking back to Chapters 2 and 3, we see that the core dynamic is not necessarily solely one of inhibition as T cells get deactivated through the PD-1-PD-L1 pathway. This dynamic can be modeled in multiple ways, but the decision to go for inhibition is as valid as e.g. the manipulation of the death term instead [60], [69]. The anti-PD-1 immunotherapy medication is depleted through binding to PD-1 at rate $\mu_{DA}$ and leaves the system through decay and other causes at rate $d_A$. The accumulation of PD-1 is a multiple of the accumulation of T cells, as all T cells are assumed to express an equal amount of PD-1 (expression rate $\rho_{PD}$). Similarly to $A$, PD-1 is depleted through binding to anti-PD1 at equal rate $\mu_{DA}$ ([60]) and leaves the system through other causes at rate $d_T$ (with T cells leaving the system).

## 6.2 Fundamental Analysis of the Introduced System of Ordinary Differential Equations

### 6.2.1 Treatment-Free Model

To further our understanding of the core dynamic of the T cell and cancer cell interaction we reduce system (6.3) - (6.6) by setting the population $A$ to be zero constantly (de facto eliminating it from the system and creating a treatment-free model). This results in:

$$\frac{dC}{dt} = \lambda_C C(1 - \frac{C}{C_M}) - \eta CT \tag{6.7}$$

$$\frac{dT}{dt} = (\theta_{I_{12}} + \theta_{I_2}T) \cdot F(Q) - d_T T \tag{6.8}$$

$$\frac{dD}{dt} = \rho_{PD} \cdot (\theta_{I_{12}} + \theta_{I_2}T) \cdot F(Q) - d_T D. \tag{6.9}$$

with $\theta_{I_{12}} = \lambda_{I_{12}} \frac{I_{12}}{K_{I_{12}}+I_{12}} T_0$ and $\theta_{I_2} = \lambda_{I_2} \frac{I_2}{K_{I_2}+I_2}$. Here we can deduce that equation (6.9) is somewhat superfluous, as the main reason for including it, the occupation by anti-PD-1, is no longer present in the system. Furthermore, it does not influence equations (6.7), (6.8). Indeed, with corresponding initial conditions, where $PD_0 = \rho_{PD}T_0$, with $\rho_{PD}$ as before the expression level of PD-1 on T cells, it becomes clear that the right-hand side of (6.9) is now a multiple of the right hand-side of (6.8). We take a look at equation (6.9):

$$\frac{dD}{dt} = \rho_{PD} \cdot (\theta_{I_{12}}T_0 + \theta_{I_2}T) \cdot F(Q) - d_T\rho_{PD}T = \rho_{PD} \cdot \frac{dT}{dt},$$

where we manipulate the death term $d_T D$, which accounts for the loss of PD-1 through death of T cells. Without any other ways of depletion of PD-1 this is a multiple of the death term of T cells in equation (6.8) as per assumption every T cell expresses an equal amount of PD-1. Therefore, we can conclude

$$\frac{\frac{dD}{dt}}{\frac{dT}{dt}} = \rho_{PD}$$

$$\Rightarrow \frac{dD}{dT} = \rho_{PD} \Rightarrow D(t) = \rho_{PD}T(t),$$

if initial conditions satisfy $D_0 = \rho_{PD} \cdot T_0$ (which they should per our model assumptions). A simulation of the reduced system with initial conditions satisfying this requirement led to the same conclusions numerically. The solutions for free PD-1 ($D(t)$) were close to being a multiple of the solutions for T cells ($T(t)$) by a factor of $\rho_{PD}$. The equality holds up to an error of magnitude $-25$. We conclude that it is a reasonable assumption, that the solution for free PD-1 will be equal to the solution for T cells multiplied by $\rho_{PD}$ in the treatment-free case. For the purposes of the treatment-free model we can therefore write

$$D(t) = \rho_{PD}T(t). \tag{6.10}$$

This finally leads to a further reduced system:

$$\frac{dC}{dt} = \lambda_C C(1 - \frac{C}{C_M}) - \eta CT \tag{6.11}$$

$$\frac{dT}{dt} = (\theta_{I_{12}} + \theta_{I_2}T) \cdot F(Q) - d_T T, \tag{6.12}$$

where we can substitute for $D$ with the help of (6.10) when calculating the term $F(Q) = F_1(C, T) = \frac{1}{1 + \frac{\gamma T(T + \epsilon C)}{K_{TQ}}}$ with $\gamma = \frac{\alpha_{DL}}{d_Q} \rho_{PD} \rho_L$. Note, that $F(Q) = F_1(C, T)$ only holds in this treatment-free case.

### Proposition 6.1

*Solutions to an Initial Value Problem for the system (6.11) - (6.12) with positive initial conditions will remain positive and are bounded under the assumption that all parameters are positive.*

**Proof.** First we examine the populations' behavior on the boundaries of a biologically relevant domain $\Omega := \{(C, T) \in \mathbb{R}^2 \mid C \geq 0, T \geq 0\}$. We obtain:

$$\frac{dT}{dt}\Big|_{T=0} = \theta_{I_{12}} \geq 0, \qquad\qquad \frac{dC}{dt}\Big|_{C=0} = 0.$$

Evidently the trajectories on the boundary $\partial\Omega$ stay on the boundary or even point in positive direction. After ensuring that solutions stay non-negative, we will proceed to examine boundedness. For $C$ it holds that

$$\frac{dC}{dt} = \lambda_C C(1 - \frac{C}{C_M}) - \eta CT \leq \lambda_C C(1 - \frac{C}{C_M}),$$

because of non-negativity. This leaves a standard logistic growth expression and is therefore bounded by $max\{C_0, C_M\}$ ([63]). Furthermore, according to [63] it holds that

$$\lim_{t \to \infty} C(t) = C_M,$$

for positive initial condition. For $T$ we look to the right-hand side of (6.12). Clearly

$$(\theta_{I_{12}} + \theta_{I_2}T) \cdot F_1(C, T) - d_T T \leq (\theta_{I_{12}} + \theta_{I_2}T) \cdot F_1(0, T) - d_T T,$$

as $F_1(C, T) = \frac{1}{1 + \frac{\gamma T(T + \epsilon C)}{K_{TQ}}}$ and solutions were shown to be non-negative. Now define

$$G(T) := \frac{\theta_{I_{12}} + \theta_{I_2}T}{1 + \hat{\gamma}T^2} = (\theta_{I_{12}} + \theta_{I_2}T) \cdot F_1(0, T)$$

with $\hat{\gamma} = \frac{\gamma}{K_{TQ}}$. By differentiation we can find the sole maximum of $G(T)$ as

$$\frac{dG(T)}{dT} = \frac{-T^2\hat{\gamma}\theta_{I_2} - 2T\hat{\gamma}\theta_{I_{12}} + \theta_{I_2}}{(1 + \hat{\gamma}T^2)^2},$$

and the numerator of this expression produces two roots. By checking the second derivative and the limits of $G(T)$, one of these roots, $\frac{\sqrt{\hat{\gamma}(\hat{\gamma}\theta_{I_{12}}^2 + \theta_{I_2}^2)}}{\hat{\gamma}\theta_{I_2}} - \frac{\theta_{I_{12}}}{\theta_{I_2}} =: \kappa$, can be identified as producing a global maximum $G(\kappa)$. Therefore, ultimately

$$\frac{dT}{dt} = (\theta_{I_{12}} + \theta_{I_2}T) \cdot F_1(C, T) - d_T T \leq \max_{T \geq 0} G(T) - d_T T = G(\kappa) - d_T T.$$

It holds further by separation of variables:

$$\frac{dT}{dt} \le G(\kappa) - d_T T,$$

$$\Leftrightarrow \quad \frac{1}{G(\kappa) - d_T T} dT \le dt,$$

$$\Leftrightarrow \quad \int \frac{1}{G(\kappa) - d_T T} dT \le \int dt,$$

$$\Leftrightarrow \quad -\frac{1}{d_T} ln(G(\kappa) - d_T T) \le t + C,$$

$$\Leftrightarrow \quad e^{-d_T(t+C)} \le G(\kappa) - d_T T,$$

$$\Leftrightarrow \quad T \le \frac{G(\kappa) - e^{-d_T(t+C)}}{d_T},$$

and finally this implies:

$$\lim_{t \to \infty} T(t) \le \frac{G(\kappa)}{d_T}.$$

Similarly to before it is $T \le max\{T_0, \frac{G(\kappa)}{d_T}\}$ where $T_0$ is the initial condition and therefore $T$ bounded. $\qquad \square$

### 6.2.2 Steady States of the Treatment-Free Model

***Proposition 6.2***
*The system (6.11) - (6.12) has a unique tumor-free equilibrium $X_*^1 = (0, T_*^1)$ and, if $\frac{\eta \epsilon C_M}{\lambda_C} \le 1, \frac{\theta_{I_2}}{d_T} \le 1, \rho(\frac{\lambda_C}{\eta}) > 0$ or $\frac{\eta \epsilon C_M}{\lambda_C} \le 1, \frac{\theta_{I_2}}{d_T} > 1, \rho(\frac{\lambda_C}{\eta}) > 0$, a unique tumorous equilibrium $X_*^2 = (C_*^2, T_*^2)$.*

**Proof.** We begin with the tumor-free equilibrium. Let therefore $C = 0$. Now to find a steady state, set $\frac{dT}{dt}$ to zero and solve for $T$.

$$\Rightarrow G(T) = \frac{\theta_{I_{12}} + \theta_{I_2} T}{1 + \hat{\gamma} T^2} - d_T T = 0.$$

We are looking for roots to the function

$$h(T) = \hat{\gamma} d_T T^3 + (d_T - \theta_{I_2}) T - \theta_{I_{12}}.$$

First, if we set $\theta_{I_{12}}$, the activation of T cells through IL-12, to zero, $h(T)$ simplifies to

$$\hat{h}(T) = \hat{\gamma} d_T T^3 + (d_T - \theta_{I_2}) T = T \left( \hat{\gamma} d_T T^2 + (d_T - \theta_{I_2}) \right).$$

39

For $d_T \geq \theta_{I_2}$, $\hat{h}$ has one root at $T_{11} = 0$. For $d_T < \theta_{I_2}$, two additional roots appear in $T_{22,23} = \pm\sqrt{\frac{\theta_{I_2} - d_T}{\hat{\gamma} d_T}}$ along with $T_{21} = 0$.

Clearly $h(T)$ is monotonously decreasing in $\theta_{I_{12}}$. Shifting the graph down by increasing $\theta_{I_{12}}$ will create only one positive root in the case $d_T \geq \theta_{I_2}$ and eventually eliminate the roots $T_{21} = 0, T_{22} = -\sqrt{\frac{\theta_{I_2} - d_T}{\hat{\gamma} d_T}}$, leaving only one positive real root in the case $d_T < \theta_{I_2}$. Even having $\theta_{I_{12}} > 0$ suffices to leave only one positive, real root in the case $d_T < \theta_{I_2}$. Hence, in either possible case, one unique positive real root exists, proving the existence of a unique tumor-free equilibrium $X_*^1 = (0, T_*^1)$.

For the tumorous equilibrium $X_*^2 = (C_*^2, T_*^2)$ we follow the approach *Kumar et al.* in [57] and employ Descartes rule (Theorem 6.3) to find the unique steady state. Descartes rule was first formulated by René Descartes in [28] and became known in the following form [6]:

### Theorem 6.3
*Let $\rho(x)$ be a polynomial function with real coefficients and the terms arranged in decreasing power of $x$. Then the number of positive zeroes of $\rho$ is equal to the number of variations in sign of $\rho(x)$ or to that number decreased by an even integer.*

Now let $C, T \neq 0$ and set $\frac{dT}{dt} = 0$ and $\frac{dC}{dt} = 0$ from (6.11), (6.12). This implies

$$\eta CT = \lambda_C C \left(1 - \frac{C}{C_M}\right), \tag{6.13}$$

$$\Leftrightarrow \quad C = C_M - \frac{C_M \eta T}{\lambda_C}, \tag{6.14}$$

and

$$d_T T = (\theta_{I_{12}} + \theta_{I_2} T) \cdot F(Q),$$
$$\Leftrightarrow \quad d_T T \left[1 + \hat{\gamma} T (T + \epsilon C)\right] = \theta_{I_{12}} + \theta_{I_2} T. \tag{6.15}$$

Substituting (6.14) into (6.15) finally yields the following

$$\rho(T) = \hat{\gamma} d_T \left(1 - \frac{\eta \epsilon C_M}{\lambda_C}\right) T^3 + \hat{\gamma} \epsilon d_T C_M T^2 + d_T \left(1 - \frac{\theta_{I_2}}{d_T}\right) T - \theta_{I_{12}} = 0 \tag{6.16}$$

Now we can examine the number of variations in sign of $\rho(T)$. Four different configurations are possible as seen in Table 6.3 (and the redundant cases created by multiplication by minus one)[7]:

---

[7]Note, that including the equality, sets the respective coefficient to zero and thus eliminating the corresponding power of $T$ from the polynomial. In our case this does not change the number of sign variations. Notably, zero coefficients are allowed per Theorem 6.3 [28].

| Case | Number of Variations |
|------|---------------------|
| 1.) $\frac{\eta\epsilon C_M}{\lambda_C} \leq 1 \wedge \frac{\theta_{I_2}}{d_T} \leq 1$ | $1\ (+++-)$ |
| 2.) $\frac{\eta\epsilon C_M}{\lambda_C} > 1 \wedge \frac{\theta_{I_2}}{d_T} \leq 1$ | $2\ (-++-)$ |
| 3.) $\frac{\eta\epsilon C_M}{\lambda_C} \leq 1 \wedge \frac{\theta_{I_2}}{d_T} > 1$ | $1\ (++--)$ |
| 4.) $\frac{\eta\epsilon C_M}{\lambda_C} > 1 \wedge \frac{\theta_{I_2}}{d_T} > 1$ | $2\ (-+--)$ |

**Table 6.3:** Overview over possible number of variations of sign in $\rho(T)$ as defined in (6.16).

In cases 2.) and 4.) we have either two real positive roots or none. But in cases 1.) and 3.) we have exactly one real positive root $T_*^2$. Of note aside from the general case: The parameters found in literature and introduced in section 6.3 (see Section 6.3 for an exhaustive justification for parameters) fall under case 1.) and thus produce a unique real positive root.

This leaves only to ensure positivity of $C_*^2$. For this we examine (6.14):

$$C_*^2 > 0$$
$$\Leftrightarrow \quad 1 - \frac{C_*^2}{C_M} < 1$$
$$\Leftrightarrow \quad \frac{\eta T_*^2}{\lambda_C} < 1$$
$$\Leftrightarrow \quad T_*^2 < \frac{\lambda_C}{\eta},$$

where in the second step we used (6.13). We therefore require $0 < T_*^2 < \frac{\lambda_C}{\eta}$. Subsequently we need to ensure that the unique positive real root of $\rho(T)$ indeed lies within the specified boundaries. As we operate in a case where it is the unique positive root, we can apply the Intermediate Value Theorem [55].

***Theorem 6.4 (Intermediate Value Theorem)***
*A continuous function $f : [a, b] \to \mathbb{R}$ takes every value $\delta$ between $f(a)$ and $f(b)$ in at least one point $c \in [a, b]$ with $f(c) = \delta$.*

If $\rho(\frac{\lambda_C}{\eta}) > 0$, since $\rho(0) = -\theta_{I_{12}} < 0$, we must have $T_*^2 \in (0, \frac{\lambda_C}{\eta})$ per Theorem 6.4, where $\rho$ is the polynomial above and satisfies the conditions imposed in Theorem 6.3.
Ultimately this shows that, under the conditions in the second part of Proposition 6.2, we have a biologically meaningful and unique tumorous equilibrium. $\qquad\square$

## 6.2.3 Stability Analysis

Having shown the existence of these steady states, we move on to examine the stability. The Jacobian of the system (6.11) - (6.12) reads as:

$$J(C,T) = \begin{pmatrix} \lambda_C(1 - 2\frac{C}{C_M}) - \eta T & -\eta C \\ (\theta_{I_{12}} + \theta_{I_2}T) \cdot \frac{\partial}{\partial C}F_1(C,T) & \theta_{I_2}F_1(C,T) + (\theta_{I_{12}} + \theta_{I_2}T) \cdot \frac{\partial}{\partial T}F_1(C,T) - d_T \end{pmatrix}$$

Now we evaluate the Jacobian at the tumor-free equilibrium $X^1 = (0, T^1_*)$:

$$J(0, T^1_*) = \begin{pmatrix} \lambda_C - \eta T^1_* & 0 \\ (\theta_{I_{12}} + \theta_{I_2}T^1_*) \cdot \frac{\partial}{\partial C}F_1(0, T^1_*) & \theta_{I_2}F_1(0, T^1_*) + (\theta_{I_{12}} + \theta_{I_2}T^1_*) \cdot \frac{\partial}{\partial T}F_1(0, T^1_*) - d_T \end{pmatrix}$$

As this results in a lower triangular matrix, we can directly deduce the eigenvalues of the matrix:

$$\lambda_1 = \lambda_C - \eta T^1_*$$

$$\lambda_2 = \theta_{I_2}F_1(0, T^1_*) + (\theta_{I_{12}} + \theta_{I_2}T^1_*) \cdot \frac{\partial}{\partial T}F_1(0, T^1_*) - d_T$$

$F_1(C,T)$ is a strictly monotonously decreasing function in both variables $C$ and $T$ on $\mathbb{R}^+_0 \times \mathbb{R}^+_0$, therefore we know $\frac{\partial}{\partial C}F_1(0, T^1_*)$ and $\frac{\partial}{\partial T}F_1(0, T^1_*)$ to be negative. If $\frac{\lambda_C}{\eta} \neq T^1_*$, $\lambda_1$ has a non-zero real part. As long as $d_T \geq \theta_{I_2}$, $\lambda_2 < 0$ and has therefore non-zero real part as well. This last condition is fulfilled in case 1.) as outlined in Table 6.3. These conditions assumed, we can use the Hartman–Grobman theorem to examine stability of $X^1_*$ by utilizing the linearization of the system. We present here a formulation close to the one found in [81] as it is very descriptive and perfectly suited to our intended applications[8]:

***Theorem 6.5 (Theorem of Hartman Grobman)***
*Suppose $x^*$ is a fixed point of the Differential Equation $\dot{x}(t) = f(x)$ with $f \in C^1(\mathbb{R}^n, \mathbb{R}^n)$. The corresponding linearized system is $\dot{z} = Az$, where $A = f'(x^*)$. If $x^*$ is hyperbolic, there is a neighborhood $U$ of $x^*$ and a homeomorphism $H : U \to \mathbb{R}^n$ with $H(x^*) = 0$, which maps the trajectories of $\dot{x}(t) = f(x)$ one-to-one into trajectories of $\dot{z} = Az$, with respect to the time course.*

In our case, this means that all solution curves of our non-linear system (6.11) - (6.12) show the same qualitative behavior around a fixed point as those of the linearized system, given the fixed point is hyperbolic. We may, under these conditions, therefore use the linearized system to examine stability of fixed points. As shown above, the fixed point $X^1_* = (0, T^1_*)$ is hyperbolic as long as $\frac{\lambda_C}{\eta} \neq T^1_*$ and we can apply the classification of phase portraits and critical points for 2D systems of Ordinary Differential Equations as

---

[8]A more general formulation of the theorem (including rigorous proof) can be found in various literature such as [93] or [18].

outlined for example in [8] to the eigenvalues of the linearized system (Note that we have even better information as we know all the eigenvalues, but simply for completion's sake let it be mentioned that the trace is equal the sum of eigenvalues [75] and the determinant is equal to the product of eigenvalues [75] as [8] uses this classification). A comprehensive visualization of said classification can be seen in Figure 6.1.
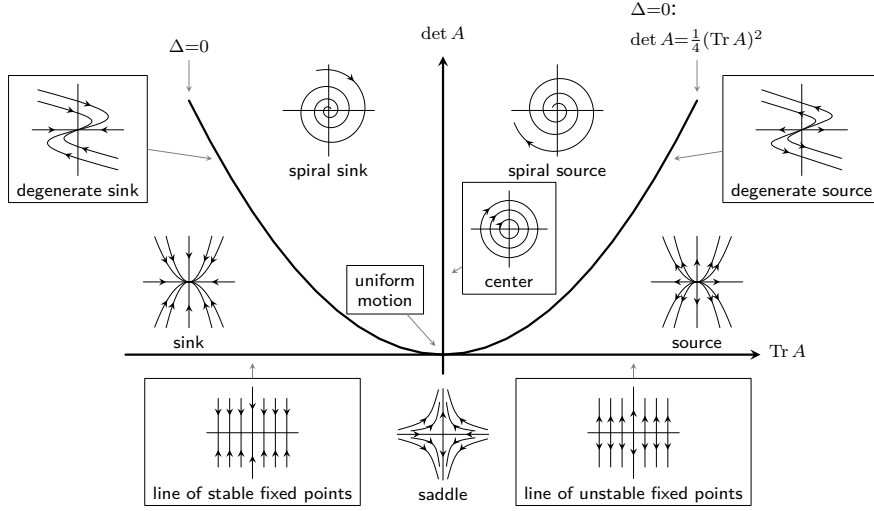


**Figure 6.1:** Classification of Phase Portraits for two-dimensional Ordinary Differential Equation systems in the $(\det A, \operatorname{Tr} A)$-plane. Source: Own Work, Code based largely on [110].

From this, we can see that $X_*^1 = (0, T_*^1)$ is either locally asymptotically stable, if $\frac{\lambda_C}{\eta} < T_*^1$ or a saddle point, if $\frac{\lambda_C}{\eta} > T_*^1$.

We employ a similar approach for the tumorous equilibrium $X_*^2 = (C_*^2, T_*^2)$. Assume therefore the conditions $\frac{\eta \epsilon C_M}{\lambda_C} \leq 1, \frac{\theta_{I_2}}{d_T} \leq 1, \rho(\frac{\lambda_C}{\eta}) > 0$ from Proposition 6.2 hold. Inserting in the Jacobian yields:

$$J(C_*^2, T_*^2) = \begin{pmatrix} \lambda_C(1 - 2\frac{C_*^2}{C_M}) - \eta T_*^2 & -\eta C_*^2 \\ (\theta_{I_{12}} + \theta_{I_2} T_*^2) \cdot \frac{\partial}{\partial C} F_1(C_*^2, T_*^2) & \theta_{I_2} F_1(C_*^2, T_*^2) + (\theta_{I_{12}} + \theta_{I_2} T_*^2) \cdot \frac{\partial}{\partial T} F_1(C_*^2, T_*^2) - d_T \end{pmatrix}.$$

We now move on to examine trace and determinant of the Jacobian evaluated at $X^2 = (C_*^2, T_*^2)$. For the trace this yields:

$$\operatorname{Tr} J(C_*^2, T_*^2) = \lambda_C(1 - 2\frac{C_*^2}{C_M}) - \eta T_*^2 + \theta_{I_2} F_1(C_*^2, T_*^2) + (\theta_{I_{12}} + \theta_{I_2} T_*^2) \cdot \frac{\partial}{\partial T} F_1(C_*^2, T_*^2) - d_T$$

$$= \underbrace{-\lambda_C \frac{C_*^2}{C_M}}_{< 0} + \underbrace{\theta_{I_2} F_1(C_*^2, T_*^2) - d_T}_{< 0} + \underbrace{(\theta_{I_{12}} + \theta_{I_2} T_*^2) \cdot \frac{\partial}{\partial T} F_1(C_*^2, T_*^2)}_{< 0} < 0,$$

because of (6.14) and $\frac{\theta_{I_2}}{d_T} \leq 1$. As for the determinant, we obtain:

$$\det J(C_*^2, T_*^2) = -\lambda_C \frac{C_*^2}{C_M}[\theta_{I_2}F_1(C_*^2, T_*^2) + (\theta_{I_{12}} + \theta_{I_2}T_*^2) \cdot \frac{\partial}{\partial T}F_1(C_*^2, T_*^2) - d_T]$$
$$+ \eta C_*^2[(\theta_{I_{12}} + \theta_{I_2}T_*^2) \cdot \frac{\partial}{\partial C}F_1(C_*^2, T_*^2)].$$

Rearranging to make use of familiar terms and formulations leads to:

$$\det J(C_*^2, T_*^2) = \underbrace{-\lambda_C \frac{C_*^2}{C_M}}_{< 0} \underbrace{(\theta_{I_2}F_1(C_*^2, T_*^2) - d_T)}_{< 0}$$
$$\underbrace{\phantom{-\lambda_C \frac{C_*^2}{C_M}(\theta_{I_2}F_1(C_*^2, T_*^2) - d_T)}}_{> 0}$$
$$+ \underbrace{(\theta_{I_{12}} + \theta_{I_2}T_*^2)C_*^2}_{> 0} \cdot \underbrace{\left[ -\frac{\lambda_C}{C_M}\frac{\partial}{\partial T}F_1(C_*^2, T_*^2) + \eta\frac{\partial}{\partial C}F_1(C_*^2, T_*^2) \right]}_{=:\Delta}.$$

In order for $X_*^2 = (C_*^2, T_*^2)$ to be locally asymptotically stable, we are looking to have $\det J(C_*^2, T_*^2) > 0$. One way to ensure this is having $\Delta \geq 0$ upheld ([8]). We use a reparameterization as proposed in [85] and reintroduce $F(Q)$ in place of $F_1(C, T)$. $\frac{\partial}{\partial T}F_1(C, T) = \frac{dF(Q)}{dQ}\frac{\partial Q}{\partial T}$ and $\frac{\partial}{\partial C}F_1(C, T) = \frac{dF(Q)}{dQ}\frac{\partial Q}{\partial C}$ and recall $Q(C, T) = \gamma T(T + \epsilon C)$. Using this simplifies the expression $\Delta$:

$$\Delta = \frac{dF(Q)}{dQ} \cdot \left[ -\frac{\lambda_C}{C_M}\frac{\partial Q}{\partial T} + \eta\frac{\partial Q}{\partial C} \right],$$

with $\frac{\partial Q}{\partial T} = 2\gamma T_*^2 + \gamma\epsilon C_*^2$ and $\frac{\partial Q}{\partial C} = \gamma\epsilon T_*^2$. By a similar argument as before for the variables $C, T$ and $F_1(C, T)$ it is clear, that $F(Q)$ is a monotonously decreasing function in $Q$ on $\mathbb{R}_0^+$ and therefore $\frac{dF(Q)}{dQ} < 0$ on this domain. Hence, if

$$\frac{\lambda_C}{C_M}(2\gamma T_*^2 + \gamma\epsilon C_*^2) \geq \eta\gamma\epsilon T_*^2$$
$$\Leftrightarrow \frac{\lambda_C}{C_M}(2T_*^2 + \epsilon C_*^2) \geq \eta\epsilon T_*^2,$$

$\Delta \geq 0$ will hold. One of the conditions in Proposition 6.2 requires $\frac{\eta\epsilon C_M}{\lambda_C} \leq 1$. This is an even stricter requirement as

$$\frac{\eta\epsilon C_M}{\lambda_C} \leq 1$$
$$\Rightarrow \frac{\lambda_C}{C_M} \geq \eta\epsilon$$
$$\Rightarrow \frac{\lambda_C}{C_M}(2T_*^2 + \epsilon C_*^2) \geq \eta\epsilon T_*^2,$$

and positivity is ensured through the parameters and $C_*^2, T_*^2$ in some critical spots. Ultimately, under the conditions proposed in the second part of Proposition 6.2, $\det J(C_*^2, T_*^2) > 0$ was shown to hold. We can deduce that in this case $X_*^2 = (C_*^2, T_*^2)$ is locally asymptotically stable and we can move on to examine global stability. For this we will utilize the *Theorem of Poincaré-Bendixson* in conjunction with *Dulac's Criterion.*

**Theorem 6.6 (Poincaré-Bendixson)**
*Let D be an open subset of the plane and a differentiable real dynamical system on D be given. Fix $(x, y) \in D$ and suppose $\omega(x, y) \neq \emptyset$, the limit set of $(x, y)$, is compact, connected and contains only finitely many fixed points. Then one of the following holds:*

- *$\omega(x, y)$ is a fixed point*

- *$\omega(x, y)$ is a regular periodic orbit*

- *$\omega(x, y)$ consists of (finitely many) fixed points and a set of orbits connecting them.*

A more general version, related Lemmata and extensive proofs can be found in [20],[106].

**Theorem 6.7 (Dulac's Criterion)**
*Suppose D is a simply connected region of the plane and suppose there exists a continuously differentiable function B(x,y) where*

$$\frac{\partial}{\partial x}\left[B(x, y) \cdot f(x, y)\right] + \frac{\partial}{\partial y}\left[B(x, y) \cdot g(x, y)\right]$$

*is of constant sign, then the dynamical system*

$$\frac{dx}{dt} = f(x, y)$$
$$\frac{dy}{dt} = g(x, y)$$

*has no closed orbits wholly contained in D. In particular, the system has no periodic solutions lying fully in D.*

A proof and further explanation can be found in [32]. For our system (6.11) - (6.12) we formulate:

**Proposition 6.8**
*Assume Case 1.) of Table 6.3 (our relevant case, see Section 6.3 for system parameters). If additionally $\rho(\frac{\lambda_C}{\eta}) > 0$ and $X_*^1 = (0, T_*^1)$ a saddle point, $X_*^2 = (C_*^2, T_*^2)$ is globally asymptotically stable.*

**Proof.** We first examine the existence of closed orbits (periodic or otherwise) in the system. This leads us to formulate

### Lemma 6.9

*The system (6.11) - (6.12) has no closed orbits on $D := \{(C, T) \in \mathbb{R}^2 \mid C > 0, T > 0\}$ and thus, no positive periodic solutions, that are nontrivial, provided $\frac{\theta_{I_2}}{d_T} \leq 1$.*

**Proof.** We employ Theorem 6.7. For this we set $B(C, T) = \frac{1}{C}$. We then evaluate

$$
\frac{\partial}{\partial C}\left(\frac{1}{C} \cdot \left[\lambda_C C(1 - \frac{C}{C_M}) - \eta CT\right]\right) + \frac{\partial}{\partial T}\left(\frac{1}{C} \cdot \left[(\theta_{I_{12}} + \theta_{I_2}T) \cdot F_1(C, T) - d_T T\right]\right)
$$

$$
= \frac{\partial}{\partial C}\left[\lambda_C - \frac{\lambda_C C}{C_M} - \eta T\right] + \frac{1}{C} \cdot \frac{\partial}{\partial T}\left[(\theta_{I_{12}} + \theta_{I_2}T) \cdot F_1(C, T) - d_T T\right]
$$

$$
= -\frac{\lambda_C}{C_M} + \frac{1}{C} \cdot \left[\theta_{I_2}F_1(C, T) + (\theta_{I_{12}} + \theta_{I_2}T) \cdot \frac{\partial F_1(C, T)}{\partial T} - d_T\right] < 0,
$$

on $D := \{(C, T) \in \mathbb{R}^2 \mid C > 0, T > 0\}$. Thus, we can apply Dulac's criterion and conclude Lemma 6.9. □

Now, going back to the *Theorem of Poincaré-Bendixson* (6.6), Proposition 6.8 directly follows. In our case we previously stated that solutions remain non-negative and are bounded in Proposition 6.1. Under the conditions in Proposition 6.8 the system allows for a unique positive equilibrium, $X_*^2 = (C_*^2, T_*^2)$, which is locally asymptotically stable. The tumor-free equilibrium is a saddle point. Because of Lemma 6.9, we can use Theorem 6.6 to directly show, that all positive solutions will tend to a fixed point. This directly implies, that $X_*^2 = (C_*^2, T_*^2)$ attracts all positive solutions and therefore we have shown global stability under the conditions of Proposition 6.8. □

As a side note, using the same methodology, we can conclude global stability for the tumor-free equilibrium, when $X_*^1 = (0, T_*^1)$ is locally asymptotically stable (and not a saddle point) and the system does not allow for a tumorous equilibrium.

## 6.3 Numerical Simulation and Parameter Fitting

After obtaining a first understanding of the core interactions between tumor cells and T lymphocytes, we reintroduce anti-PD-1 medication into the system and move back to system (6.3) - (6.6). We are interested in finding the rate of activation for T cells. This could also give us some indication if activated T cells are able to enter the tumor microenvironment. For this, respecting the difference in treatment between patients, we will perform parameter fitting for $\lambda_{I_{12}}$ using the data set of one patient. We use P1, as P1 presents with a significantly higher number of metastases than other patients (see Chapter 5 and Figure 5.1), hopefully mitigating the problem of heterogeneity in tumors somewhat. As outlined in Chapter 5 P1 also presents several other advantages over the remaining data.

We will perform the fitting using the complete tumor burden as reference values and then qualitatively compare the results with single metastases and other patients. The location of the observed metastases is also an interesting one, as the blood-brain barrier filters the blood flow to and from the brain [23] and, to some degree, protects the brain (relative to other locations) from cancerous cells [114]. We thus have a more isolated environment when examining tumor burden as a whole; this can only be beneficial to our results. In addition to the parameters (exhaustive list in Table 6.4, explanations below) we will need a value for the concentration of anti-PD-1 after admission. We assume that anti-PD-1 is instantly homogeneously distributed in the blood volume, which is reasonable especially for the brain, as the cerebral blood flow is quite high [19]. We calculate the amount of blood present at a given point in time (i.e. the cerebral blood volume). From [51] we know that the blood volume per $cm^3$ brain tissue is about $3.1 \times 10^{-2}$ ml and through measurements in *Slicer 3D* we can calculate the volume of the brain of P1 to be $1410\,cm^3$. Together this equates to a blood volume of $43.7\,$ml in the brain at one given point in time. An average male of the appropriate age group has a total blood volume of about $4.7\,$l in the body [25]. Through the body weight and thus total dose of anti-PD-1 ($225\,$mg from our data), we can now calculate the concentration of anti-PD-1 present in the brain after administration (given our assumptions) as about $1.5 \times 10^{-6}\,\mathrm{g/cm^3}$.

There are additional effects in place, such as the high cerebral blood flow, making overall more anti-PD-1 available in the brain. We try to emulate this, by multiplying the identified concentration with a factor of 10. The specific value the anti-PD-1 concentration increases after each treatment cycle (within a reasonable range) does not qualitatively change the behavior of the system (not shown here), so the exact amount administered to the brain is secondary. For our purposes we will use $1.5 \times 10^{-5}\,\mathrm{g/cm^3}$ as reasoned above and increase the concentration of anti-PD-1 by this amount at the time points corresponding to anti-PD-1 treatment cycles in our simulation.

### 6.3.1 Parameter Values Used in Simulations

As our model populations are set to be in $g/cm^3$, we need to convert the tumor sizes from Chapter 5 from volume to corresponding concentrations. For this we use the relation between volume and mass obtained in the control case of [9]. Therefore, one $cm^3$ of tumor volume will have about $1.25g$ in mass and we use the obtained mass in conjunction with the measured brain volume (see above) to obtain concentrations in $g/cm^3$. Our model (6.3) - (6.6) has a carrying capacity of tumor cells in the surrounding tissue embedded through the logistic growth function. However, this is more a local condition and indicates the maximum concentration of cancer cells, for which supply of oxygen and nutrients can still be provided. As we are examining the overall tumor burden on the brain it would be unrealistic to assume that 100% of the brain volume can be occupied by cancerous cells with a homogeneous concentration of $C_M$ (or lower, because of T cell activity - the

tumorous equilibrium) everywhere.

In addition to this local condition we therefore introduce a global restriction to limit the growth of tumor burden. By this we aim to respect restrictions on growth due to the segmentation and form of the brain as well as due to a possible lethal burden. An example for such restrictions from our data was shown before in Figure 5.3 and now, in Figure 6.2, a more extreme case is shown from P3. While the lungs in Figure 6.2 are not at maximum carrying capacity for tumor cells at every single spot, the two tumors shown are severely restricted in their growth due to spatial and structural properties.
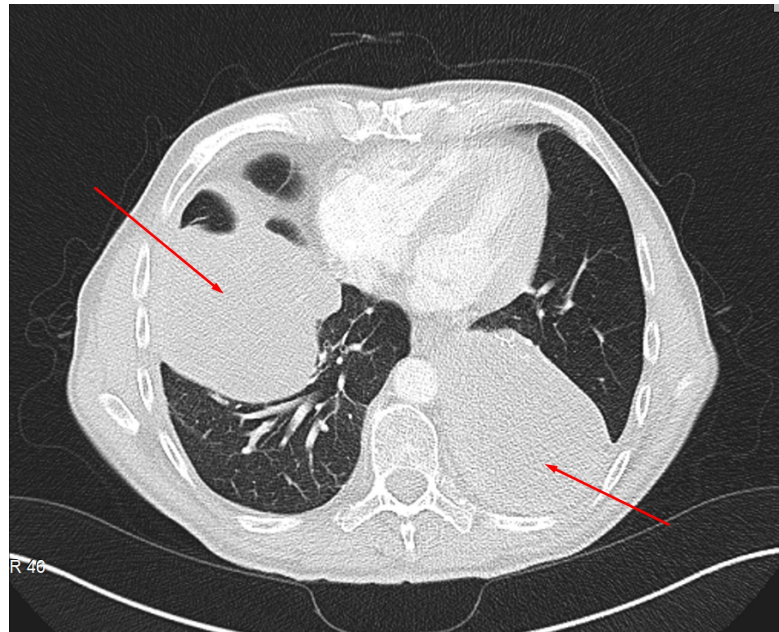


**Figure 6.2:** Two endobronchial metastases Lung1, Lung3 (indicated by red arrows) at peak size from P3. Source: Own work in conjunction with data provided by *E. Dippel.*

We assume in this model that a maximum of 10% of the brain volume can be occupied by cancerous cells (i.e. is available space for metastases) and we adjust our concentrations accordingly. Otherwise, as was observed in simulations (not shown here), the model produces unrealistically high concentrations of tumor cells throughout the brain compared to our data. Now, we can introduce values for our model parameters: the values used can be found in Table 6.4; explanations are given below.

| Parameter | Meaning | Value | Sources (if appl.) |
|---|---|---|---|
| $\lambda_C$ | Proliferation rate of cancer cells | $0.9 \, \text{day}^{-1}$ | Estimate |
| $C_M$ | Carrying capacity of cancer cells | $0.4766 \, \text{g/cm}^3$ | [97] |
| $\eta$ | Killing rate of cancer cells by T cells | $23 \, \text{day}^{-1} \cdot \text{cm}^3/\text{g}$ | [60] |
| $\lambda_{I_{12}}$ | Rate of activation of naive T cells | To determine | |
| $\lambda_{I_2}$ | Rate of proliferation of activated T cells | $0.25 \, \text{day}^{-1}$ | [40] |
| $I_{12}$ | Concentration of IL-12 | $1.5 \times 10^{-10} \, \text{g/cm}^3$ | [60] |
| $I_2$ | Concentration of IL-2 | $2.37 \times 10^{-11} \, \text{g/cm}^3$ | [60] |
| $T_0$ | Concentration of available naive T cells | $2 \times 10^{-3} \, \text{g/cm}^3$ | [40] |
| $K_{I_{12}}$ | Half saturation of IL-12 | $1.5 \times 10^{-10} \, \text{g/cm}^3$ | [60] |
| $K_{I_2}$ | Half saturation of IL-2 | $2.37 \times 10^{-11} \, \text{g/cm}^3$ | [60] |
| $\hat{K}_{TQ}$ | Inhibition of T cells through PD-1-PD-L1 | $1.365 \times 10^{-18} \, \text{g/cm}^3$ | [60] |
| $\rho_L$ | Expression of PD-L1 on T cells | $5.22 \times 10^{-7}$ | Estimate |
| $\epsilon$ | Expression of PD-L1 on tumor cells relative to $\rho_L$ | $0.01$ | [60] |
| $d_T$ | Death rate of T cells | $0.191 \, \text{day}^{-1}$ | [40] |
| $\mu_{PA}$ | Rate of depletion of PD-1 by anti-PD-1 | $2.1 \times 10^5 \, \text{cm}^3/(\text{g} \cdot \text{day})$ | Estimate |
| $d_A$ | Decay of anti-PD-1 | $2.7 \times 10^{-2} \, \text{day}^{-1}$ | [60] |
| $\rho_{PD}$ | Expression of PD-1 on T cells | $2.49 \times 10^{-7}$ | Estimate |

**Table 6.4:** Parameters used for the simulation of the system of Ordinary Differential Equations (6.3) - (6.6) unless otherwise noted. This set of parameters is utilized for the main parameter fitting process. Sources: Own work and as outlined in Table.

**Additional Explanation for Parameters**

*Proliferation rate $\lambda_C$*

Estimates for doubling times in melanoma vary greatly in literature [16]. *Lai et al.* in [60] propose a reasonable range of doubling time in 5 - 15 days and using their method to deduce a growth rate for logistic growth, we can calculate a value for $\lambda_C$. As the metastasis is extremely aggressive in our data set for P1, we opt for the more aggressive side of the spectrum (5 days) and therefore obtain $\lambda_C = 0.9\,\mathrm{day}^{-1}$.

*Carrying capacity $C_M$*

In [97] a fitting of the logistic growth dynamic is conducted for the capacity, that tissue can support (locally). We use their value obtained for $C_M$.

*Killing rate of cancer $\eta$*

Killing rates for $CD4^+$ as well as $CD8^+$ T cells are given in [60]. The ratio of $CD4^+$ to $CD8^+$ T cells varies due to several factors, but we assume a healthy state and thus can reasonably assume a $CD4^+$ to $CD8^+$ ratio of 2:1 (see [101], [60]). We average $46\,\mathrm{day}^{-1} \cdot \mathrm{cm}^3/\mathrm{g}$ for $CD8^+$ and $11.5\,\mathrm{day}^{-1} \cdot \mathrm{cm}^3/\mathrm{g}$ for $CD4^+$ accordingly and obtain $\eta = 23\,\mathrm{day}^{-1} \cdot \mathrm{cm}^3/\mathrm{g}$.

*Rate of activation of naive T cells $\lambda_{I_2}$*

The proliferation rates of both $CD4^+$ and $CD8^+$ T cells is the same and given in [40] in a set-up up similar to ours; therefore, we use the same value and set $\lambda_{I_2} = 0.25\,\mathrm{day}^{-1}$.

*Concentration of available naive T cells $T_0$*

The densities of naive T cells are given in [40] as $1.2 \times 10^{-3}\,\mathrm{g}/\mathrm{cm}^3$ for $CD4^+$ T cells and $8 \times 10^{-4}\,\mathrm{g}/\mathrm{cm}^3$ for $CD8^+$ T cells. As we assume an equal rate of activation for all T cells in our model, we combine these densities to $T_0 = 2 \times 10^{-3}\,\mathrm{g}/\mathrm{cm}^3$

*Expression of PD-L1 on T cells $\rho_L$, Expression of PD-1 on T cells $\rho_{PD}$, Expression of PD-L1 on tumor cells (relative to $\rho_L$) $\epsilon$*

All the relevant constants for calculation of $\rho_L$, $\rho_{PD}$ can be found in [60]. There are, on average, 3000 PD-1 proteins on a T cell. The mass for such a protein is known to be approximately $mass_{PD} = 8.3 \times 10^{-20}$ g and the mass of a T cell is approximately $mass_T = 10^{-9}$ g [60]. Therefore, we can calculate:

$$\rho_{PD} = 3000 \cdot \frac{mass_{PD}}{mass_T} = 2.49 \times 10^{-7}.$$

Similarly, we know 9000 PD-L1 proteins are generally found on a T cell and the weight of this protein is known to be approximately $mass_L = 5.8 \times 10^{-20}$ g and therefore:

$$\rho_L = 9000 \cdot \frac{mass_L}{mass_T} = 5.22 \times 10^{-7}.$$

Finally, for $\epsilon$, it becomes a little trickier, as this can vary from tumor to tumor and certainly from patient to patient. This is reflected in [60] and [85], who deal with exactly this expression rate factor and offer ranges $0 - 0.01$ and $1 - 100$ respectively. As we have seen previously in Section 3.2, expression of PD-L1 on tumor cells in the case of melanoma is controversial as an indicator for response to anti-PD-1 treatment and several publications state, that response and even remission can often be seen in patients with little to no expression displayed. We therefore choose a small value for $\epsilon$ in hope that our model captures this dynamic[9]. We opt for $\epsilon = 0.01$.

*Death rate of T cells $d_T$*

The rates of decay for $CD4^+$ ($0.197\,\text{day}^{-1}$) as well $CD8^+$ T cells ($0.18\,\text{day}^{-1}$) are given in [40]. We once again assume our "healthy" ratio of 2:1 for $CD4^+$ to $CD8^+$ and average accordingly to obtain $d_T = 0.191\,\text{day}^{-1}$.

*Decay of anti-PD-1 $d_A$*

The half-life of Pembrolizumab is given by the FDA [36] as 26 days and confirmed to be so in [37]. Therefore, we can calculate the rate of decay directly as $d_A = \frac{ln2}{26\,\text{day}^{-1}} = 2.7 \times 10^{-2}\,\text{day}^{-1}$.

---

[9]It should be noted here that indeed it does and even if the tumor expresses no PD-L1 at all ($\epsilon = 0$), the effects of treatment can be observed. This goes for all our modeling approaches in Chapters 6 and 7 and will not be repeated each time.

*Rate of depletion of PD-1 by anti-PD-1 $\mu_{PA}$*

For the calculation of $\mu_{PA}$ we try to estimate what percentage of the administered anti-PD-1 actually binds to receptors and how much decays naturally. As seen in Chapter 5 our prescribed dose is $(2\,\mathrm{mg/kg})$, which is also the recommended dose at current standards of treatment ([88]). *Patnaik et al.* in [91] relate dose administered to Pembrolizumab serum concentration observed and ultimately to PD-1 receptor modulation as an indicator for treatment effect. They observe, that exceeding the recommended dose has no additional benefits and indeed even going as low as $0.05\,\mathrm{mg/kg} - 0.06\,\mathrm{mg/kg}$ still leads to comparable PD-1 receptor modulation (albeit there is a benefit to upping the dose to recommended levels). Going beyond this threshold effects PD-1 receptor modulation negatively in a more significant manner. Thus, we can reasonably assume, that $0.06\,\mathrm{mg/kg}$ still leads to high saturation of PD-1 receptors on T cells and therefore only a small percentage of our dose is actually bound to PD-1 receptors. This is supported by *Ogungbenro et al.* in [88], who observe fairly similar receptor occupancy levels for doses of $10\,\mathrm{mg/kg}$ and $0.3\,\mathrm{mg/kg}$ (87% vs 77%) and *Fessas et. al* [37], who make similar observations regarding receptor occupancy.

Assuming that administering $0.06\,\mathrm{mg/kg}$ leads to almost full utilization (as this seems to be the threshold for effectiveness), we estimate that about $\frac{0.06\,\mathrm{mg/kg}}{2\,\mathrm{mg/kg}} = 3\%$ of our dose will bind to receptors whereas the rest decays. Now assuming steady state for equation (6.5), we can calculate $\mu_{PA}$. For this we assume a constant source of anti-PD1 to get a nontrivial steady state solution for $A$. This is no problem, as it doesn't affect the parameter, but we need a constant value for $D$ to execute the calculations. As a value for $D$, we examine the control (disease-free) case and obtain a range of $0.9 \times 10^{-9}\,\mathrm{g/cm^3} - 7 \times 10^{-9}\,\mathrm{g/cm^3}$ for parameters $\lambda_{I_{12}}$ between 1 and 100. For simulation we choose $4 \times 10^{-9}\,\mathrm{g/cm^3}$. As we have an estimate for how much anti-PD-1 simply decays, we can conclude $\frac{\mu_{PA}DA}{0.03} = \frac{d_A A}{0.97}$ at steady state. Therefore, finally

$$\mu_{PA} = \frac{0.03 \cdot d_A}{0.97 \cdot D} = \frac{0.03 \cdot 2.7 \times 10^{-2}\,\mathrm{day}^{-1}}{0.97 \cdot 4 \times 10^{-9}\,\mathrm{g/cm^3}} = 2.1 \times 10^5\,\mathrm{cm^3/(g \cdot day)}$$

$I_{12}$, $I_2$, $\hat{K}_{TQ}$, $K_{I_{12}}$, $K_{I_2}$ are all extracted from [60], where $I_{12}$, $I_2$ are constants as explained above.

To showcase the general parameter fit we conduct mock-up simulations with varying parameters for the unknown rate of activation $\lambda_{I_{12}}$. The results of these simulations are

visualized in Figure 6.3 along with the control case[10]. Through these simulations we can prove that the modeling approach with our parameter set in Table 6.4 can produce distinct behaviors, importantly it can produce stable disease behavior and response up to remission.
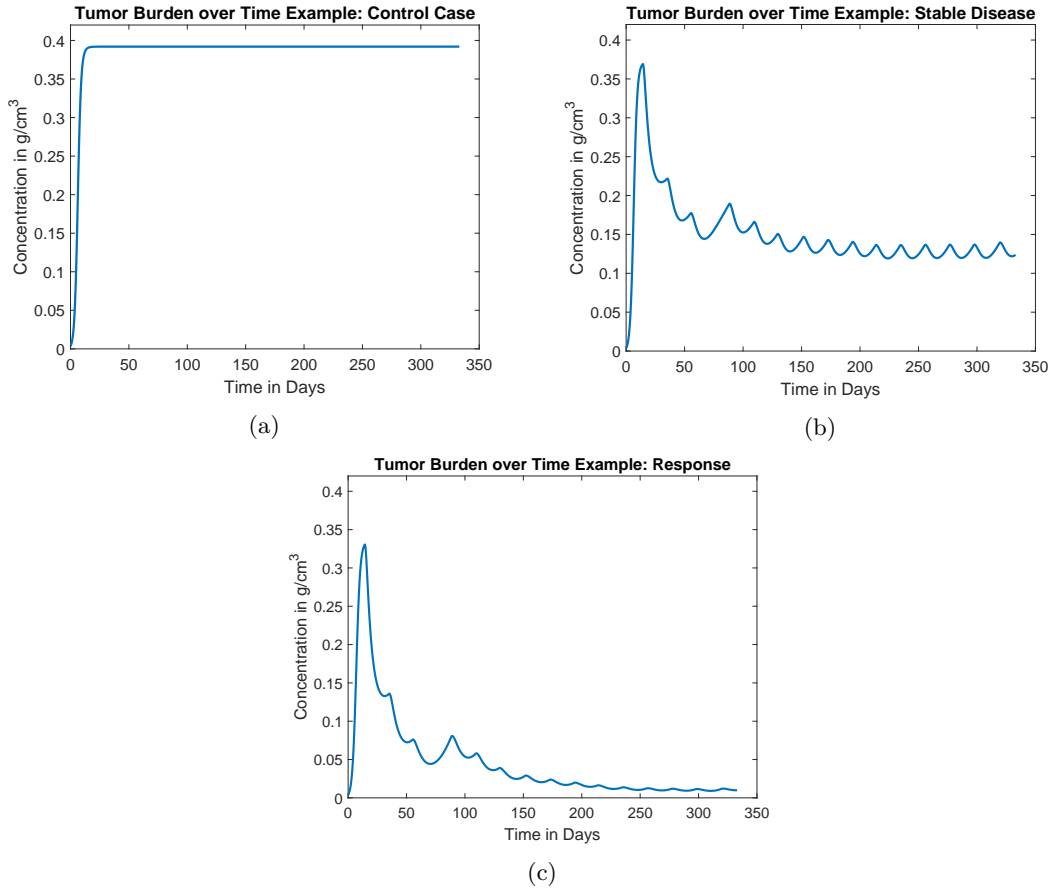


(a)



(b)



(c)

**Figure 6.3:** Exemplary simulations that display the control case (treatment-free) in (a), initial response with stable disease in (b) and response up to remission in (c) for varying parameter values for $\lambda_{I_{12}}$. Each figure tracks the concentration of cancer cells (under treatment regime and initial conditions at $t = 0$ of P1) and therefore tumor burden. Source: Own work in conjunction with data provided by *E. Dippel.*

---

[10]Note that we used the data of P1 as an orientation and set up the treatments to emulate the treatment regime of P1. As explained in the motivation of $\lambda_C$, cancer of P1 displays extremely progressive behavior thus explaining the fast growth to capacity in the control case.

### 6.3.2 Results of Parameter Fitting Simulation

We proceed to conduct a parameter fitting for $\lambda_{I_{12}}$ to our model (6.3) - (6.6) using the parameters outlined in Table 6.4. We use the exact immunotherapy treatment regime undergone by P1 as can be found in Table 5.3. The timeline is also as outlined in Chapter 5 and initial values for cancer cell concentration stem from the measurements at $t = 0$. Initial values for T cell ($T_0$) and PD-1 ($D_0$) concentration were taken from the steady state of the control case (treatment-free) and are taken to be approximately $T_0 = 6 \times 10^{-4}\,\mathrm{g/cm^3}$ and $D_0 = \rho_{PD} \cdot T_0$. Results can be seen in Figure 6.4; this gives the parameter value $\lambda_{I_{12}} = 17.6\,\mathrm{day^{-1}}$.
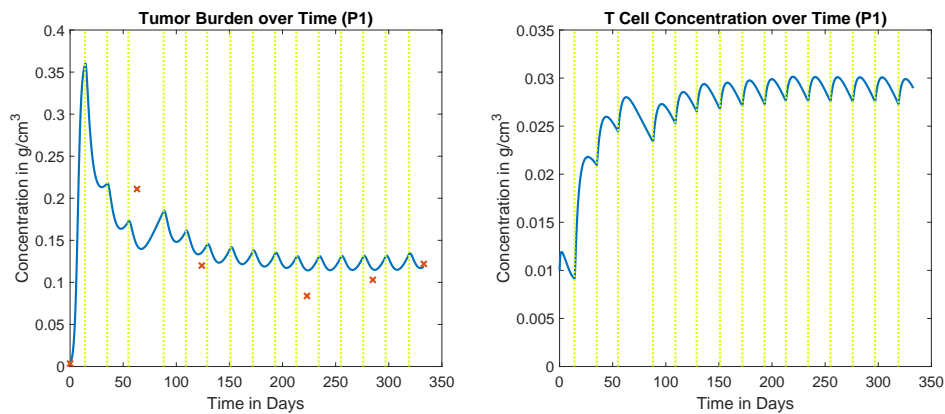


**Figure 6.4:** Behavior of simulated tumor burden of P1 (left), compared to actual measurements taken, and T cell concentration (right) over time. Treatment times are indicated through vertical lines. Source: Own work in conjunction with data provided by *E. Dippel.*

Looking back at Table 5.2, we can compare the behavior of single metastases. The volume over time for M1 - M5 is visualized in Figure 6.5. We can see that initial response agrees with the overall model from Figure 6.4, but at the last imaging date $t = 333$ we see fairly aggressive progression in size of M1 - M4, whereas our model predicts stable disease. As overall tumor burden increases only slightly it agrees with the observations, that smaller metastases do indeed not progress, but the treatment has still beneficial effects on them. This further emphasizes the need to consider the behavior of metastases more closely and focus on the exact dynamics in the tumor microenvironment. We will attempt to do so in Chapter 7. Nonetheless, our model of Ordinary Differential Equations (6.3) - (6.6) seems to capture the underlying response dynamics quite well.

In the treatment-free model with equal parameters we see the tumor rise almost to capacity (controlled only marginally by the immune system) and stagnate at this level, which is congruent with our analysis from Section 6.2. We can see the treatment having
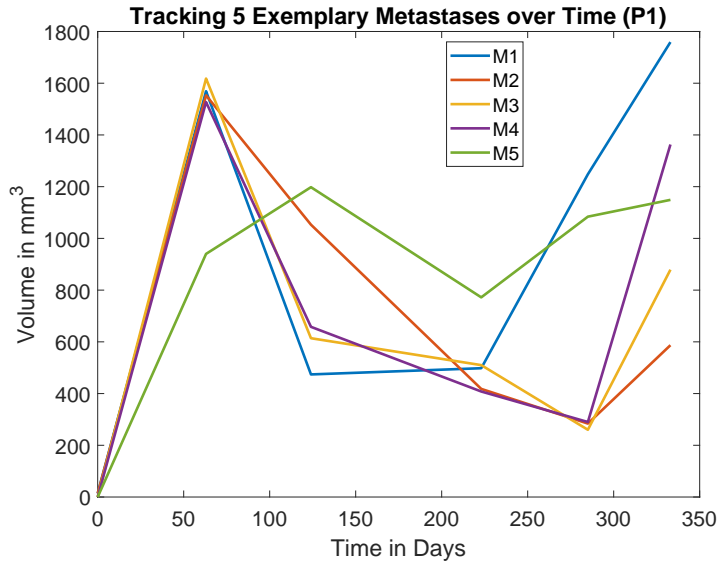
**Figure 6.5:** Volume of M1 - M5 from P1 as measured directly from data over the observed time. Source: Data provided by *E. Dippel.*

immense effect in comparison even when the tumor cells express little to no PD-L1. As we intentionally chose low PD-L1 expression on tumors in an attempt to understand the treatment effect under such conditions, we may offer some thoughts on the question of why patients respond to anti-PD-1 treatment with practically no expression of PD-L1 on tumor cells, which is still subject to discussion (as outlined in Section 3.2). We can, from our model and results, explain the effect as a sort of boost for the immune system, inhibiting its self-regulation through PD-1-PD-L1 complexes. If the tumor expresses PD-L1, this of course improves response even further (under the condition of all other factors remaining unchanged).

While the dynamics clearly reflect the data points, the parameter fit did not manage to match the curve perfectly. It appears, that the initial response is overestimated by the model, whereas, when stable disease sets in, the tumor burden is overestimated. One factor, we have so far not considered, is the radiation therapy conducted on the entire brain at $t = 68$. As discussed in Chapter 3, adjuvant therapy can play a crucial role in immunotherapy (see [111] for a comprehensive overview) and while not fully understood, there is evidence, that combined treatment offers improved response [111]. We try to include the radiotherapy and a synergy effect into our system to examine the resulting dynamics. While $\lambda_{I_{12}}$ is motivated as the activation rate of naive T cells, functionally it controls how many activated T cells enter the tumor environment. As seen in Chapter 2, penetration of the tumor by T cells (and ultimately the amount of T cells present)

is a strong indicator for response. Indeed, also from Chapters 2 and 3, we note that immunotherapy can be less effective, because of non-sufficient penetration of T cells. We therefore assume, we can reasonably introduce the effect of combination therapy through modification of parameter $\lambda_{I_{12}}$ [11].

An example of this modified response can be seen in Figure 6.6 and it is evident that the fit is improved. For this simulation we used the same set-up as before, but introduced a parameter $\lambda_{I_{12}pre} = 10\,\mathrm{day}^{-1}$ for the T cell activation pre-radiation therapy, allowing less T cells in the tumor environment and a parameter $\lambda_{I_{12}post} = 21\,\mathrm{day}^{-1}$ for the T cell activation post-radiation therapy, allowing for an improved immune response.
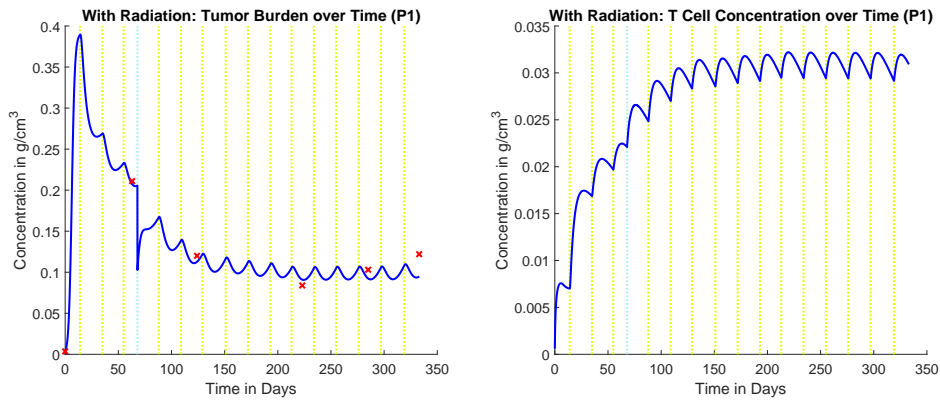


**Figure 6.6:** Behavior of simulated tumor burden of P1 (left) compared to actual measurements taken and T cell concentration (right) over time. Simulations include additional effects for radiation. Treatment times are indicated through vertical dotted lines, where green is anti-PD-1 treatment and light blue is radiation therapy. Source: Own work in conjunction with data provided by *E. Dippel.*

It should be noted, that the primary effect of radiation therapy was included in the model as an eradication of a percentage of tumor cells in the area receiving radiation treatment. The precise effect of radiation therapy on the types of cells involved is complex (as can be seen in [10]); in our case the exact percentage of tumor cells eradicated had no significant effect on the qualitative outcome (largely due to the aggressive nature of the cancer). For the simulation we used a percentage of 50%. After obtaining these improved results, we move onto the micro level and look at separate metastases: Looking back at Figure 6.5 and the progression of our "older, bigger" metastases M1-M4 towards the end of the observed period; this could be either interpreted as the wearing off of the effect of the radiation on immune response or a general development of resistance toward the

---

[11]Through the modeling approach we assume that everything is well mixed, but in reality, of course, the T cells move to the tumor sites

immunotherapy through new mutations. Resistance is developed in a significant number of patients that show initial response as outlined in [52] and [70]. This may be further indication that a resistance mechanism could be included in an Ordinary Differential Equation model to improve model accuracy.

Moving on to other patient data, we first take a look at P3, as P3 also presents with multiple metastases in the same tissue. Here, we have a total of five metastases in lung tissue, which is however significantly lower than the number of brain metastases observed in P1. We start in a similar manner to our process with P1 data and compare the simulation behavior to the overall tumor burden in lung tissue. For this we need to adjust several parameters. Firstly, in terms of increase of anti-PD-1 concentration: From [67], we obtain a range for pulmonary blood volume from about 390 ml to 481 ml in their control group with one outlier at 666 ml. We therefore assume an average pulmonary blood volume of 450 ml, which once again allows us to calculate the amount of anti-PD-1 medication dispensed to the pulmonary environment from total dose and the average blood volume of 4.7 l in the body [25]. The total volume of both male lungs was derived in [56] to be about 5858 cm$^3$. As above we calculate the increase of anti-PD-1 concentrations, which in this case is $2.5 \times 10^{-6}$ g/cm$^3$.

Similarly, we need to convert our measurements into concentrations and will again proceed as for P1 brain metastases. From Figure 6.2 we can reasonably assume, that the lung can support a higher tumor burden than we assumed for the brain (10%). There is certainly a limit as outlined in the patient history of P3, as eventually re-sections became necessary to retain organ functionality. We assume that 50% of the lung volume can be occupied by tumor mass and adjust our concentrations accordingly. As this might appear arbitrary at this point, we want to again emphasize the nature of these restrictions. They should always be thought of in the context of a spatially homogenous Ordinary Differential Equation model. The local (parameter $C_M$ in our model) and this global restriction do not impact the behavior of the system qualitatively (only in specific cases, see Section 6.2); it can essentially be thought of as a rescaling.

Further, we adjust the proliferation rate $\lambda_C$ of cancerous cells. In the case of P1 we observed an extremely aggressive progress of the cancer and thus opted for a rather aggressive growth behavior. Here we choose a value close to the one used by *Lai et al.* in [60] in $\lambda_C = 0.6$ day$^{-1}$. Lastly, we want to remind of the special standing the data-set P1 had, as we could reasonably exclude all effects from previous treatments. With P3, the treatment with *Ipilimumab* and additional chemotherapy, makes this much trickier. This might still have an impact on system parameters, such as $\lambda_C$ among other. We further don't allow the tumor a treatment-free period before initiation of *Pembrolizumab* therapy, as this showed unnaturally high growth in the first days of simulation. Compared to the timeline for P3 in Appendices C and D. we start simulations at $t = 6$, the first cycle of

treatment, and assume the measurements from $t = 0$ at that date.

A rough fitting leads to the results seen in Figure 6.7 and leads to a value $\lambda_{I_{12}} \approx 17\,\mathrm{day}^{-1}$, similar to the case of P1. It becomes evident, that the model is not suited
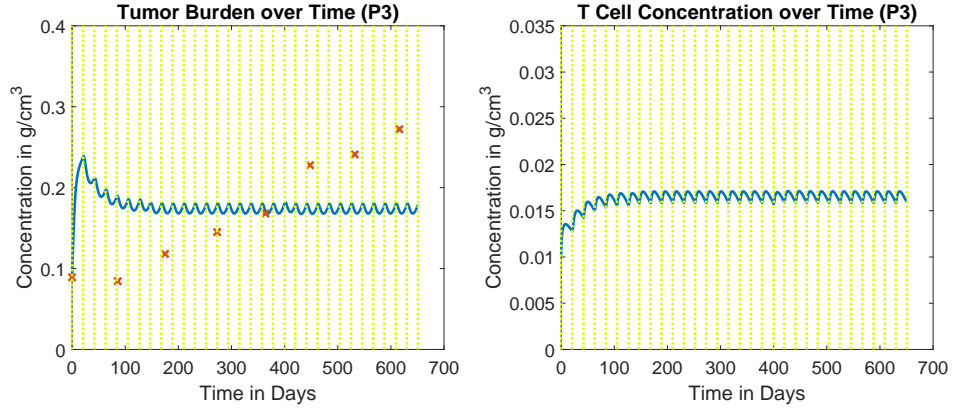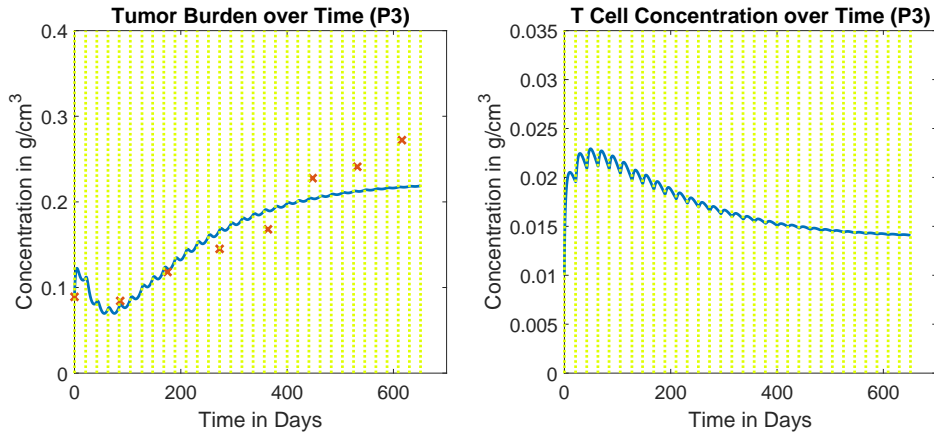


**Figure 6.7:** Behavior of simulated pulmonary tumor burden of P3 (left), compared to actual measurements taken, and T cell concentration (right) over time. Treatment times are indicated through vertical lines as before. Source: Own work in conjunction with data provided by *E. Dippel.*

to emulate the dynamic of slowed progress. Where response and stable disease can be described quite well through our model, stable disease into slow progression is not possible. This again emphasizes the need to include a resistance mechanism or something similar, when moving forward with his Ordinary Differential Equation approach. We do not want to dive too deeply into this topic, as the medicinal background is complex and the evolution of resistance in a cancer to specific treatment not fully understood. Qualitatively, we could introduce a respective dynamic at various points in our system. This should, of course, be rigorously motivated from a biological as well as mathematical point of view. Just as a brief outlook, if we take our core dynamic triggered by the presence of anti-PD-1 in the system, we could manipulate the system as follows:

$$\frac{dC}{dt} = \lambda_C C (1 - \frac{C}{C_M}) - \eta CT \tag{6.17}$$

$$\frac{dT}{dt} = (\lambda_{I_{12}} T_0 \frac{I_{12}}{K_{I_{12}} + I_{12}} + \lambda_{I_2} T \frac{I_2}{K_{I_2} + I_2}) \cdot F(Q) - d_T T \tag{6.18}$$

$$\frac{dA}{dt} = -\mu_{PA} DA \cdot e^{-\xi t} - d_A A \tag{6.19}$$

$$\frac{dD}{dt} = \rho_{PD} \cdot (\lambda_{I_{12}} T_0 \frac{I_{12}}{K_{I_{12}} + I_{12}} + \lambda_{I_2} T \frac{I_2}{K_{I_2} + I_2}) \cdot F(Q) - d_T D - \mu_{PA} DA \cdot e^{-\xi t}. \tag{6.20}$$

Specifically, we manipulated the primary effect of anti-PD-1 and complemented the term representative for depletion of free PD-1 with an exponential decay term. This means, as we move forward in time, the effect of PD-1 blocking by anti-PD-1 has less impact. With values $\lambda_{I_{12}} = 17\,\mathrm{day}^{-1}$ and $\xi = 0.007$ we get the results in Figure 6.8.



**Figure 6.8:** Behavior of simulated pulmonary tumor burden of P3 (left), compared to actual measurements taken, and T cell concentration (right). The simulation includes resistance dynamics. Treatment times are indicated through vertical lines. Source: Own work in conjunction with data provided by *E. Dippel.*

We can see, that this first adjustment already allows a much-improved fit. We will stop further examinations of resistance dynamics and this brief outlook should not be understood as rigorous from either the biological side (motivation and derivation of system and parameter values) or the mathematical side (parameter fitting). It is only intended to give an idea, what further behavior is enabled by the extension of our basic model and encourage further explorations of anti-PD-1 resistance through mathematical modeling. Looking at Figure 6.9, we once again examine the behavior of single metastases.

Figure 6.9 shows all five lung metastases as well as two additional tumors located close to the *arteria mammaria interna* and in the *mediastinum* respectively. We see that in this case the overall tumor burden might be deceptive, as a large number of metastases show full remission and only three progress in size. Looking to Appendix C for reference, we can see that Lung1 and Lung3 from Figure 6.9 are extremely large. As can be gleaned from Appendix C, P2 has two metastases of middling size and they both follow a standard stable disease behavioral pattern. As our model was proven to be well equipped to handle stable disease, we might suspect that the model was able to simulate behavior of P2 metastases. Simulations proved this to be true (not shown here due to space considerations) for the same approach and a similar parameter set as
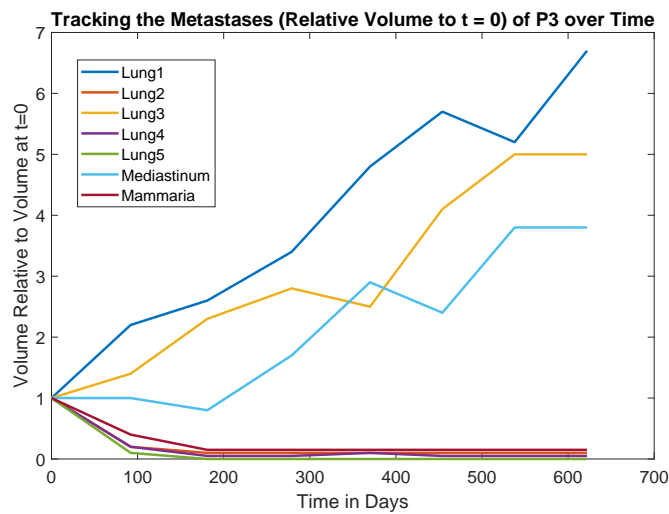
**Figure 6.9:** Metastases from P3 as measured directly from data over the observed time. To account for two extremely large metastases, the measurements were scaled in this graphic to represent size relative to measurements at $t = 0$. Source: Data provided by *E. Dippel*

utilized above.

Overall, the results from P3 (and P2) confirm our previously articulated need to examine metastases separately. It is interesting to see such heterogeneous behavior in different types of tissue and for metastases significantly bigger in size as compared to P1. Lastly, we want to once again state, that the data for P3 is not as "pure" for the reasons outlined above. Several resections of unknown date and volume (see Chapter 5) pose an additional challenge. The same goes for P2 because of adjuvant radiation. When it comes to quantitative evaluation, it appears to be important to consider adjuvant therapy strongly. Especially so when comparing between different patients as treatment histories vary greatly. We are primarily interested in further understanding the dynamics of immune response and anti-PD-1 treatment, but effects of adjuvant therapy should always be kept in mind, when dealing with data. Once the mechanics and interactions of immunotherapy and the adjuvant therapy options are better understood, it may be a promising avenue of research to pursue from a mathematical viewpoint and strive for a holistic approach. As was touched upon for the evaluation of P3 data, a resistance dynamic could possibly included in such an approach.

## 6.4 The P-Q-N Model

We previously alluded to the need to examine the tumor microenvironment (i.e. single metastases) and the cells present more closely, to be able to understand the vastly different behaviors of distinct metastases. We are looking examine additional characteristics of cancer cells and thus allow for some manner of heterogeneity while staying true to an Ordinary Differential Equation modeling approach and applying pure mass-action kinetics. One option is the utilization of several populations of cancer cells with different properties [112]. Thus, we divide the entirety of cancer cells into three populations: **P**roliferating cells, **Q**uiescent cells and **N**ecrotic cells, therefore P-Q-N model. The three types of cells have distinct characteristics, such as growth rates or rates of decay (if any). The compartment, to which a tumor cell belongs, depends on several factors. The key factor is the availability of oxygen and nutrients. Should a proliferating cell lack in supply of either of these, it will become quiescent; a quiescent cell may be reactivated and become once again proliferating, if conditions permit it [41]. In case the supply levels of nutrients and oxygen drop further, a quiescent cell may die completely and thus become necrotic [24].

The model generally assumes perfectly spheroidal shape of the tumor to justify the assumptions needed in deriving the compartment model of Ordinary Differential Equations and to apply mass-action kinetics (if needed). The tumor is assumed to be layered, where the necrotic cells occupy the center and the proliferating cells the outer layer with the quiescent cells in between (as seen schematically in Figure 6.11) [112]. These assumptions are fairly simplifying, as is supported by Figure 6.10. While showing imaging of a tumor displaying the characteristic "necrotic core", it also gives an idea of the complex structures involved. Nonetheless a good understanding of the dynamics can be obtained from the P-Q-N Model.

The following is an example of such an Ordinary Differential Equation model consisting of the three mentioned compartments:

$$\frac{dP}{dt} = G(P) - b_{PQ}P + b_{QP}Q - \delta_P P, \tag{6.21}$$

$$\frac{dQ}{dt} = b_{PQ}P - b_{QP}Q - b_{QN}Q - \delta_Q, \tag{6.22}$$

$$\frac{dN}{dt} = b_{QN}Q - \delta_N N, \tag{6.23}$$

$$P(0) = P_0, \quad Q(0) = Q_0, \quad N(0) = N_0, \tag{6.24}$$

where $P(t)$ is the concentration of proliferating (tumor) cells, $Q(t)$ the concentration of quiescent (tumor) cells, $N(t)$ the concentration of necrotic (tumor) cells and $G(P)$ is a growth function (such as for example from Table 6.2). Proliferating cells become hypoxic (i.e. quiescent) with rate $b_{PQ}$ and reoxygenate at rate $b_{QP}$. Quiescent cells
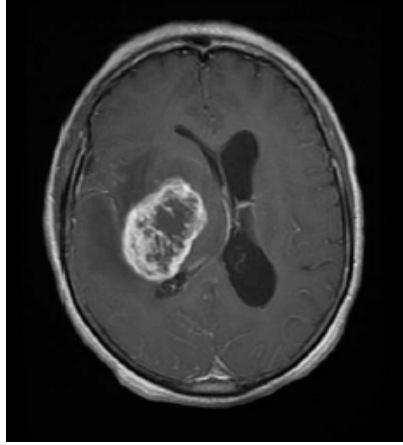
**Figure 6.10:** Axial image with contrast displaying a tumor with necrotic core at right basal ganglia. Source: [116].
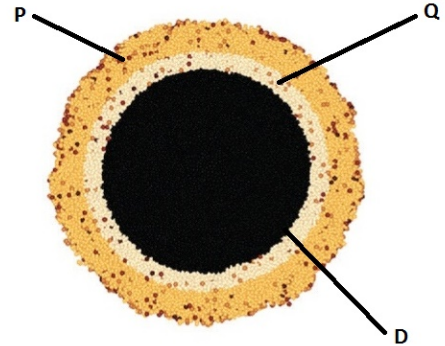


**Figure 6.11:** Schematic visualization of proliferating (P), quiescent (Q) and necrotic (N) cells in a tumor. Source: [109].

become chronically hypoxic (i.e. necrotic) at rate $b_{QN}$. Further, proliferating cells leave the microenvironment due to reasons other than hypoxia at rate $\delta_P$. Similarly, quiescent and necrotic cells are removed from the microenvironment at rates $\delta_Q$, $\delta_N$ respectively.

As proposed in [112] this approach allows the inclusion of terms $F(P, Q, N)$ and $H(P, Q, N)$ into equations (6.21) and (6.22) to account for further dynamics as e.g. the effect of necrosis on proliferation among others. The effect of necrosis in particular has been proposed often [39], though the exact mechanisms are still not fully understood [112]. It of course depends on the chosen model as well as which key interactions it aims to evaluate and therefore some do not explicitly include the dynamic (see [112] for example).

It becomes evident that the supply of nutrients and oxygen plays a vital role in the core dynamics of this model and thus we decide to introduce another cell population into the system - that of vascular cells. To allow the dynamics to play out spatially, we move away from the spatially homogeneous Ordinary Differential Equation approach.

# Chapter 7

# A Spatially Heterogeneous Partial Differential Equation Approach

We employ a spatially heterogeneous approach to emulate the spatial dynamics of the various cells involved. The key dynamics here are between the three types of cancerous cells as discussed before in Section 6.4: proliferating, quiescent and necrotic. While we keep dividing the tumor cells in these three compartments despite the existence of in-between states, we acknowledge the fact that the compartments are not strictly separate. The layers assumed in the P-Q-N Model (6.21) - (6.23) in Section 6.4 had the implicit effect that compartments were unable to mix. To account for a more realistic model we explore a system of Partial Differential Equations that depicts the concentrations of our three compartments in a given point in space in addition to the change over time. This allows mingling between tumor cell types and thus creates a more realistic, less "black-and-white" model of the tumor.

Additionally we introduce a new type of cell into the system in the form of vascular cells. The role of vascular cells in tumor growth is critical, as can be seen in Section 2.2, with the tumor initiating angiogenesis early on in order to survive and support its growth. Further, as evident from Section 2.4, the vascular system also plays a pivotal role in the body's immune response. We employ a similar modeling approach as *Gallaher et al.* in [41] and try to combine the dynamics of spatial tumor growth with the key dynamics of immune response and anti-PD-1 immunotherapy as previously evaluated in Chapter 6. This is of course a simplification as tumor vasculature differs from "normal" vasculature and is quite chaotic (see Figure 7.1).

While a tumor is certainly a three-dimensional (3D) object, we examine the dynamics in only one dimension. For simplicity we assume spherically symmetric behavior of the tumor and involved components; this allows for a quasi three-dimensional approach without complicating the system as we can move to spherical coordinates. Here, all functions solely depend on the radius, i.e. the distance from the center of the tumor. With this simplifying assumption we basically obtain a one-dimensional (1D) system - the only additional effect is on the Laplacians involved [12]. The Laplacian for a three-dimensional
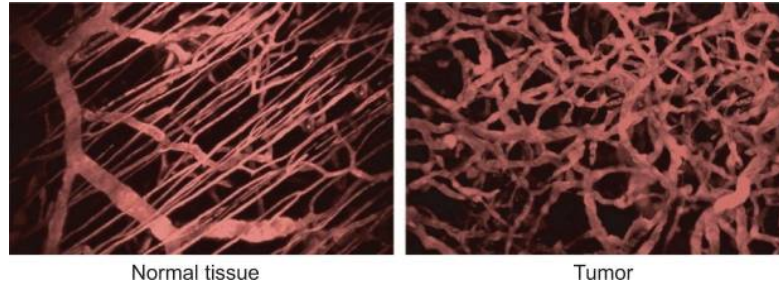
**Figure 7.1:** Side-by-side comparison between an example of "normal" blood vessels and more chaotic tumor vasculature. Source: [38].

domain in Cartesian coordinates $(x, y, z)$ and a one-dimensional domain reads as:

$$\Delta f = \nabla^2 f = \frac{\partial^2 f}{\partial x^2} + \frac{\partial^2 f}{\partial y^2} + \frac{\partial^2 f}{\partial z^2} \quad (3D), \qquad \Delta f = \frac{\partial^2 f}{\partial x^2} \quad (1D).$$

For spherical coordinates $(r, \theta, \phi)$ the Laplacian is:

$$\Delta f = \nabla^2 f = \frac{1}{r^2} \frac{\partial}{\partial r}\left(r^2 \frac{\partial f}{\partial r}\right) + \frac{1}{r^2 \sin\theta} \frac{\partial}{\partial \theta}\left(\sin\theta \frac{\partial f}{\partial \theta}\right) + \frac{1}{r^2 \sin^2\theta} \frac{\partial^2 f}{\partial \phi^2}, \qquad (7.1)$$

where, for the three dimensional case, cartesian and spherical coordinates relate in the following way:

$$x = r \sin\theta \cos\phi, \qquad y = r \sin\theta \sin\phi, \qquad z = r \cos\theta.$$

It is evident from (7.1), that if we apply our assumption of spherical symmetry, i.e. the function $f$ only depends on $r$, the Laplacian reduces to $\Delta = \frac{1}{r^2} \frac{\partial}{\partial r}\left(r^2 \frac{\partial f}{\partial r}\right)$. The gradient in spherical coordinates writes as:

$$\nabla f = \frac{\partial f}{\partial r}\hat{r} + \frac{1}{r}\frac{\partial f}{\partial \theta}\hat{\theta} + \frac{1}{r \sin\theta}\frac{\partial f}{\partial \phi}\hat{\phi}$$

Under the assumption of spherical symmetry, this simplifies to $\nabla f = \frac{\partial f}{\partial r}\hat{r}$, which is a multiple of the vector unit vector $\hat{r}$ for all values and is therefore equivalent to the gradient in a one dimensional Partial Differential Equation, $\nabla f = \frac{\partial f}{\partial x}\hat{x}$.

## 7.1 The Model

This assumption of spherical symmetry allows us to formulate a model of one-dimensional Partial Differential Equations to describe the interactions of the immune response to

| State Variable | Meaning |
|:---:|:---:|
| $P$ | Concentration of proliferating cancerous cells in $g/cm^3$ |
| $Q$ | Concentration of quiescent cancerous cells in $g/cm^3$ |
| $N$ | Concentration of necrotic cancerous cells in $g/cm^3$ |
| $V$ | Concentration of vascular cells in percentage of volume occupied |
| $A$ | Concentration of anti-PD-1 in $g/cm^3$ |
| $T$ | Concentration of activated T cells in $g/cm^3$ |
| $D$ | Concentration of free PD-1 expressed on T cells in $g/cm^3$ |
| $L$ | Concentration of PD-L1 expressed on T and cancer cells in $g/cm^3$ |
| $Q$ | Concentration of PD-1-PD-L1 complexes in $g/cm^3$ |

**Table 7.1:** List of variables involved in the system of Partial Differential Equations (7.2) - (7.8).

metastasized melanoma in the tumor microenvironment on a fixed region (sphere in three dimensions). We introduce the populations proliferating cancer cells ($P$), quiescent cancer cells ($Q$), necrotic cancer cells ($N$) as introduced in the P-Q-N model, vascular cells ($V$) and as before T cells ($T$), free PD-1 ($D$) and anti-PD-1 medication ($A$). A full overview over populations involved can be gleaned from Table 7.1. We formulate the system of Partial Differential Equations:

$$\frac{\partial P}{\partial t} = D_P \Delta P + \lambda_P PV \left[1 - G\right] + \alpha_{QP} QV - \alpha_{PQ} P(1-V) - \delta_P P - \eta_P PT \qquad (7.2)$$

$$\frac{\partial Q}{\partial t} = D_Q \Delta Q - \alpha_{QP} QV + \alpha_{PQ} P(1-V) - \alpha_{QN} Q - \delta_Q Q - \eta_Q QT \qquad (7.3)$$

$$\frac{\partial N}{\partial t} = \alpha_{QN} Q - \delta_n N \qquad (7.4)$$

$$\frac{\partial V}{\partial t} = D_V \Delta V + \chi \nabla \left(V \nabla Q\right) + \lambda_V VQ[1 - G] - \delta_V V \qquad (7.5)$$

$$\frac{\partial A}{\partial t} = D_A \Delta A - \mu_{DA} DA - d_A A \qquad (7.6)$$

$$\frac{\partial T}{\partial t} = D_T \Delta T + \left[\theta_{I_{12}} V + \theta_{I_2} T\right] \cdot F(Q) - d_T T \qquad (7.7)$$

$$\frac{\partial D}{\partial t} = D_T \Delta D + \rho_{PD} \left[\theta_{I_{12}} V + \theta_{I_2} T\right] \cdot F(Q) - d_T D - \mu_{DA} DA \qquad (7.8)$$

where $\theta_{I_{12}} = \lambda_{T I12} T_0 \frac{I_{12}}{K_{I12}+I_{12}}$, $\theta_{I_2} = \lambda_{T I2} \frac{I_2}{K_{I2}+I_2}$ as before and

$$G = G(t) = \frac{4}{5} \left[P(t) + Q(t) + N(t)\right] + V(t).$$

All populations are given again as concentrations in $g/cm^3$ with the exception of vascular cells. Vascular cells are given in percentage of volume occupied. Along with these equations we employ zero-flux boundary conditions (see Section 4.2). As initial conditions we will set an appropriate percentage of vascular cells (depending on location and tissue) throughout the tissue, an appropriate T cell and PD-1 concentration and start with a solid sphere of proliferating cancer cells in the center of our 3-dimensional region. That is to say we begin simulations (unless otherwise noted; this is necessary in e.g. P3 due to data availability) at the theoretical onset of angiogenesis. As seen in Section 2.2 this happens roughly above 1 mm in diameter for malignant tumors. So, we will start with initial conditions of about 0.5 mm radius, where all volume is occupied by solely proliferating tumor cells, as there are no vascular structures inside the tumor yet and therefore no significant amount of T cells should be contained within.

We set the percentage of volume occupied for this tumor initial condition to 95% to account for some room for stroma and irregularities. The rest of our simulated region has the appropriate percentage of vasculature and concentrations of T cells and PD-1. As we are interested in the size of the tumor, we need to define the tumor border (which moves over time). Through the properties of mathematical diffusion, in our simulation, extremely small concentrations will occur on the entire region. We define the tumor border as the point farthest away from the center ($r = 0$) which still has a concentration of $0.02\,\mathrm{g/cm^3}$ of proliferating cancer cells. One needs to be careful with increasing tumor size, as the center tends to be made up almost solely of necrotic cells. This is somewhat arbitrary (however proposed as a reasonable choice in [41]), but the border is well behaved as tumor concentration drops quickly when moving over a certain point on $[0, L]$, the interval on which we conduct our simulation (see below). Other values for the cut-off point (border) in a similar region ($0.005\,\mathrm{g/cm^3} - 0.05\,\mathrm{g/cm^3}$) work as well in simulations (not shown here). We now give some motivation and explanations for equations (7.2) - (7.8).

*Proliferating (Normoxic) Cells (P)*

As in the P-Q-N Model, proliferating cells are the only tumorous cells that proliferate and they do so at rate $\lambda_P$ while under the regime of a logistic growth function [60]. Different from Ordinary Differential Equation approaches, they do so only in presence of sufficient vascular cells $V$. Proliferating cells become hypoxic at rate $\alpha_{PQ}$ in the absence of vasculature (modeled through the term $(1 - V)$). Quiescent cells can reoxygenate and become proliferating cells once more at rate $\alpha_{QP}$, when vascular cells are present. As compared to the Ordinary Differential approach we can regulate proliferation more elegantly. Through the introduction of quiescent and necrotic cells, we can exclude the factors nutrients and oxygen from the growth function. This is now regulated through

the exchange between these three compartments $(P, Q, N)$. It allows us to adjust the capacity to only represent volume restrictions. Thus, the limiting factor in our logistic growth term is equal to $[1 - G(t)]$, where $G(t)$ is the percentage of volume occupied by tumor cells (all kinds) and vascular cells and therefore the expression from above:

$$G(t) = \frac{4}{5} \left[ P(t) + Q(t) + N(t) \right] + V(t),$$

as $1.25\,\mathrm{g}$ of tumor mass equate to $1\,\mathrm{cm}^3$ of tumor volume [9] and vascular cells are given in percentage of volume occupied. The other populations are neglected, as concentrations are extremely low in comparison or are not relevant to volume restrictions (e.g. PD-1 is part of the T cells). Also, in comparison to the Ordinary Differential Equation approach, we need not worry with overall space available, since our model only examines one metastasis at a time and we can evaluate each case separately when comparing to data. $\eta_P$ represents the killing rate of proliferating cells by T cells. Similar to the P-Q-N model, proliferating cells can leave the system through other causes and they are expunged from the microenvironment at rate $\delta_P$. Proliferating cells undergo random diffusion at rate $D_P$. Therefore

$$\frac{\partial P}{\partial t} = D_P \Delta P + \lambda_P PV \left[ 1 - G \right] + \alpha_{QP} QV - \alpha_{PQ} P(1 - V) - \delta_P P - \eta_P PT,$$

and specifically in spherically symmetric polar coordinates:

$$\frac{\partial P}{\partial t} = D_p \left[ \frac{\partial^2 P}{\partial r^2} + \frac{2}{r} \frac{\partial P}{\partial r} \right] + \lambda_P PV \left[ 1 - G \right] + \alpha_{QP} QV - \alpha_{PQ} P(1 - V) - \delta_P P - \eta_P PT.$$

*Quiescent (Hypoxic) Cells (Q)*

Quiescent cells become chronically hypoxic and thus necrotic at rate $\alpha_{QN}$. They undergo random diffusion at rate $D_Q$ and are killed by T cells at rate $\eta_Q$. Much like proliferating cells they can leave the system for other causes and do so at rate $\delta_Q$. Therefore

$$\frac{\partial Q}{\partial t} = D_Q \Delta Q - \alpha_{QP} QV + \alpha_{PQ} P(1 - V) - \alpha_{QN} Q - \delta_Q Q - \eta_Q QT,$$

and specifically in spherically symmetric polar coordinates:

$$\frac{\partial Q}{\partial t} = D_Q \left[ \frac{\partial^2 Q}{\partial r^2} + \frac{2}{r} \frac{\partial Q}{\partial r} \right] - \alpha_{QP} QV + \alpha_{PQ} P(1 - V) - \alpha_{QN} Q - \delta_Q Q - \eta_Q QT.$$

67

*Necrotic Cells (N)*

Necrotic cells will not reoxygenate and become quiescent or even proliferating again. They are expunged from the system at rate $\delta_N$ and do not undergo random migratory dispersal. Therefore (same equation for spherically symmetric polar coordinates):

$$\frac{\partial N}{\partial t} = \alpha_{QN} Q - \delta_n N.$$

*Vascular Cells (V)*

Vascular cells primarily occur when the tumor initiates angiogenesis. Vascular cells will therefore proliferate at rate $\lambda_V$ through logistic growth only in dependence of $Q$. The same spatial restriction as on proliferating cancer cells is imposed through the inclusion of the term $[1 - G(t)]$. It should be noted, that there are three types of vasculature involved in the tumor microenvironment [31]. These can be classified as mother vessels, glomeruloid bodies, and vascular malformations [31]. This leads to a vastly heterogenous structure of the local vasculature, which further depends on the type of surrounding tissue. The key dynamic is the expression of VEGF-A, which can be found in the vast majority of malignant tumors. In a hypoxic environment the expression of VEGF-A increases and therefore facilitates the proliferation of vascular cells. We include this dynamic implicitly through the dependence of $Q$ in the proliferation term. The VEGF-A cytokine is multifunctional (it also plays a key role in lymphangiogenic activity, [31]) and has another relevant feature for our model. In addition to inducing proliferation it also has a chemotactic effect on vascular cells [41], which we include in the basic Keller-Segel form (see [32] for further explanation) with chemotactic constant $\chi$ [47]. As a stand in for VEGF-A, we again use the quiescent cells that cause its expression, as attractant in this chemotactic approach. Lastly, vascular cells do undergo random migratory dispersal at rate $D_V$ and leave the system at rate $\delta_V$. Therefore

$$\frac{\partial V}{\partial t} = D_V \Delta V + \chi \nabla \Big( V \nabla Q \Big) + \lambda_V V Q [1 - G] - \delta_V V,$$

and specifically in spherically symmetric polar coordinates:

$$\frac{\partial V}{\partial t} = D_V \left[ \frac{\partial^2 V}{\partial r^2} + \frac{2}{r} \frac{\partial V}{\partial r} \right] + \chi \left[ \frac{\partial V}{\partial r} \frac{\partial Q}{\partial r} + V \left( \frac{\partial^2 Q}{\partial r^2} + \frac{2}{r} \frac{\partial Q}{\partial r} \right) \right] + \lambda_V V Q [1 - G] - \delta_V V.$$

*Anti-PD-1 Immunotherapy Medication (A)*

Anti-PD-1 medication is depleted through binding to PD-1 at rate $\mu_{DA}$ and decays in the microenvironment at rate $d_A$. In terms of adding medication to the system, we - in simulations - add the appropriate amount instantaneously. While the administration of the medication may take up to one hour (source:[45], obtained data), including an additional regime to alternate between the system under treatment and not under treatment proved to introduce unnecessary instability and no improved results. While doing so may be interesting in other forms of cancer treatments, such as chemo-, radio- or targeted therapy, the dynamics at play in our model act more slowly as medicine empowers the body's own immune system and doesn't attack tumor cells directly. The addition of anti-PD-1 is dependent on the concentration of vascular cells, $V$, as we assume anti-PD-1 to travel quickly through the vascular system. In the local tumor environment, it then undergoes random diffusion at rate $D_A$. Therefore

$$\frac{\partial A}{\partial t} = D_A \Delta A - \mu_{DA} DA - d_A A,$$

and specifically in spherically symmetric polar coordinates:

$$\frac{\partial A}{\partial t} = D_A \left[ \frac{\partial^2 A}{\partial r^2} + \frac{2}{r} \frac{\partial A}{\partial r} \right] - \mu_{DA} DA - d_A A.$$

*Active, relevant T Cells (T)*

The T cells in our model undergo the same dynamics as previously discussed in the Ordinary Differential Equations (6.3) - (6.6). This includes the activation of naive T cells and the local proliferation of T cells induced by IL-12 and IL-2 respectively. The activation of T cells happens proportionally to the local vasculature, as T cells are transported to the tumor site via blood vessels. In comparison to the Ordinary Differential Equation system, we can here model the arrival of T cells in the system more accurate. The heterogeneity of the tumor plays a critical role in the initial arrival and subsequent distribution of T cells. Both processes, activation and proliferation, are inhibited by the presence of PD-1-PD-L1 complexes, which is included in the model through the term $F(Q)$.

$$F(Q) = \frac{1}{1 + Q/K_{TQ}} == \frac{1}{1 + (DL)/\hat{K}_{TQ}},$$

as before. However, $L = \rho_L(T + \epsilon(P + Q))$, where we include PD-L1 expressed on (the still active) proliferating ($P$) and quiescent ($Q$) cancer cells. In the previous system of

Ordinary Differential Equation (6.3) - (6.6) we incorporated the concentration of cancer cells $C$ for PD-L1 expression, as we had only included one type of cancer cell in our model. T cells further undergo natural death at rate $d_T$ and random diffusion at rate $D_T$. Therefore

$$\frac{\partial T}{\partial t} = D_T \Delta T + \left[\theta_{I_{12}} V + \theta_{I_2} T\right] \cdot F(Q) - d_T T,$$

and specifically in spherically symmetric polar coordinates:

$$\frac{\partial T}{\partial t} = D_T \left[\frac{\partial^2 T}{\partial r^2} + \frac{2}{r}\frac{\partial T}{\partial r}\right] + \left[\theta_{I_{12}} V + \theta_{I_2} T\right] \cdot F(Q) - d_T T.$$

*Free PD-1 (not bound by anti-PD-1) (D)*

Finally, as before, PD-1 is introduced into the system through the addition of further T cells and thus underlies the same dynamics and inhibition mechanism. Because of the assumption that every cell in one population behaves alike, the natural death rate of PD-1 is equal to that of T cells, i.e. $d_T$. Because PD-1 is expressed on T cells, it undergoes the same random diffusion at rate $D_T$. Lastly, PD-1 depletes through binding to anti-PD-1 at rate $\mu_{DA}$ [60]. Therefore

$$\frac{\partial D}{\partial t} = D_T \Delta D + \rho_{PD}\left[\theta_{I_{12}} V + \theta_{I_2} T\right] \cdot F(Q) - d_T D - \mu_{DA} D A,$$

and specifically in spherically symmetric polar coordinates:

$$\frac{\partial D}{\partial t} = D_T \left[\frac{\partial^2 D}{\partial r^2} + \frac{2}{r}\frac{\partial D}{\partial r}\right] + \rho_{PD}\left[\theta_{I_{12}} V + \theta_{I_2} T\right] \cdot F(Q) - d_T D - \mu_{DA} D A.$$

Additionally, to these motivations of each equation, a brief explanation of the origins of separate killing rates $\eta_P, \eta_Q$ shall be given. We previously discussed the complex behavior and patterns of movement for T cells in Section 2.4. When it comes to the behavior of T cells in our system (7.2) - (7.8), it is clear, that the movement is fairly simplified. In [72] it was shown, that T cells, after activation, move very different if the local concentration of active (proliferating) cancer cells is high as compared to lower concentrations. As outlined in [49] it appears that T cells are possibly attracted to high numbers (i.e. higher concentrations) of active cancer cells in the local environment. This

is supported by their trajectories and might be part of the explanation why many tumors are not penetrated as often the core is far more necrotic compared to the outer layers. Indeed, in preliminary simulations it was observed, that in absence of sophisticated T cell dynamics the tumor border will grow outwards regardless of immune response (while the local concentrations are reduced).

Initially this was addressed by introducing chemotaxis into the T cell (and subsequently the PD-1) equation, so that T cell movement is regulated by concentration of proliferating cancer cells $P$. While hinting at the desired effect and the possibility of stable disease (resting tumor border) in this modeling approach it proved to be somewhat unstable, as the model now contained three terms of chemotaxis, terms that can be a complication even in implicit and Crank-Nicolson methods of simulation (see Section 7.2 and [5]). In system (7.2) - (7.8) we try to emulate this behavior by assigning a higher killing rate $\eta_P$ in the case of proliferating cells as compared to quiescent cells ($\eta_Q$). This gives T cells more potency overall when (at same tumor cell density) the share of proliferating cells increases. In simulations this turned out to be close to the tumor border, which agrees with the general behavior of tumors as outlined in Chapters 2 and 6.

We leave $\eta_P$ as in the previous Ordinary Differential Equation system and set $\eta_Q = 5\,\mathrm{day}^{-1}$. As seen in following simulations these values fit the overall dynamic, though some thought may be given to choosing higher values, as T cells no longer (as before in the Ordinary Differential Equation system) attack all cancer cells, but merely proliferating and quiescent cells. With this dynamic of two separate killing rates, the model is now equipped to produce a temporarily stagnant tumor border.

Having formulated the system, we can now simulate it numerically to investigate the behavior over time.

## 7.2 Numerical Simulation Methods

The system (7.2) - (7.8) was simulated utilizing a Finite Differences approach in the form of an adjusted Crank–Nicolson method. Finite Differences are commonly used in three variations [89]. Given the Partial Differential Equation

$$\frac{\partial u}{\partial t} = F\Big(u, x, t, u_x, u_{xx}\Big),$$

we discretize the system. We have one-dimension for space and time in our case - resulting in evenly spaced gridpoints as visualized in Figure 7.2. The distance between two adjacent gridpoints at the same time point is set to be $\Delta x$ and vice versa $\Delta t$ in such a manner that $\frac{T}{\Delta t}, \frac{L}{\Delta x}$ are integers, where we examine solutions on the domain $[0, L]$ for the time interval $[0, T]$. From now on let the indices $i, n$ indicate the position on the grid,

so that $u_i^n = u(i \cdot \Delta x, n \cdot \Delta t)$. The gridpoint $(0,0)$ would here equate to the point $r = 0$ at time $t = 0$. We now use the grid in one of three ways to approximate time derivatives on the left-hand side of each Partial Differential Equation (7.2) - (7.8):

*Explicit Method (Forward Euler):*

$$\frac{u_i^{n+1} - u_i^n}{\Delta t} = F_i^n\left(u, x, t, u_x, u_{xx}\right)$$

*Implicit Method (Backward Euler):*

$$\frac{u_i^{n+1} - u_i^n}{\Delta t} = F_i^{n+1}\left(u, x, t, u_x, u_{xx}\right)$$

*Crank-Nicolson Method:*

$$\frac{u_i^{n+1} - u_i^n}{\Delta t} = \frac{1}{2}\left[F_i^n\left(u, x, t, u_x, u_{xx}\right) + F_i^{n+1}\left(u, x, t, u_x, u_{xx}\right)\right] \tag{7.9}$$

The derivation of these finite difference methods shall not be given here, but for extensive literature on derivation through Taylor series expansion and discussion on accuracy of different methods, the reader may be referred to [66]. A visual representation of how the methods operate can be found in Figure 7.2.
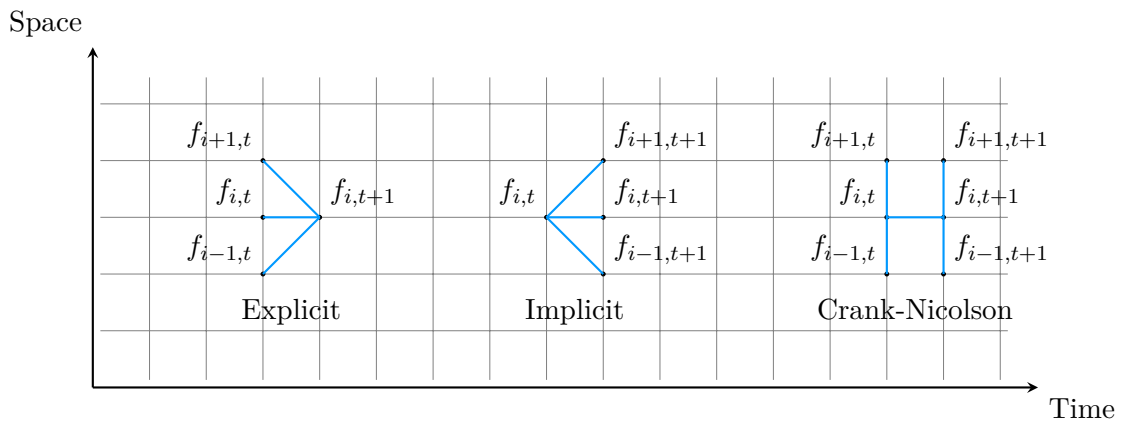


**Figure 7.2:** Visual representation of the manner in which Explicit, Implicit and Crank-Nicolson Methods utilize the discretization of the domain to approximate solutions in each step. Source: Own work.

While the Explicit Method - through direct calculation in each time step - is easiest to implement and offers simplicity computationally, it needs to meet certain requirements for stability [89]. Specific stability criteria can be formulated for a Partial Differential Equation under given conditions (e.g. the classic Heat Equation in one dimension) [79]. The Explicit Method turned out to not offer the necessary stability for system (7.2) - (7.8), even for critically small time steps. Both the Implicit Method and the Crank-Nicolson Method proved to be stable; we therefore opt to employ Crank-Nicolson for the improved accuracy. Both Implicit and Crank-Nicolson method are often thought of as unconditionally stable, but chemotaxis terms need to be handled with care nonetheless (see [5]). It has to be noted, that the computational complexity is significantly higher, as a system of equations needs to be solved for each time step. This gets especially tedious with a high number of non-linear terms (see below).

In conjunction with (7.9), we utilize a central difference approach for the space derivatives, i.e. we approximate those derivatives as follows:

$$\frac{\partial u}{\partial x} \approx \frac{u_{i+1}^{n+1} - u_{i-1}^{n+1} + u_{i+1}^n - u_{i-1}^n}{4\Delta x},$$
$$\frac{\partial^2 u}{\partial x^2} \approx \frac{u_{i+1}^{n+1} - 2u_i^{n+1} + u_{i-1}^{n+1} + u_{i+1}^n - 2u_i^n + u_{i-1}^n}{2(\Delta x)^2}.$$

As system (7.2) - (7.8) is highly non-linear, we opt for a simplified Crank-Nicolson approach as indicated above. The coupled Differential Equations lead to the necessity of solving a system of non-linear equations when advancing in time. We mitigate this by reducing the complexity similar to the concept demonstrated in [5]. Specifically, we elect to use an explicit approach when it comes to the reaction terms (not involving derivatives) of (7.2) - (7.8). For this we only utilize the previously known values for the reaction terms when moving forward in time, whereas Crank-Nicolson in pure form would require both the previously known values as well as unknown values (of the current time step). The system of equations needed to be solved in each step reduces to a tridiagonal matrix, which can be solved by the Thomas Algorithm and thus avoids high computational complexity.

To illustrate the numerical process we followed to implement our adjusted Crank-Nicolson method, we look at $P$, the proliferating cells, in time step $n \to n+1$: Assuming we know all values at time $n \cdot \Delta t$, we obtain the following discretization of equation (7.1):

$$\frac{P_i^{n+1} - P_i^n}{\Delta t} = D_P \left[ \frac{P_{i+1}^{n+1} - 2P_i^{n+1} + P_{i-1}^{n+1}}{2(\Delta x)^2} + \frac{P_{i+1}^n - 2P_i^n + P_{i-1}^n}{2(\Delta x)^2} \right]$$
$$+ D_P \frac{2}{i\Delta x} \left[ \frac{P_{i+1}^{n+1} - P_{i-1}^{n+1}}{4\Delta x} + \frac{P_{i+1}^n - P_{i-1}^n}{4\Delta x} \right]$$
$$+ \lambda_P P_i^n V_i^n \left[ 1 - G_i^n \right] + \alpha_{QP} Q_i^n V_i^n - \alpha_{PQ} P_i^n (1 - V_i^n) - \delta_P P_i^n - \eta_P P_i^n T_i^n.$$

Rearranging the terms gives:

$$(-\tau - \psi) P_{i+1}^{n+1} + \zeta P_i^{n+1} + (-\tau + \psi) P_{i-1}^{n+1} =$$
$$(\tau + \psi) P_{i+1}^n + \hat{\zeta} P_i^n + (\tau - \psi) P_{i-1}^n + \lambda_P P_i^n V_i^n \left[ 1 - G_i^n \right]$$
$$+ \alpha_{QP} Q_i^n V_i^n - \alpha_{PQ} P_i^n (1 - V_i^n) - \delta_P P_i^n - \eta_P P_i^n T_i^n,$$

with

$$\tau = \frac{D_P}{2(\Delta x)^2}, \qquad \psi = \frac{D_P}{i2(\Delta x)^2}, \qquad \zeta = \frac{1}{\Delta t} + \frac{D_P}{(\Delta x)^2}, \qquad \hat{\zeta} = \frac{1}{\Delta t} - \frac{D_P}{(\Delta x)^2}.$$

The boundary conditions, in conjunction with our discretization, help us obtain similar equations for the first and last gridpoints at a given timestep $n$. As outlined in [5], we assume it holds for all $n > 0$ (though it would hold for our initial conditions as well):

$$P_0^n = P_1^n, \qquad\qquad P_{(T/\Delta x)+1}^n = P_{(T/\Delta x)-1}^n$$

With this we can formulate a linear system of equations in the manner of $A \cdot x = b$ where

$$A = \begin{bmatrix} \zeta - \tau + \psi & -\tau - \psi & 0 & \cdots & 0 \\ -\tau + \psi & \zeta & -\tau - \psi & \ddots & \vdots \\ 0 & \ddots & \ddots & \ddots & 0 \\ \vdots & \ddots & -\tau + \psi & \zeta & -\tau - \psi \\ 0 & \cdots & 0 & -2\tau & \zeta \end{bmatrix}, \quad x = \begin{bmatrix} P_1^{n+1} \\ P_2^{n+1} \\ \vdots \\ \vdots \\ P_{(T/\Delta x)}^{n+1} \end{bmatrix}, \quad b = \begin{bmatrix} b_1 \\ b_2 \\ \vdots \\ \vdots \\ b_{(T/\Delta x)} \end{bmatrix},$$

with

$$b_i = (\tau + \psi) P_{i+1}^n + \hat{\zeta} P_i^n + (\tau - \psi) P_{i-1}^n + \lambda_P P_i^n V_i^n \left[ 1 - G_i^n \right] + \alpha_{QP} Q_i^n V_i^n$$
$$- \alpha_{PQ} P_i^n (1 - V_i^n) - \delta_P P_i^n - \eta_P P_i^n T_i^n$$

known. This system of equations can now be solved to obtain the values for $P_i^{n+1}$, $\quad i \in [0, (L/\Delta x)]$. We employ the same process for all other populations and then proceed to the next time step. This works exactly the same way for all other indicator variables and shall not be demonstrated here to avoid repetition. The only difference is the vasculature $V$ as it encompasses the chemotaxis term and thus not only first and second order derivatives of $V$, but also first order derivatives of $Q$: We can solve this problem by simply ensuring that $Q$ is handled first for each time step, so the values $Q_{i+1}^{n+1}, Q_1^{n+1}, Q_{i-1}^{n+1}$ are known and can be included in the right-hand side of the linear system solved for $V$. From the calculations shown, we can better understand, why we can employ the Thomas Algorithm: as mentioned above, $A$ - as defined above - is clearly a tridiagonal matrix. This cuts our computation time down; we get $\mathcal{O}(n)$ instead of $\mathcal{O}(n^3)$, which would be the case for a full matrix [5].

## 7.3 Parameter Fitting and Results

### 7.3.1 Parameter Values

Unless otherwise noted below, we carry over all parameters from the Ordinary Differential Equation model. For the remaining parameters we chose the values given in Table 7.2. Some additional explanations are given below.

*Diffusion coefficients $D_P, D_Q, D_A, D_T$*

For $D_P$ we use the value given in [41]. The relation of $D_P$ and $D_Q$ is also given in [41]. For anti-PD-1, we set our diffusion coefficient $D_A$ to be comparatively low to other diffusion as anti-PD-1 medication are monoclonal antibodies and therefore not prone to self-induced migration. Looking at [60] for reference we can see a diffusion coefficient of higher magnitude, but this becomes necessary as the presented system does not include vasculature. Anti-PD-1 does get spread quite rapidly through the blood stream, which is addressed in our model through instantaneous distribution of anti-PD-1 upon administration proportional to the vasculature present. The medication does get distributed very well in this manner. Once introduced into the local environment, the diffusion dynamic takes over the motility of anti-PD-1. For $D_T$ we choose a relatively high diffusion coefficient as compared to e.g. [60]. This has several reasons. For one this gives the immune system flexibility and allows T cells to migrate quickly as they have been shown to do albeit not all the time [14]. The high diffusion coefficient also emulates the flexibility of the immune system as it reacts to the other cell populations' behavior. In [60] this is included through the high motility of IL-12 and IL-2. As we have not included these cell populations in our model, we set the diffusion coefficient to the

75

| Parameter | Meaning | Value | Sources (if appl.) |
|---|---|---|---|
| $D_P$ | Diffusion coefficient of proliferating cancer cells | $6.3 \times 10^{-4} \, \mathrm{cm^2/day}$ | [41] |
| $D_Q$ | Diffusion coefficient of quiescent cancer cells | $1.7 \cdot D_P$ | [41] |
| $D_V$ | Diffusion coefficient of vascular cells | $0.8 \cdot D_P$ | [41] |
| $D_A$ | Diffusion coefficient of anti-PD-1 medicine | $7.9 \times 10^{-7} \, \mathrm{cm^2/day}$ | Estimate |
| $D_T$ | Diffusion coefficient of T cells | $8.6 \times 10^{-2} \, \mathrm{cm^2/day}$ | Estimate |
| $\lambda_P$ | Proliferation rate of proliferating cells | $3.15 \, \mathrm{day^{-1}}$ | Estimate |
| $\alpha_{PQ}$ | Rate of hypoxia of proliferating cells | $3.0 \times 10^{-2} \, \mathrm{day^{-1}}$ | Estimate |
| $\alpha_{QP}$ | Rate of quiescent cell reoxygenation | $0.5 \, \alpha_{PQ}$ | Estimate |
| $\delta_P = \delta_Q = \delta_N = \delta_V$ | Rate of expunging of various cells | $2.4 \times 10^{-4} \, \mathrm{day^{-1}}$ | [41] |
| $\eta_P$ | Killing rate of proliferating cancer cells by T cells | $23 \, \mathrm{day^{-1}}$ | [60] |
| $\eta_Q$ | Killing rate of quiescent cancer cells by T cells | $5 \, \mathrm{day^{-1}}$ | Estimate |
| $\alpha_{QN}$ | Rate of necrosis of quiescent cells | $1.7 \times 10^{-3} \, \mathrm{day^{-1}}$ | [41] |
| $\chi$ | Chemotaxis coefficient of vascular cells | $1.3 \times 10^{-3} \, \mathrm{cm^2/day}$ | [41] |
| $\lambda_V$ | Proliferation rate of vascular cells | $0.6 \, \mathrm{day^{-1}}$ | Estimate |
| $\lambda_{I_{12}}$ | Activation rate of naive T cells (adjusted) | To be determined | Estimate |

**Table 7.2:** Parameters used for the simulation of the system of Partial Differential Equations (7.2) - (7.8) unless otherwise noted. Further parameters are carried over from the Ordinary Differential Equation model in Chapter 6. This set of parameters is utilized for the main simulations for tumor growth and behavior (P1). Deviations from this parameter set for other simulations are indicated appropriately. Sources: Own work and as outlined in Table.

same magnitude as the diffusion coefficients for IL-12 and IL-2 from [60] to allow our immune response the same reactive nature and spatial flexibility.

### *Proliferation rate $\lambda_P$*

Compared to the Ordinary Differential case the proliferation rate is increased here to account for two factors: The proliferating cancer cells account for the sole source of new cancer cells, whereas before we included all cancer cells as one species. Furthermore, proliferation only happens proportionally to vasculature, i.e. if sufficient nutrients and oxygen is available.

### *Rate of hypoxia $\alpha_{PQ}$ and rate of reoxygenation $\alpha_{QP}$*

In [41] a range of $0.0014\,\text{day}^{-1} - 0.096\,\text{day}^{-1}$ is given for different environments ranging from high to low vascular content. We choose a value in the middle of this range. It is also commented in [41] that rate of reoxygenation is significantly lower than rate of hypoxia, though a precise value was not derived. We account for this by setting $\alpha_{QP} = 0.5\,\alpha_{\text{PQ}}$.

### *Rates of expunging $\delta_P$,$\delta_Q$,$\delta_N$,$\delta_V$*

Extracted from [41] and similar magnitudes found in other literature, these parameters do not have a big influence on overall dynamics, but allow the system to behave naturally, as in reality sometimes cells are lost to the local environment through displacements or other reasons leading to expunging.

### *Rate of necrosis $\alpha_{QN}$*

Direct necrosis is not possible in our model, as cells would first become quiescent before undergoing necrosis. This dynamic is similarly represented in [41], where we obtained the rate of necrosis.

### *Chemotaxis coefficient $\chi$*

The same is true for the characterization of chemotactic dynamics between quiescent cells and vascular cells - we adapt the value derived in [41].

*Proliferation rate $\lambda_V$*

A range for vascular cell proliferation is given in [41] for different environments (much like before for $\alpha_{PQ}, \alpha_{QP}$. The range is $0.28\,\text{day}^{-1} - 0.83\,\text{day}^{-1}$ and to complement our choice for rate hypoxia we again choose a value from the middle of this range.

In addition, different from our Ordinary Differential Equation approach, we insert medication proportionally to vasculature. We keep the same method of instantaneous injection at the given treatment times and subsequent simulation with adjusted anti-PD-1 levels. Where before we simply upped the concentration by the appropriate amount calculated from treatment data, we now consider the manner of arrival in the tumor microenvironment (i.e. through the vascular system). Therefore, we need to adjust the dose added in each treatment cycle, so the same amount still arrives in the local system. In the previous system we increased the concentration by $1.5 \times 10^{-5}\,\text{g/cm}^3$ to represent treatment for P1. As in the tumorless case we know the percentage of vasculature in the brain to be 3.1% from [51], we add:

$$1.5 \times 10^{-5}\,\text{g/cm}^3 \times \frac{1}{0.031} \approx 5 \times 10^{-4}\,\text{g/cm}^3$$

proportionally to the concentration of vascular cells in each treatment cycle. As the tumor undergoes angiogenesis and accumulates additional vasculature, more anti-PD-1 will reach the tumor microenvironment, which is covered in our model dynamics.

## 7.3.2 Numerical Results

For initial simulation we again employ our set of data from P1, as we can exclude preexisting treatment effects with reasonable certainty. We simulate the system in the manner outlined above and choose the following initial conditions: As discussed above we will have $P(i,0) = \frac{5}{4} \times 0.95\,\text{g/cm}^3$ with $i \in [0, 0.5\,\text{mm}]^{12}$, so that we have solid tumor sphere with diameter $1\,\text{mm}$. In the rest of the tissue, not occupied by tumor cells, we will set appropriate concentrations for vascular cells, T cells and PD-1, so that $V(j,0) = V_0, \quad T(j,0) = T_0, \quad D(j,0) = \rho_{PD} \cdot T_0$ with $j \in (0.5\,\text{mm}, L]$, where $L$ is the radius of our spherical region.

We have previously calculated the percentage of vascular tissue in the brain in Chapter 6 to be about 3.1%. It should be noted, that while we will assume the same initial conditions for all metastases, depending on location some may have better access to the heterogeneous structures of blood vessels in the brain. Through first simulations it

---

[12]This will be about $0.5\,\text{mm}$ depending on the actual numerical grid used in our simulation

became evident that this percentage is not able to sustain the aggressive initial growth observed in data P1 from $t = 0$ to $t = 63$. We therefore opted for an initial vascular percentage of 5% throughout the tissue. This might be an indicator that vascular volume can be limited as an indicator for tumor behavior and possibly an alternative could be considered in blood volume circulated. Initial T cell concentration (and therefore PD-1 concentration as well) is set to the same as before in the Ordinary Differential Equation system.

**Exemplary Treatment-Free Case**

We start by simulating a treatment-free system for the duration of 365 days to get an idea of the dynamics at play. For this we use the same approach as outlined above, but simulate an environment with lower vascular activity. We decrease the associated parameters from Table 7.2 [41]: We set the proliferation rate of vascular cells, $\lambda_V$ equal to $0.3\,\text{day}^{-1}$ and increase the rate of hypoxia $\alpha_{QP}$ to $0.04\,\text{day}^{-1}$, which in turn increases the rate of reoxygenation $\alpha_{QP}$. To complement this, we increase the rate of necrosis $\alpha_{QN}$ to $0.05\,\text{day}^{-1}$. These changes do not qualitatively change the simulation results, but avoid an overly aggressive tumor, allowing an easier display of the dynamics at play. The results can be seen in Figure 7.3.

We can observe the tumor growing over time through Figures 7.3a - 7.3c, which display the constitution of the tumor at three distinct time points. In Figures 7.3b, 7.3c we can start to see the typical structure of a tumor, with an outer layer of largely proliferating cells, followed (moving inward) by an increased concentration of quiescent cells. Finally, closer to the center the concentration of necrotic cells increases and in Figure 7.3c we can clearly see the characteristic necrotic core being formed, whereas the concentrations of proliferating and quiescent cells become very low. Figure 7.3d displays the average concentration of vascular cells - through fraction of volume occupied - within the tumor over time. This is defined to be the area between the center and our self-defined and moving boundary, where the concentration of proliferating tumor cells falls below $0.02\,\text{g/cm}^3$. The onset of angiogenesis is clearly observable and with growing size, the tumor develops a more extensive system of vasculature to support itself.

To understand the effect of anti-PD-1 on this system, we now introduce an exemplary treatment regime (such as imposed on P1), with treatment beginning at $t = 44$. We use the dosage calculated above and administer treatment in regular cycles of 21 days. Results can be seen in Figure 7.4.

The effect of anti-PD-1 treatment is immediately visible between Figures 7.3, 7.4. The concentrations of tumor cells are fairly low and the spatial spread is very contained.
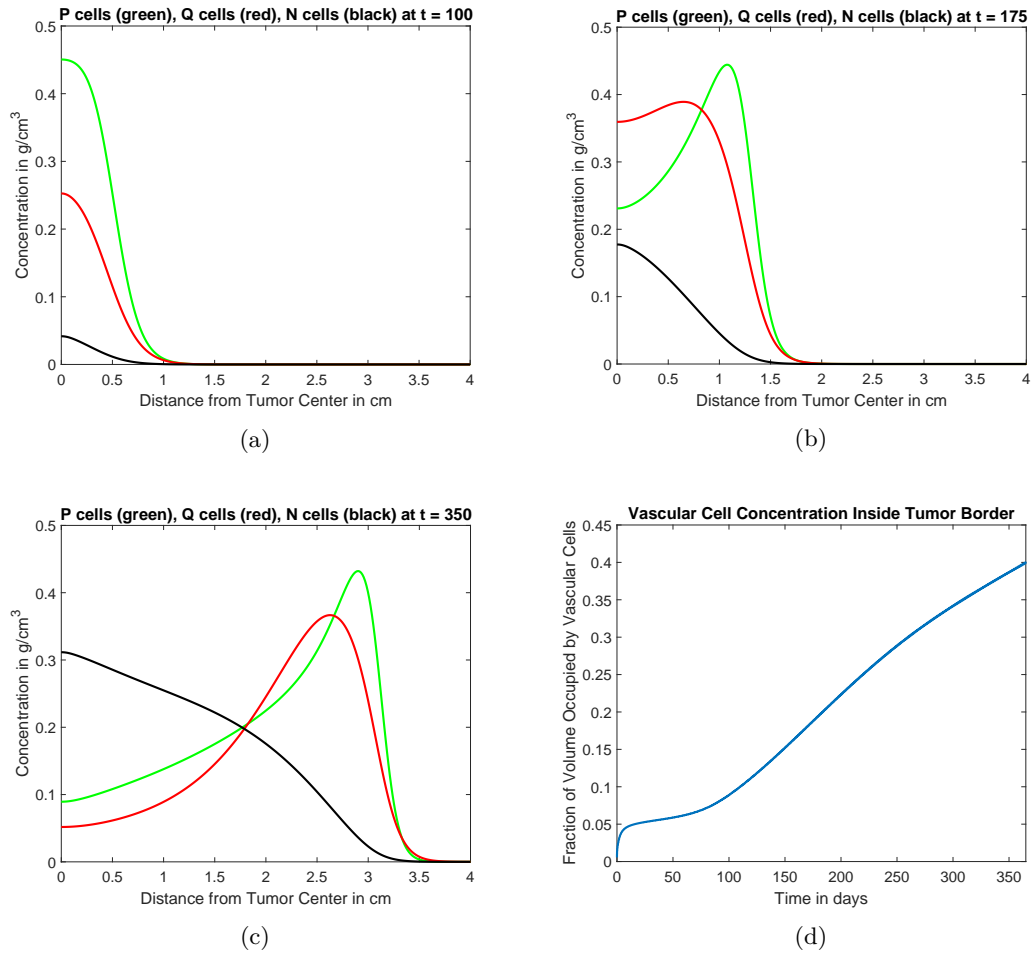
**Figure 7.3:** Constitution of tumor at different times in a treatment-free simulation with reduced vascular proliferation. Concentrations of proliferating (P), quiescent (Q) and necrotic (N) cancer cells from the center to the edge of the simulated region are given at three different time points: 100 days (a), 175 days (b) and 350 days(c). In (d) the development of the average concentration of vascular cells inside the tumor over time is shown. Source: Own work.

In the simulation including treatment, from $t = 100$ (Figure 7.4a) to $t = 175$ (Figure 7.4b) the tumor size and tumor cell concentration are almost stagnant. Towards the end of the simulation the tumor starts to spread despite continued treatment (one cycle of anti-PD-1 is even included at $t = 349$). This is insofar interesting, because in reality - even after a patient reaches stable disease, an acquired resistance to anti-PD-1 treatment can be observed. In the simulation, after treatment initiation the tumor shrinks down,
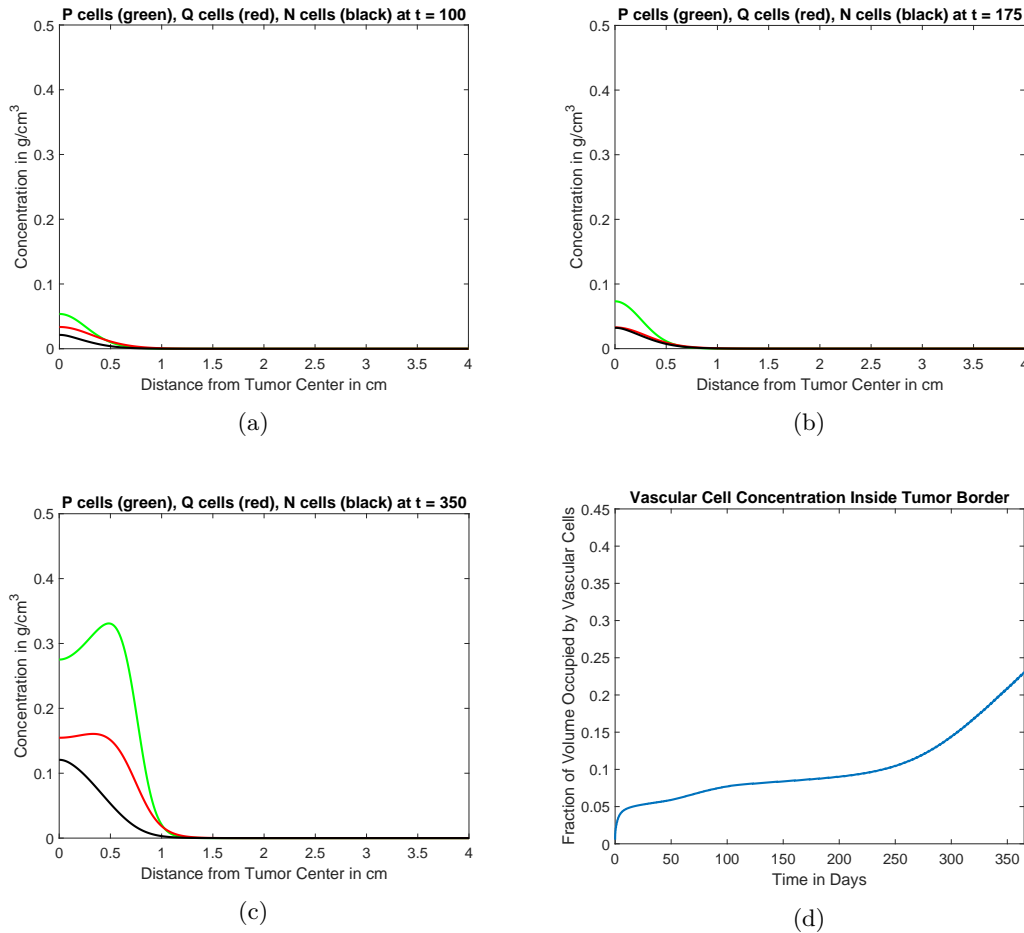
**Figure 7.4:** Constitution of tumor at different times in a treatment simulation in similar environment and parameter set-up to Figure 7.3. Concentrations of proliferating (P), quiescent (Q) and necrotic (N) cancer cells from the center to the edge of the simulated region are given at three different time points: 100 days (a), 175 days (b) and 350 days(c). In (d) the development of the average concentration of vascular cells inside the tumor over time is shown. Source: Own work.

but stabilizes after continued treatment and presents with de facto stable disease as concentrations and tumor volume stay constant over several weeks. It turns out that the vascular cells, which are only affected implicitly (decreased $Q$ cell concentration) through anti-PD-1, continue proliferating - albeit slowly - inside the tumor as can be seen in Figure 7.4d. This in turn induces proliferation of cancer cells $P$, as more nutrients and oxygen become available. As the tumor builds up, it furthers vascular growth and entering the involved cells in a cycle which then leads to abnormal tumor growth once

again. It seems that in the system the tumor adjusts to increased T cell activity, by shrinking and then changing its structure to a point where growth can once again be supported.

Through the adjustment of $\lambda_{I_{12}}$, which regulates how many active T cells arrive in the tumor microenvironment, the system behavior can move from response to stable disease (with delayed progress) to progress. We will visualize this in the following adaptation and comparison to data P1.

**Comparison of Numerical Results to Data**

We move back to our initial set-up in a higher vasculature environment and examine the system behavior compared to data set P1. We use the parameters from Table 7.2 and attempt to find a suitable value for $\lambda_{I_{12}}$. As discovered in Section 6.3 the inclusion of the effect of radiation therapy allowed for a better fit in the Ordinary Differential Equation system. Here, it was not too important how many cells were killed off directly by radiation therapy, but more so that T cell activity was increased after radiation. We therefore include this dynamic as well and divide our simulation in two parts - pre-radiation and post-radiation with two distinct parameters $\lambda_{I_{12}(pre)}$ for the time before radiation and $\lambda_{I_{12}(post)}$ for the time after radiation. This in turn allows for increased T cell activity post-radiation, which makes anti-PD-1 treatment more effective and thus allows for a synergistic effect as discussed in Section 6.3. In comparison to the Ordinary Differential Equation system values for $\lambda_{I_{12}(pre)}$ and $\lambda_{I_{12}(post)}$ should here be higher than their respective counterparts in Section 6.3 as activation of naive T cells (i.e. arrival at the tumor site) happens proportionally to vascular cell concentration, which is initially set to be 5%.

In terms of data comparison, we first need to extract the desired measurements from our data. As outlined in Chapter 5, we measured volume of metastases. Since our model assumes a spherically symmetric tumor shape, volume depends solely on tumor radius. We assume perfect spherical shape for our measured volumes as well and calculate the corresponding radii from Table 5.2 to compare to the spatial growth in our simulation. To get a first idea of model fit we average the radii from M1-M5 at every observed point in time (average of all that are visible at a given time). We choose fitting values for $\lambda_{I_{12}(pre)} = 25 \, \text{day}^{-1}$ and $\lambda_{I_{12}(post)} = 143 \, \text{day}^{-1}$. The results can be seen in Figure 7.5. The first slowing of expansion (plateau around $t = 10$ in Figure 7.5) marks the first big impact of lack of oxygen and nutrients. The tumor started out with aggressive growth and expansion (as he had adapted before angiogenesis). This dynamic dominates the beginning of our simulation. Then the vascular dynamics set in and the tumor needs to build up sufficient vasculature to sustain further growth, which results in a momentary slowing of tumor growth.
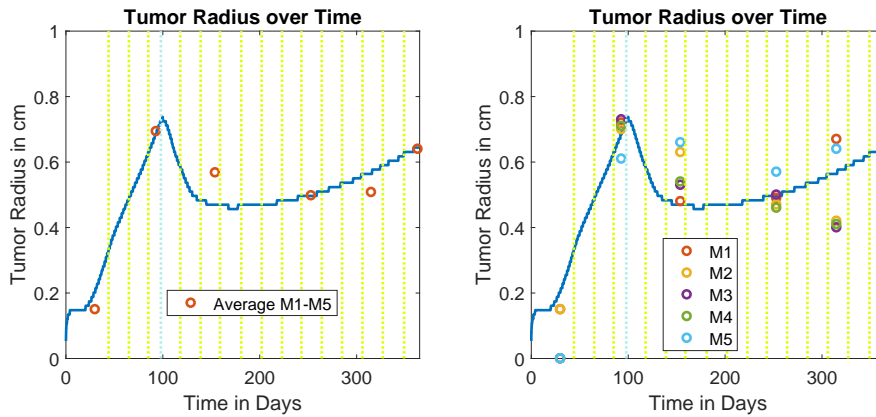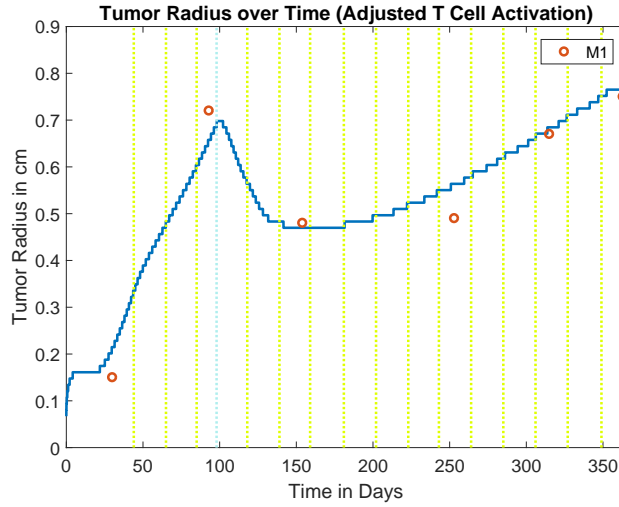
**Figure 7.5:** Tumor radius over time from simulation of model (7.2) - (7.8) with appropriate parameters as outlined including treatment regime of P1. In comparison the measurements from P1 are shown as average of M1-M5 through red circles (left) and M1-M5 separately in different colors (right). Treatment cycles are indicated as before through vertical, dotted lines. Source: Own work in conjunction with data provided by *E. Dippel.*

The dynamic (and even the slight progress after stable disease) is well represented by the model. Through the adjustment of $\lambda_{I_{12}(post)}$ the model is able to represent several characteristic types of cancer progressions. In Figure 7.6 we can see exemplary simulations for three different values for $\lambda_{I_{12}(post)}$ leading to progress, stable disease and response respectively. In our model the adjusted $\lambda_{I_{12}(post)}$ could mean that the radiation wasn't able to hit a certain metastasis as well as another. Or that the tumor has developed additional mutations that disallow T cells entry to the tumor microenvironment for some reason.

It should be noted, that we primarily focus on the T cell activation and if T cells can enter the tumor at a high rate, because, as discussed in Section 2.4, the degree of penetration of the tumor by T cells is thought to be a good indicator for response to treatment. However, the model dynamics are also influenced to a degree by different types of vasculature environment (thus respecting the different locations of metastasis). This can be included in the model through different initial percentages of vascular cells and the associated parameters describing vascular proliferation, hypoxia of proliferating cancer cells and reoxygenation of quiescent cancer cells. For example, let's assume - compared to the average, M1 from P1 was initially more susceptible to penetration by T cells, but got a weak dose of radiation, thus having a decreased activation rate compared to the average post-radiation. We set $\lambda_{I_{12}(pre)} = 27\,\mathrm{day}^{-1}$ and $\lambda_{I_{12}(post)} = 123\,\mathrm{day}^{-1}$ to represent this in our model and obtain the tumor simulation as seen in Figure 7.7.

We see that the fit to data points is much better. Similarly, we can fit the activation rate of T cells and the local properties of vasculature in order for the simulation to

(a)



(b)



(c)
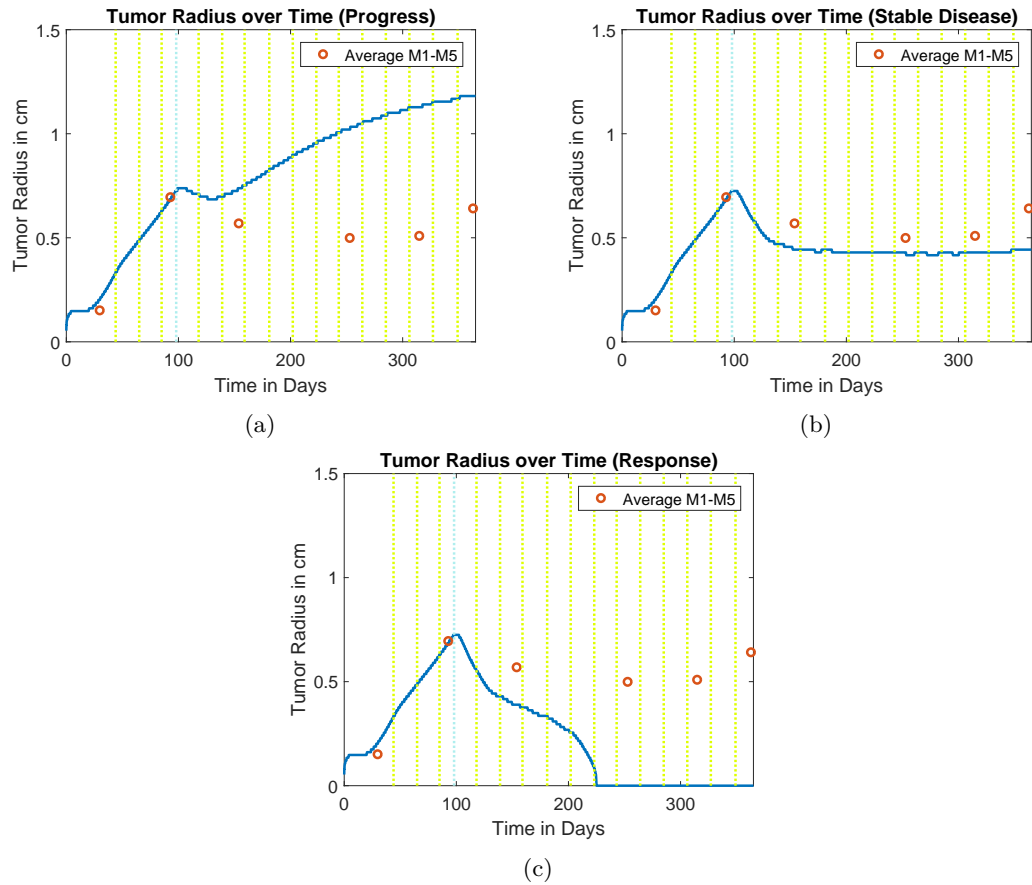
**Figure 7.6:** Exemplary progress (a), stable disease (b) and response (c) behavior under P1 treatment regime for different values of $\lambda_{I_{12}(post)}$ ($83\,\mathrm{day}^{-1}$,$136.25\,\mathrm{day}^{-1}$,$147\,\mathrm{day}^{-1}$ respectively). Graphs show tumor border over time compared to averages of observed measurements M1-M5 (red circles) for reference. Source: Own work in conjunction with data provided by *E. Dippel*.

represent a single metastasis better. This makes even more evident the need to consider metastases individually to really understand the dynamics at play from a medicinal point of view.

We have already demonstrated through simulations (Figures 7.6a - 7.6c) that the model is able to emulate all relevant tumor behaviors. We want to cement this by examining our data sets P2,P3. Moving on to other patients, we want to - one last time - emphasize the special status of data set P1. We were reasonably able to start simulations from the
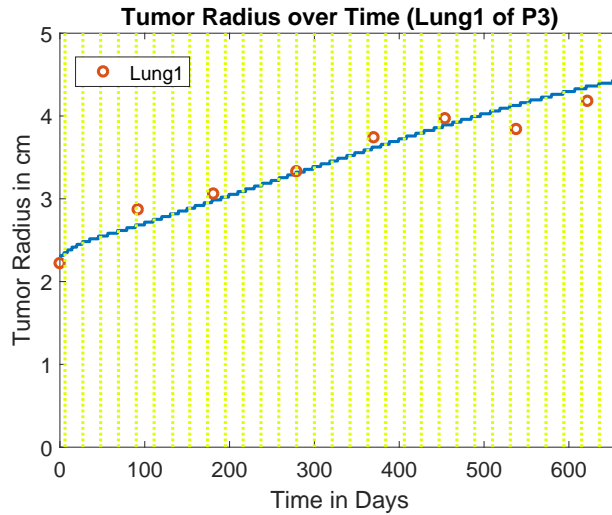
**Figure 7.7:** Tumor radius over time from simulation of model (7.2) - (7.8) with appropriate
parameters as outlined (including treatment regime of P1). The activation of T
cells was fitted to better represent the growth behavior of M1 in P1. Measurements
for M1 are given for comparison as red circles. Source: Own work in conjunction
with data provided by *E. Dippel.*

initiation of angiogenesis as metastases occur just before the first treatment cycle. Due
to this timing and the aggressive nature of the cancer we were able to confidently exclude
effects from previous treatments.

In the case of P2,P3 the circumstances are different. The metastases we track during
*Pembrolizumab* treatment had existed previously and underwent a variety of treatments
(not all of which were well documented). In the case of P2,P3 we run a control case simu-
lation until the tumor reaches the radius (size) observed at $t = 0$ and then use these values
as initial conditions. This poses the problem that we have a naturally grown structure of
the tumor at $t = 0$, where in reality the structure might be adapted or distorted due to
treatment effects. In a model that emphasizes the tumor structure and dynamics between
cell populations spatially, this might pose a problem and we should keep that in mind
discussing results. Nonetheless, this is our best approach and we employ it for simulations.

As in Chapter 6, we start with P3. We will not demonstrate the fit of each metastasis
here, but showcase process of simulation and fit for one exemplary lung metastasis Lung1.
As in Chapter 6 we have to adjust some parameters. From above we know the average
pulmonary blood volume and the average volume of a lung, so we can calculate the

approximate percentage of vascular cells, $vper_{pul}$ in the lung as about:

$$vper_{pul} \approx \frac{450}{5858} \approx 0.077$$

As for P1 this enables us to deduce the increase of anti-PD-1 concentration in each treatment cycle from the value we used for our Ordinary Differential Equation approach:

$$2.5 \times 10^{-6}\,\mathrm{g/cm}^3 \times \frac{1}{0.077} \approx 3.2 \times 10^{-5}\,\mathrm{g/cm}^3$$

As lung tissue is a high vasculature environment [41], we leave the parameters $\lambda_V$, $\alpha_{PQ}$, $\alpha_{QN}$ and the initial vascular cell density unchanged. As in the Ordinary Differential Equation case we reduce the rate of proliferation for proliferating cancer cells. We reduce it by the same fraction and set $\lambda_P = 2.1\,\mathrm{day}^{-1}$. The results can be seen in Figure 7.8 for $\lambda_{I_{12}} = 57\,\mathrm{day}^{-1}$. We can see that the fit is quite good for Lung1 of P3 as well, since



**Figure 7.8:** Tumor radius over time from simulation of model (7.2) - (7.8) with appropriate parameters and initial conditions as outlined (including treatment regime of P3). Measurements for Lung1 of P3 are given for comparison as red circles. Source: Own work in conjunction with data provided by *E. Dippel*.

the model captures the slowing progress with continuous anti-PD-1 treatment. While it doesn't hit the data points perfectly, it comes pretty close and most importantly the growth of tumor radius (and thus size) slows with progressing time. An improved screening/fitting process might produce better adjusted parameters for the vascular environment to maybe produce a better fit. However, as noted above, the data is to be handled with care and above else it is important for us to see, that the model is able to

reproduce the core dynamics seen in tumor behavior of our data set. It is also interesting to evaluate a metastasis of this size as compared to the smaller brain metastases of P1.



(a)

(b)
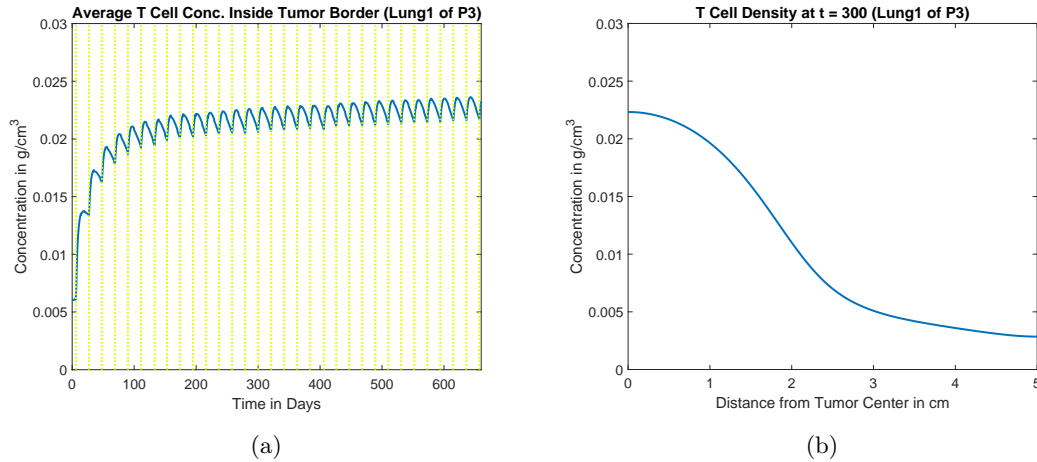
**Figure 7.9:** T cell concentration over time throughout entire simulation of Figure 7.8 (a) and spatial distribution of T cells at exemplary timepoint $t = 300$. The simulation was conducted with appropriate parameters as outlined in this Chapter and with the specific *Pembrolizumab* treatment regime of P3. Source: Own work in conjunction with data provided by *E. Dippel*.

Another thing we can highlight is the distribution of T cells. As broadly discussed in this Chapter and Chapter 2, T cell movement and distribution appears to be quite complex. In Figure 7.9a we can see the average T cell concentration for Lung1 of P3 over time inside the defined tumor border. The behavior of this average T cell concentration is very reminiscent of the Ordinary Differential Equation model (see Section 6.3) and even displays similar levels. However, looking at Figure 7.9b, we can see that the distribution of T cells is very heterogeneous on our domain. Figure 7.9b is an exemplary snapshot at $t = 300$, but the distribution is similar at other times[13]. Also, we have further introduced a T cell dynamic not explicitly seen in these Figures: T cells attack proliferating cancer cells much more aggressively than quiescent cancer cells and they do not attack necrotic cancer cells at all. That means we have increased T cell activity near the border, where the density of proliferating cancer cells is highest. This mimics the attraction of T cells toward active cancer cells. The accumulation of T cells toward the center of the tumor stems from high densities of vascular cells, which the tumor builds up to sustain growth.

---

[13]This behavior is not exclusive to the special case of Lung1 of P3, but can be observed in other simulations as well. The exact behavior depends on choice of parameter set among others, but the qualitative behavior seen in Figure 7.9b is similar in other simulations

Moving on to P2, we can see in Appendix C, that only two metastases were observed during *Pembrolizumab* treatment, one of which is a brain metastasis displaying typical stable disease behavior. We know that our model is able to emulate stable disease in a brain environment. Therefore, we turn to the other metastasis of P2, which is a lymph node and something very different. We have seen in Chapters 2 and 3, that lymph nodes take a special place when it comes to melanoma (and indeed all cancers). The metastatic lymph node is not from the first onset of metastasis in the patient history of P2, as it appears several months after first diagnosis of metastatic melanoma (with distant metastasis). However, this does not really matter for our model as we are merely interested in the behavior under an anti-PD-1 treatment regime. Lymph nodes introduce another complication in our model and data handling, as the lymph node is a preexisting structure and gets bigger with cancerous cells developing.

Another factor may be the role of lymph nodes in the cascade of immune response to cancer. Lymph nodes can be seen as gateways used by T cells when undergoing activation as they move from lymph system into blood vessels [105]. This might lead to a more focused supply of T cells for the tumor microenvironment. A lymph node also displays a very heterogeneous structure and thus, this environment merits some evaluation. In terms of angiogenesis we can turn to the research of *Li et al.* in [68], who produce evidence that a lymph node metastasis behaves similar to metastases in other tissue and induces angiogenesis. In fact, they propose density of vascular cells (blood vessels) in the lymph node as a better diagnostic indicator as opposed to size of the lymph node. This further emphasizes the complexity in evaluating tumor growth in a lymph node, as evidently, cancerous cells develop and cause angiogenesis, before increased size of the lymph node can be observed. As angiogenesis only happens in ("normal") metastases over about 1 mm diameter, this indicates that significant growth may have happened before it can be detected in measurements of the lymph node.

The findings in [65] further underline the special role of blood vessels in the lymph node environment when it comes to cancer. Several indicators for survival are derived concerning the blood vessel structure in the lymph node in [65]. From the results in [68] we can assume a "healthy" vascular cell density of approximately 6.5%. So, we are again dealing with a high vasculature environment as compared to the initial conditions proposed in [41]. It is reasonable to once again employ the same parameter values $\lambda_V$, $\alpha_{PQ}$, $\alpha_{QN}$ and the same initial vascular cell density. It should be noted that while initial vascular cell density played a role in supporting the aggressive cancer of P1, other initial values (e.g. 2% or 7%) do not change our results in the simulations of P2,P3 in a significant manner. This might be, because we let our initial conditions develop naturally in a previous simulation. Therefore, the growth speed in our first simulation is neglected. For our second, main simulation, the tumor has already built up a supporting vascular

structure, so initial vascular cell density does not play a big role. To keep things simple, we stay with initial vascular percentage of 5% and conduct our two-stage simulation.
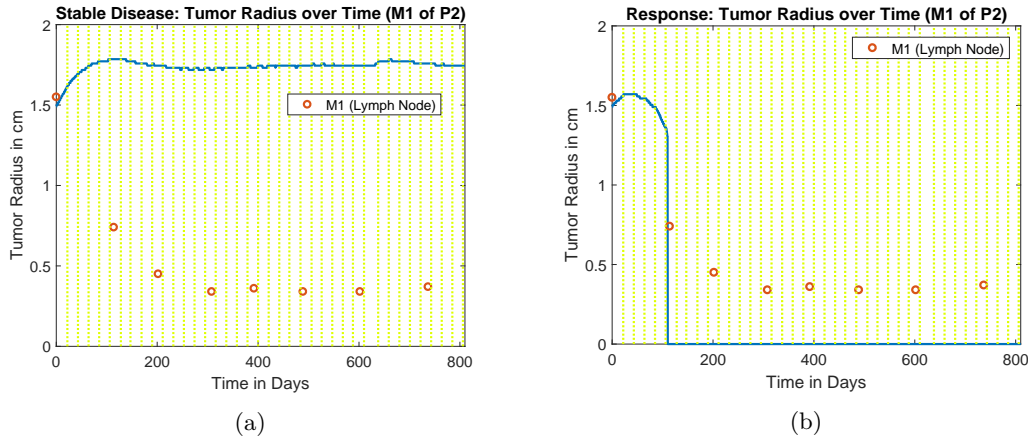


**Figure 7.10:** Simulation for lymph node metastasis of P2 displaying stable disease for $\lambda_{I_{12}} = 57 \, \text{day}^{-1}$ (a) and remission for $\lambda_{I_{12}} = 157 \, \text{day}^{-1}$ (b). Measurements for said metastasis are given for reference (red circles). Source: Own work in conjunction with data provided by *E. Dippel*.

The model had some problems capturing the exact behavior displayed by this lymph node metastasis. It was able to reproduce stable disease, but on a higher level (higher tumor radius) than suggested by data. This can be seen in Figure 7.10a for $\lambda_{I_{12}} = 57 \, \text{day}^{-1}$. It was also able to produce response up to full remission for e.g. $\lambda_{I_{12}} = 157 \, \text{day}^{-1}$ as seen in Figure 7.10b. The behavior of the tumor in this simulation is qualitatively quite similar to previous simulations.

With initiation of therapy the concentration of active cancer cells decreases everywhere as T cells attack the tumor more vigorously. At the same time the tumor adjusts and develops a new constitution which leads to a new surge of growth. If T cells do too much damage the tumor will collapse fully, before it gets new fuel, so to speak. This leads to remission. If treatment initiation merely slows growth we will see further progress - possibly leading to stable disease when the tumor reaches a certain size.

Lastly, if the initial response is not too strong, the tumor may display stable disease (and possibly further growth later on). While this is a simplification of all dynamics involved it roughly captures what is happening in terms of tumor behavior. In the specific case of the lymph node metastasis M1 of P2, the model cannot produce stable disease on a level corresponding to data points. This could have several reasons. For one it could be

attributed to data shortcomings or the special environment, that is a lymph node. The last measurements do not actually deviate from normal lymph node size, so we could in fact be witnessing remission. This emphasizes the problem with measuring lymph node size and using it in quantitative context such as our system of Partial Differential Equations (7.2) - (7.8). It might also indicate some shortcomings of the model not being able to handle a big response into stable disease.

Finally, it is possible that through a more sophisticated screening and fitting process we could find fitting vascular parameters to better represent the behavior.

Despite the problem with the single metastasis M1 of P3, the model gives a very good first step in being able to encompass several key dynamics in a spatial simulation and displaying a good fit as well as the possibility to describe the vastly different responses to anti-PD-1 therapy (ranging from no response to full response). We were able to reproduce the behavior of brain and lung metastases of varying size and emulate a variety of different behaviors, while maintaining the characteristic constitution of a tumor.

To conclude, it should be mentioned that the expression rate of PD-L1 $\epsilon$ also differs between tumors. While this expression may not be a reliable indicator for response and/or survival, the effect of increased expression should not be discarded in its entirety. PD-L1 expression may not be a necessary requisite to allow response or facilitate it, but it is another factor contributing to heterogeneity of tumors. Finally, the precise moment of formation of a tumor and the exact onset of angiogenesis cannot be determined beyond all doubt. We may obtain a starting point for our simulations by calculating backwards from our images with a simple logistic growth approach to get an idea. Especially the two stage simulations adopted for P2,P3 are not necessarily representative as the observed metastases had previously existed and different treatments had been applied. The fit to data can further be improved by simulating from different starting points and then adjusting parameters; this does neither add to nor take away from our results, but should be mentioned for completion's sake as another small factor of uncertainty linked to incomplete data.

# Chapter 8

# Conclusion and Outlook

Both the Ordinary Differential Equation model and the Partial Differential Equation model were able to display the qualitative behavior of tumor burden and single metastasis well. Whereas the former is more suited to represent the overall tumor burden in a larger volume, the latter was able to - through the utilization of spatial dynamics - recreate the growth of single metastases. The assumption of homogeneous constitution and "well-mixedness" of an Ordinary Differential Equation approach comes with some drawbacks, and it became evident, that to really understand the tumor dynamics of one single tumor it is not sufficient. The Ordinary Differential Equation model gave strong indication, that the effect of adjuvant therapy plays an important role and should not be discarded from further examinations. This complicates things somewhat, as a number of adjuvant therapy options are still used and their interplay with anti-PD-1 medication is not fully understood.

The Partial Differential Equation model was able to, through the inclusion of vascular cells, simulate the restrictions on oxygen and nutrients in a more detailed way. The way the tumor undergoes angiogenesis depends on several factors and the model showed modified responses to T cell activity with the tumor adapting and developing a different vascular structure. Especially interesting was the fact that the simulation was able to show initial stable disease for several weeks and even months with the tumor slowly adapting its constitution to adjust to increased T cell activity (e.g. post anti-PD-1 treatment initiation). This might indicate that the tumor in reality is able to adapt, which manifests as acquired resistance to treatment. This can happen through additional mutations or simply due to the fact that the dynamics between vascular and cancer cells change with increased T cell activity (as in our model). This may offer some interesting paths of further research - overall the dynamics with vasculature proved to be crucial in tumor growth and development (with the model responding drastically to changes in vasculature properties) indicating the key role the location of metastasis plays.

Both models were set up to examine dynamics with zero to low PD-L1 expressions and both models were able to display good response to anti-PD-1 treatment. The models explain this response with an inhibition of the self-regulation of the immune system, with

cells such as T cells or cytokines also expressing PD-L1. Ultimately not only the evasion mechanism of the tumor (PD-L1 expression) is affected, but the immune system appears to be put in overdrive and is thus better able to combat the cancer in relevant locations. This may explain, why patients or single tumors with no PD-L1 expression show response to anti-PD-1 medication. As for limitations, it should be noted that our models are fully deterministic, which is justifiable with high cell populations, but somehow violates the key component of cancer. It is after all caused by a single random mutation. Especially in the early stages, random behavior may still play a large role and affect growth. Further (apparent) randomness is introduced through the behavior of T cells which varies greatly (see below). In addition, the measurements for smaller size metastases are unreliable. For our heterogeneous modeling approach, we assumed perfect spheres in terms of tumor shape, which is far from reality, as was already seen and broadly discussed in Chapter 5. Complex shapes can have an impact on growth behavior and the evolution of blood vessels in the tumor.

In terms of moving forward it may be of interest to evaluate the role of blood circulation as an indicator over local percentage of volume occupied by vascular cells. If a lower volume blood vessel has increased blood flow, more T cells (and medication) may nonetheless be able to arrive at such locations. This is supported by the fact that simulations in the brain showed improved fit with a higher vasculature percentage than was calculated. Another factor is tumor density. Our model only reacts implicitly to tumor density. If T cell activity is increased the tumor cell concentration is attacked at each point of the tumor. Through this change, growth is no longer supported and the tumor shrinks. It may be worthwhile to explore explicit effects and examine if some tumors show a more solid constitution through higher cell density and if this is related to improved response to treatment as T cells may be able to move less freely.

Lastly, it became evident, that T cell movement is very complex and pushes the limits of a "simple" Partial Differential Equation model. While we were able to account for the complexity of T cell activity through our spatial dynamics and increased killing rate for proliferating cells, this is still a strong simplification. This is a call to both mathematics and medicine to better understand the behavior of T cells and to explore further ways of modeling said behavior.

To conclude this thesis, we revisit a statement from Chapter 3. It is an often stated hope in the oncology community, that given time, treatment methods such as surgery or chemotherapy, used widely today, will become increasingly irrelevant as research gives rise to better treatment options. Targeted therapy and immunotherapy are precision tools exploiting the understanding of cancer obtained in decades of research, whereas chemotherapy, radiation therapy and surgery appear blunter. To further hone these

precision tools, a better and more detailed understanding of cancer and the dynamics at play is of vital importance and we can only keep research standards high and hope that a day is not too far off, where we can treat cancer by applying targeted treatment that roots it out completely. It is my sincere hope, that through this thesis a stepping stone (however small it may be) was created to further move in this direction.

# Appendix A: Overview over Staging Classification of Malignant Melanoma

Staging classification of malignant melanoma; Figure on the next page. Source: [3]

## A m e r i c a n   J o i n t   C o m m i t t e e   o n   C a n c e r

# Melanoma of the Skin Staging

7th EDITION

### Definitions

#### Primary Tumor (T)

**TX** Primary tumor cannot be assessed (for example, curettaged or severely regressed melanoma)

**T0** No evidence of primary tumor

**Tis** Melanoma in situ

**T1** Melanomas 1.0 mm or less in thickness

**T2** Melanomas 1.01–2.0 mm

**T3** Melanomas 2.01–4.0 mm

**T4** Melanomas more than 4.0 mm

**NOTE:** a and b subcategories of T are assigned based on ulceration and number of mitoses per $mm^2$, as shown below:

| T CLASSIFICATION | THICKNESS (mm) | ULCERATION STATUS/MITOSES |
|---|---|---|
| T1 | ≤1.0 | a: w/o ulceration and mitosis $<1/mm^2$<br>b: with ulceration or mitoses $≥1/mm^2$ |
| T2 | 1.01–2.0 | a: w/o ulceration<br>b: with ulceration |
| T3 | 2.01–4.0 | a: w/o ulceration<br>b: with ulceration |
| T4 | >4.0 | a: w/o ulceration<br>b: with ulceration |

#### Regional Lymph Nodes (N)

**NX** Patients in whom the regional nodes cannot be assessed (for example, previously removed for another reason)

**N0** No regional metastases detected

**N1-3** Regional metastases based upon the number of metastatic nodes and presence or absence of intralymphatic metastases (in transit or satellite metastases)

**NOTE:** N1–3 and a–c subcategories assigned as shown below:

| N CLASSIFICATION | NO. OF METASTATIC NODES | NODAL METASTATIC MASS |
|---|---|---|
| N1 | 1 node | a: micrometastasis[1]<br>b: macrometastasis[2] |
| N2 | 2–3 nodes | a: micrometastasis[1]<br>b: macrometastasis[2]<br>c: in transit met(s)/satellite(s) *without* metastatic nodes |
| N3 | 4 or more metastatic nodes, or matted nodes, or in transit met(s)/satellite(s) with metastatic node(s) | |

**ajcc**®

**American Cancer Society**®

Financial support for AJCC
7th Edition Staging Posters
provided by the American Cancer Society
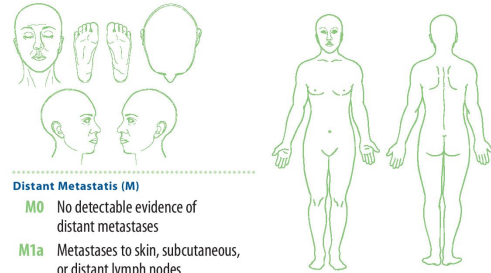
#### Distant Metastatis (M)

**M0** No detectable evidence of distant metastases

**M1a** Metastases to skin, subcutaneous, or distant lymph nodes

**M1b** Metastases to lung

**M1c** Metastases to all other visceral sites or distant metastases to any site combined with an elevated serum LDH

**NOTE:** Serum LDH is incorporated into the M category as shown below:

| M CLASSIFICATION | SITE | SERUM LDH |
|---|---|---|
| M1a | Distant skin, subcutaneous, or nodal mets | Normal |
| M1b | Lung metastases | Normal |
| M1c | All other visceral metastases | Normal |
| | Any distant metastasis | Elevated |

| ANATOMIC STAGE/PROGNOSTIC GROUPS | | | | | | |
|---|---|---|---|---|---|---|
| Clinical Staging[1] | | | | Pathologic Staging[4] | | |
| Stage 0 | Tis | N0 | M0 | 0 | Tis | N0 | M0 |
| Stage IA | T1a | N0 | M0 | IA | T1a | N0 | M0 |
| Stage IB | T1b | N0 | M0 | IB | T1b | N0 | M0 |
| | T2a | N0 | M0 | | T2a | N0 | M0 |
| Stage IIA | T2b | N0 | M0 | IIA | T2b | N0 | M0 |
| | T3a | N0 | M0 | | T3a | N0 | M0 |
| Stage IIB | T3b | N0 | M0 | IIB | T3b | N0 | M0 |
| | T4a | N0 | M0 | | T4a | N0 | M0 |
| Stage IIC | T4b | N0 | M0 | IIC | T4b | N0 | M0 |
| Stage III | Any T | ≥ N1 | M0 | IIIA | T1-4a | N1a | M0 |
| | | | | | T1-4a | N2a | M0 |
| | | | | IIIB | T1-4b | N1a | M0 |
| | | | | | T1-4b | N2a | M0 |
| | | | | | T1-4a | N1b | M0 |
| | | | | | T1-4a | N2b | M0 |
| | | | | | T1-4a | N2c | M0 |
| | | | | IIIC | T1-4b | N1b | M0 |
| | | | | | T1-4b | N2b | M0 |
| | | | | | T1-4b | N2c | M0 |
| | | | | | Any T | N3 | M0 |
| Stage IV | Any T | Any N | M1 | IV | Any T | Any N | M1 |

#### Notes

[1] Micrometastases are diagnosed after sentinel lymph node biopsy and completion lymphadenectomy (if performed).

[2] Macrometastases are defined as clinically detectable nodal metastases confirmed by therapeutic lymphadenectomy or when nodal metastasis exhibits gross extracapsular extension.

[3] Clinical staging includes microstaging of the primary melanoma and clinical/radiologic evaluation for metastases. By convention, it should be used after complete excision of the primary melanoma with clinical assessment for regional and distant metastases.

[4] Pathologic staging includes microstaging of the primary melanoma and pathologic information about the regional lymph nodes after partial or complete lymphadenectomy. Pathologic Stage 0 or Stage IA patients are the exception; they do not require pathologic evaluation of their lymph nodes.

# Appendix B: Approved Drugs For Melanoma Treatment

Overview over FDA approved drugs for melanoma treatment. For more information on each drug (including survival rates in Stage III trials) see [96]. Source: [96]

| Drug, Brand name, Marketed by | Mechanism of action | FDA approval year | Common adverse effects |
|---|---|---|---|
| Dacarbazine, DTIC-Dome, Bayer | It causes DNA damage by methylating the DNA guanines and induces apoptosis | 1975 | Anorexia, nausea, vomiting and in some cases diarrhea |
| IFN-α2b, Intron-A, Merck | It acts by mimicking the action of human IFN-α2b | 1995 | Fatigue, flu-like symptoms and depression |
| Aldesleukin, Proleukin Prometheus Laboratories Inc | It is a highly purified human recombinant IL-2 analog that resembles the functions of human IL-2 | 1998 | Hypotension, reduced renal function and supraventricular tachycardia |
| p-IFN-α2b, Sylatron, Merck | Pegylated-IFN-α2b has enhanced bioavailability compared to IFN-α2b | March, 2011 | Side effect profile is similar to IFN-α2b |
| Vemurafenib, Zelboraf, Roche | It is a selective inhibitor of mutated forms (V600E) of BRAF kinase | August, 2011 | Skin disorders and cutaneous SCC |
| Ipilimumab, Yervoy, Bristol-Myers Squibb | It binds to the negative regulatory CTLA-4 receptors on T-cells and blocks their activity | March, 2011 | Immune-mediated enterocolitis, hepatotoxicity and endocrine disorders |
| Dabrafenib, Tafinlar Novartis | It is a selective inhibitor of mutated forms (V600E) of BRAF kinase | May, 2013 | Similar to vemurafenib |

| | | | |
|---|---|---|---|
| Pembrolizumab Keytruda, Merck | It acts by binding to the PD-1 receptors on T-cells and blocks their activity | September, 2014 | Renal failure, dyspnea, pneumonitis and cellulitis |
| Nivolumab, Opdivo, Bristol-Myers Squibb | It acts by binding to the PD-1 receptors on T-cells and blocks their activity | December, 2014 | Fatigue, diarrhea, nausea, pneumonitis, liver and kidney toxicity |
| Trametinib, Mekinist, Novartis | It is a reversible inhibitor of MAPK, MEK1 and MEK2 | September, 2015 | Rash, diarrhea, lymphedema, hypertension and altered liver function |
| T-VEC, Imlygic, BioVex/Amgen | T-VEC is a live, attenuated, HSV-1 genetically modified to express human GM-CSF in tumor cells | October, 2015 | Cellulitis, fatigue, chills, pyrexia, nausea, influenza-like illness and injection site pain |
| Cobimetinib, Cotellic, Roche | It is a reversible inhibitor of MAPK, MEK1 and MEK2 | November, 2015 | Similar to trametinib |

# Appendix C: Tumor Measurements for Patients P2,P3

Here we present the measurements obtained from P2,P3. It should be noted that measurements are less reliable as compared to P1 due to incomplete information on adjuvant therapy. In case of Lung4 of P3, we can assume excision as the tumor is no longer visible on images and a resection took place around the same time it disappears. Other resections are less clear and this creates the need for caution when handling the data of P3. For P2 we are in the same boat, as adjuvant radiation therapy may distort data (see Chapter 5 and Appendix D).

| Time of Measurement | M1 | M2 |
|:---:|:---:|:---:|
| $t = 0$ | $15\,551\,\mathrm{mm}^3$ | $2945\,\mathrm{mm}^3$ |
| $t = 114$ | $1681\,\mathrm{mm}^3$ | $302\,\mathrm{mm}^3$ |
| $t = 202$ | $385\,\mathrm{mm}^3$ | $170\,\mathrm{mm}^3$ |
| $t = 308$ | $165\,\mathrm{mm}^3$ | $157\,\mathrm{mm}^3$ |
| $t = 392$ | $197\,\mathrm{mm}^3$ | $161\,\mathrm{mm}^3$ |
| $t = 489$ | $160\,\mathrm{mm}^3$ | $158\,\mathrm{mm}^3$ |
| $t = 602$ | $170\,\mathrm{mm}^3$ | $183\,\mathrm{mm}^3$ |
| $t = 737$ | $206\,\mathrm{mm}^3$ | $177\,\mathrm{mm}^3$ |

Measurement data of metastases M1-M2 of P2, including time of measurement and size of metastases. Source: Own work in conjunction with data provided by *E. Dippel.*

| Time of Measurement | Lung1 | Lung2 | Lung3 | Lung4 |
|:---:|:---:|:---:|:---:|:---:|
| $t = 0$ | $45\,616\,\text{mm}^3$ | $20\,580\,\text{mm}^3$ | $65\,928\,\text{mm}^3$ | $65\,928\,\text{mm}^3$ |
| $t = 92$ | $98\,543\,\text{mm}^3$ | $4241\,\text{mm}^3$ | $90\,612\,\text{mm}^3$ | $3780\,\text{mm}^3$ |
| $t = 181$ | $119\,866\,\text{mm}^3$ | $1357\,\text{mm}^3$ | $152\,966\,\text{mm}^3$ | $2949\,\text{mm}^3$ |
| $t = 279$ | $155\,094\,\text{mm}^3$ | $1077\,\text{mm}^3$ | $182\,160\,\text{mm}^3$ | $2053\,\text{mm}^3$ |
| $t = 370$ | $218\,590\,\text{mm}^3$ | $838\,\text{mm}^3$ | $164\,217\,\text{mm}^3$ | $9651\,\text{mm}^3$ |
| $t = 454$ | $261\,307\,\text{mm}^3$ | $785\,\text{mm}^3$ | $271\,434\,\text{mm}^3$ | $0\,\text{mm}^3$ |
| $t = 538$ | $237\,394\,\text{mm}^3$ | $679\,\text{mm}^3$ | $326\,356\,\text{mm}^3$ | $0\,\text{mm}^3$ |
| $t = 622$ | $306\,928\,\text{mm}^3$ | $594\,\text{mm}^3$ | $329\,702\,\text{mm}^3$ | $0\,\text{mm}^3$ |

Measurement data of metastases of P3 (Lung1 - Lung5), including time of measurement and size of metastases. Source: Own work in conjunction with data provided by *E. Dippel.*

| Time of Measurement | Lung5 | Mediastinum | Mammaria |
|:---:|:---:|:---:|:---:|
| $t = 0$ | $10\,973\,\text{mm}^3$ | $467\,\text{mm}^3$ | $10\,145\,\text{mm}^3$ |
| $t = 92$ | $551\,\text{mm}^3$ | $416\,\text{mm}^3$ | $4241\,\text{mm}^3$ |
| $t = 181$ | $105\,\text{mm}^3$ | $369\,\text{mm}^3$ | $468\,\text{mm}^3$ |
| $t = 279$ | $0\,\text{mm}^3$ | $785\,\text{mm}^3$ | $92\,\text{mm}^3$ |
| $t = 370$ | $0\,\text{mm}^3$ | $1357\,\text{mm}^3$ | $59\,\text{mm}^3$ |
| $t = 454$ | $0\,\text{mm}^3$ | $1140\,\text{mm}^3$ | $28\,\text{mm}^3$ |
| $t = 538$ | $0\,\text{mm}^3$ | $1638\,\text{mm}^3$ | $21\,\text{mm}^3$ |
| $t = 622$ | $0\,\text{mm}^3$ | $1770\,\text{mm}^3$ | $19\,\text{mm}^3$ |

Measurement data of metastases of P3 (Lung5, Mediastinum, Mammaria), including time of measurement and size of metastases. Source: Own work in conjunction with data provided by *E. Dippel.*

# Appendix D: Treatment Regime Data for Patients P2,P3

We present the available data on treatment during the relevant time interval. For previous treatments see Chapter 5. In terms of therapy measures, only treatments, that could at least be roughly attributed to a date, were included in the following tables. As touched upon in Chapter 5, further adjuvant therapies occurred, but the available information is incomplete. Specifically, this includes several resection procedures for P3 in addition to the ones included in the Table below. In the case of P2 it includes radiation therapy of unknown location and time.

| Time of Administration | Cycle, Medication and Amount |
|:---:|:---:|
| $t = 22$ | 1.) Cycle *Pembrolizumab* (2 mg/kg) |
| $t = 43$ | 2.) Cycle *Pembrolizumab* (2 mg/kg) |
| $t = 64$ | 3.) Cycle *Pembrolizumab* (2 mg/kg) |
| $t = 85$ | 4.) Cycle *Pembrolizumab* (2 mg/kg) |
| $t = 106$ | 5.) Cycle *Pembrolizumab* (2 mg/kg) |
| $t = 128$ | 6.) Cycle *Pembrolizumab* (2 mg/kg) |
| $t = 147$ | 7.) Cycle *Pembrolizumab* (2 mg/kg) |
| $t = 169$ | 8.) Cycle *Pembrolizumab* (2 mg/kg) |
| $t = 190$ | 9.) Cycle *Pembrolizumab* (2 mg/kg) |
| $t = 211$ | 10.) Cycle *Pembrolizumab* (2 mg/kg) |
| $t = 232$ | 11.) Cycle *Pembrolizumab* (2 mg/kg) |
| $t = 253$ | 12.) Cycle *Pembrolizumab* (2 mg/kg) |
| $t = 274$ | 13.) Cycle *Pembrolizumab* (2 mg/kg) |
| $t = 295$ | 14.) Cycle *Pembrolizumab* (2 mg/kg) |
| $t = 316$ | 15.) Cycle *Pembrolizumab* (2 mg/kg) |
| $t = 337$ | 16.) Cycle *Pembrolizumab* (2 mg/kg) |
| $t = 358$ | 17.) Cycle *Pembrolizumab* (2 mg/kg) |
| $t = 379$ | 18.) Cycle *Pembrolizumab* (2 mg/kg) |
| $t = 400$ | 19.) Cycle *Pembrolizumab* (2 mg/kg) |
| $t = 421$ | 20.) Cycle *Pembrolizumab* (2 mg/kg) |
| $t = 442$ | 21.) Cycle *Pembrolizumab* (2 mg/kg) |
| $t = 462$ | 22.) Cycle *Pembrolizumab* (2 mg/kg) |
| $t = 484$ | 23.) Cycle *Pembrolizumab* (2 mg/kg) |
| $t = 506$ | 24.) Cycle *Pembrolizumab* (2 mg/kg) |
| $t = 526$ | 25.) Cycle *Pembrolizumab* (2 mg/kg) |
| $t = 547$ | 26.) Cycle *Pembrolizumab* (2 mg/kg) |
| $t = 568$ | 27.) Cycle *Pembrolizumab* (2 mg/kg) |
| $t = 588$ | 28.) Cycle *Pembrolizumab* (2 mg/kg) |
| $t = 610$ | 29.) Cycle *Pembrolizumab* (2 mg/kg) |
| $t = 638$ | 30.) Cycle *Pembrolizumab* (2 mg/kg) |
| $t = 659$ | 31.) Cycle *Pembrolizumab* (2 mg/kg) |
| $t = 680$ | 32.) Cycle *Pembrolizumab* (2 mg/kg) |
| $t = 701$ | 33.) Cycle *Pembrolizumab* (2 mg/kg) |
| $t = 722$ | 34.) Cycle *Pembrolizumab* (2 mg/kg) |
| $t = 743$ | 35.) Cycle *Pembrolizumab* (2 mg/kg) |
| $t = 764$ | 36.) Cycle *Pembrolizumab* (2 mg/kg) |
| $t = 785$ | 37.) Cycle *Pembrolizumab* (2 mg/kg) |
| $t = 806$ | 38.) Cycle *Pembrolizumab* (2 mg/kg) |

Treatment data of P2, including time of treatment, medication administered and amount of medication for each treatment cycle, if applicable. Source: Data provided by *E. Dippel.*

| Time of Administration | Cycle, Medication and Amount |
|---|---|
| $t = 6$ | 1.) Cycle *Pembrolizumab* ($2\,\mathrm{mg/kg}$) |
| $t = 27$ | 2.) Cycle *Pembrolizumab* ($2\,\mathrm{mg/kg}$) |
| $t = 48$ | 3.) Cycle *Pembrolizumab* ($2\,\mathrm{mg/kg}$) |
| $t = 69$ | 4.) Cycle *Pembrolizumab* ($2\,\mathrm{mg/kg}$) |
| $t = 90$ | 5.) Cycle *Pembrolizumab* ($2\,\mathrm{mg/kg}$) |
| $t = 111$ | 6.) Cycle *Pembrolizumab* ($2\,\mathrm{mg/kg}$) |
| $t = 133$ | 7.) Cycle *Pembrolizumab* ($2\,\mathrm{mg/kg}$) |
| $t = 153$ | 8.) Cycle *Pembrolizumab* ($2\,\mathrm{mg/kg}$) |
| $t = 174$ | 9.) Cycle *Pembrolizumab* ($2\,\mathrm{mg/kg}$) |
| $t = 195$ | 10.) Cycle *Pembrolizumab* ($2\,\mathrm{mg/kg}$) |
| $t = 216$ | 11.) Cycle *Pembrolizumab* ($2\,\mathrm{mg/kg}$) |
| $t = 237$ | 12.) Cycle *Pembrolizumab* ($2\,\mathrm{mg/kg}$) |
| $t = 258$ | 13.) Cycle *Pembrolizumab* ($2\,\mathrm{mg/kg}$) |
| $t = 279$ | 14.) Cycle *Pembrolizumab* ($2\,\mathrm{mg/kg}$) |
| $t = 300$ | 15.) Cycle *Pembrolizumab* ($2\,\mathrm{mg/kg}$) |
| $t = 321$ | 16.) Cycle *Pembrolizumab* ($2\,\mathrm{mg/kg}$) |
| $t = 342$ | 17.) Cycle *Pembrolizumab* ($2\,\mathrm{mg/kg}$) |
| $t = 363$ | 18.) Cycle *Pembrolizumab* ($2\,\mathrm{mg/kg}$) |
| $t = 384$ | 19.) Cycle *Pembrolizumab* ($2\,\mathrm{mg/kg}$) |
| $t = 406$ | 20.) Cycle *Pembrolizumab* ($2\,\mathrm{mg/kg}$) |
| *unknown* | 2 separate resections (volume unknown) |
| $t = 426$ | 21.) Cycle *Pembrolizumab* ($2\,\mathrm{mg/kg}$) |
| $t = 447$ | 22.) Cycle *Pembrolizumab* ($2\,\mathrm{mg/kg}$) |
| $t = 468$ | 23.) Cycle *Pembrolizumab* ($2\,\mathrm{mg/kg}$) |
| *unknown* | Further resections (volume unknown) |
| $t = 489$ | 24.) Cycle *Pembrolizumab* ($2\,\mathrm{mg/kg}$) |
| $t = 510$ | 25.) Cycle *Pembrolizumab* ($2\,\mathrm{mg/kg}$) |
| $t = 531$ | 26.) Cycle *Pembrolizumab* ($2\,\mathrm{mg/kg}$) |
| $t = 552$ | 27.) Cycle *Pembrolizumab* ($2\,\mathrm{mg/kg}$) |
| $t = 573$ | 28.) Cycle *Pembrolizumab* ($2\,\mathrm{mg/kg}$) |
| $t = 594$ | 29.) Cycle *Pembrolizumab* ($2\,\mathrm{mg/kg}$) |
| $t = 615$ | 30.) Cycle *Pembrolizumab* ($2\,\mathrm{mg/kg}$) |
| $t = 636$ | 31.) Cycle *Pembrolizumab* ($2\,\mathrm{mg/kg}$) |
| $t = 657$ | 32.) Cycle *Pembrolizumab* ($2\,\mathrm{mg/kg}$) |

Treatment data of P3, including time of treatment, medication administered and amount of medication for each treatment cycle, if applicable. Source: Data provided by *E. Dippel.*

# Appendix E: MATLAB Codes Used in This Thesis

**Listing 1**

This function runs an optimization for activation rate of T cells $\lambda_{I_{12}}$ and then plots the results. For this it utilizes a function simulating the system of Ordinary Differential Equations (6.3) - (6.6) dependent on $\lambda_{I_{12}}$. In this case all of this is tailored to timeline, measurements and treatment regime of P1. It can easily be adjusted to work for other data.

```matlab
    function fit_para = fit_P1_lamI12()
    %runs optimization for parameter fitting through fminsearch. Fits to data
    %set P1

5   %initial value for optimization
    k_0 = 10;

    %run optimization
    k_fit = fminsearch(@simulation_P1_dep_lamI12,k_0);
10  fit_para = k_fit;

    %simulate system with fitted parameter lambda_I12
    sol_for_sim = only_sim_P1_dep_lamI12(k_fit);

15  %timepoints for treatment cycles
    timepoints_med = [14 35 55 88 109 129 151 172 193 213 234 255 276 297 ...
        ↪ 319];
    %timepoints for measurements
    timepoints_pic = [0 63 124 223 285 333];
    %concentration of cancer cells obtained from data increased by factor ...
        ↪ of 10
20  measurements_pic = [3.54E-03 2.11E-01 1.20E-01 8.39E-02 1.03E-01 ...
        ↪ 1.22E-01];

    %plot results
    figure
    subplot(1,2,1)
25  plot(sol_for_sim(:,1),sol_for_sim(:,2))
    hold on
    scatter(timepoints_pic,measurements_pic)
```

```matlab
     for i = 1:length(timepoints_med)
         line([timepoints_med(i) timepoints_med(i)], [0 0.4], ...
             ↪ 'LineWidth',2,'Color',[223/255 255/255 ...
             ↪ 0/255],'LineStyle',':')
30   end
  hold off
  title('Cancer Cells')

  subplot(1,2,2)
35 plot(sol_for_sim(:,1),sol_for_sim(:,3))
  hold on
     for i = 1:length(timepoints_med)
         line([timepoints_med(i) timepoints_med(i)], [0 0.035], ...
             ↪ 'LineWidth',2,'Color',[223/255 255/255 ...
             ↪ 0/255],'LineStyle',':')
     end
40 hold off
  title('T Cells')

  end
```

## Listing 2

This function simulates the system of Ordinary Differential Equations (6.3) - (6.6) for a given set of parameters. In this case all of this is tailored to timeline, measurements and treatment regime of P1. It can easily be adjusted to work for other data. The function demonstrated here performs a two-stage simulation separated by radiation therapy, as P1 receives adjuvant radiation therapy. This concept can be simplified into a one stage simulation or further extended.

```matlab
   function [ output ] = only_sim_P1_dep_lamI12_inclrad()
   %runs simulation of ODE system for P1 treatment regime including ...
       ↪ effect of
   %adjuvant radiation. This is included through eradication of cancer cells
   %and increased parameter lambda_I12 post radiation.
5
   %initial conditions
   ini_T = 0.0006;
   roh_P = 2.49e-7;
   ini_PD = roh_P * ini_T;
10 ini = [3.54E-03, ini_T, 0, ini_PD];

   %increase in anti-PD-1 concentration in each treatment cycle
   medicine = 0.000015;
   %percentage of cancer cells killed by radiation
15 radio_perc = 0.5;

   %timepoints for measurements
   timepoints_pic = [0 63 124 223 285 333];
   %concentration of cancer cells obtained from data increased by factor ...
       ↪ of 10
20 measurements_pic = [3.54E-03 2.11E-01 1.20E-01 8.39E-02 1.03E-01 ...
       ↪ 1.22E-01];
   %timepoints for treatment cycles
   timepoints_med = [14 35 55 88 109 129 151 172 193 213 234 255 276 297 ...
       ↪ 319 333];
   %timepoints for treatment cycles including timepoint for radiation
   timepoints_med_incl_radio = [14 35 55 68 88 109 129 151 172 193 213 ...
       ↪ 234 255 276 297 319 333];
25
   %timevector for first simulation iteration
   t_ode = [0 timepoints_med(1)];

   %simulation for each interval between treatments
30 for i = 0:length(timepoints_med_incl_radio)-1
       %under 4 -> pre radiation, 4 and over -> post radiation
       if i < 4
           [sol_ti, sol_yi] = ode45(@Melanoma_ODE, t_ode, ini);
       else
```

```matlab
35          [sol_ti, sol_yi] = ode45(@Melanoma_ODE_postrad, t_ode, ini);
       end
       if i == 0
           sol_t = sol_ti;
           sol_y = sol_yi;
40     else
           sol_ti = sol_ti + timepoints_med_incl_radio(i);
           sol_y = sol_y(1:end-1,:);
           sol_t = sol_t(1:end-1);

45         %add solution of current interval to overall solution
           sol_t = vertcat(sol_t,sol_ti);
           sol_y = vertcat(sol_y,sol_yi);
       end

50     %create timevector for next simulation iteration
       if i < length(timepoints_med_incl_radio)-1
           new_endpoint = timepoints_med_incl_radio(i+2) - ...
               ↪ timepoints_med_incl_radio(i+1);
           t_ode =[0 new_endpoint];
       end
55
       %killing of cancer cells due to radiation and new initial conditions
       if i == 3
           transfer1 = sol_yi(:,1);
           ini(1) = transfer1(end)*(1-radio_perc);
60
           transfer2 = sol_yi(:,2);
           ini(2) = transfer2(end);

           transfer3 = sol_yi(:,3);
65         ini(3) = transfer3(end);

           transfer4 = sol_yi(:,4);
           ini(4) = transfer4(end);
       else
70         transfer1 = sol_yi(:,1);
           ini(1) = transfer1(end);

           transfer2 = sol_yi(:,2);
           ini(2) = transfer2(end);
75
           transfer3 = sol_yi(:,3);
           ini(3) = transfer3(end) + medicine;

           transfer4 = sol_yi(:,4);
80         ini(4) = transfer4(end);
       end
   end
```

```matlab
    output = [sol_t sol_y(:,1) sol_y(:,2)];
85
    %plot results
    figure
    subplot(1,2,1)
    hold on
90  for i = 1:length(timepoints_med)-1
        line([timepoints_med(i) timepoints_med(i)], [0 0.4], ...
            ↪ 'LineWidth',2,'Color',[223/255 255/255 0/255],'LineStyle',':')
    end
    line([68 68], [0 0.4], 'LineWidth',2,'Color',[175/255 238/255 ...
        ↪ 238/255],'LineStyle',':')
    plot(sol_t,sol_y(:,1),'b')
95  scatter(timepoints_pic,measurements_pic,'red','x')
    hold off

    subplot(1,2,2)
    hold on
100 for i = 1:length(timepoints_med)-1
        line([timepoints_med(i) timepoints_med(i)], [0 0.035], ...
            ↪ 'LineWidth',2,'Color',[223/255 255/255 0/255],'LineStyle',':')
    end
    line([68 68], [0 0.035], 'LineWidth',2,'Color',[175/255 238/255 ...
        ↪ 238/255],'LineStyle',':')
    plot(sol_t,sol_y(:,2),'b')
105 title('With Radiation: T Cell Concentration over Time (P1)')
    xlabel('Time in Days')
    ylabel('Concentration in g/cm^3')


110 function dydt = Melanoma_ODE(t,y)

    lambda_c = 0.9; %proliferation rate cancer cells
    eta = 23; %killing rate T cells
    C_M = 0.4766; %carrying capacity for cancer cells
115 roh_P = 2.49e-7; %expression rate PD-1 of T cells
    lambda_T_I12 = 10; %activation of T cells
    T_0  = 2e-3; %concentration of naive T cells
    I_12 = 1.5e-10; %concentration IL-12
    K_I12 = 1.5e-10; %half saturation IL-12
120 lambda_T_I2 = 0.25; %proliferation T cells
    I_2 = 2.37e-11; %concentration IL-2
    K_I2 = 2.37e-11; %half saturation IL-12
    K_TQhat = 1.365e-18; %inhibition of T cells
    roh_L = 5.22e-7; %expression of PD-L1 on T cells
125 eps = 0.01; %expression PD-L1 on tumor cells (realtive to T cells)
    d_t = 0.191; %death rate T cells
    mu_PA = 2.1e5; %depletion of anti-PD-1 through PD-1
    d_A = 0.027; %decay of anti-PD-1
```

109

```matlab
130  %ODE system
     dydt = zeros(4,1);
     dydt(1) = lambda_c * y(1) * (1 - y(1)/C_M) - eta * y(1) * y(2);
     dydt(2) = (lambda_T_I12 * T_0 * (I_12/(K_I12 + I_12)) + lambda_T_I2 * ...
         ↪ y(2) * (I_2/(K_I2 + I_2))) * 1/(1 + (y(4) * (roh_L * (y(2) + ...
         ↪ eps * y(1))))/K_TQhat) - d_t * y(2);
     dydt(3) = - mu_PA * y(3) * y(4) - d_A * y(3);
135  dydt(4) = roh_P * (lambda_T_I12 * T_0 * (I_12/(K_I12 + I_12)) + ...
         ↪ lambda_T_I2 * y(2) * (I_2/(K_I2 + I_2))) * 1/(1 + (y(4) * ...
         ↪ (roh_L * (y(2) + eps * y(1))))/K_TQhat) - d_t * y(4) - mu_PA * ...
         ↪ y(3) * y(4);
     end

     function dydt = Melanoma_ODE_postrad(t,y)
     lambda_c = 0.9; %proliferation rate cancer cells
140  eta = 23; %killing rate T cells
     C_M = 0.4766; %carrying capacity for cancer cells
     roh_P = 2.49e-7; %expression rate PD-1 of T cells
     lambda_T_I12 = 21; %activation of T cells
     T_0  = 2e-3; %concentration of naive T cells
145  I_12 = 1.5e-10; %concentration IL-12
     K_I12 = 1.5e-10; %half saturation IL-12
     lambda_T_I2 = 0.25; %proliferation T cells
     I_2 = 2.37e-11; %concentration IL-2
     K_I2 = 2.37e-11; %half saturation IL-12
150  K_TQhat = 1.365e-18; %inhibition of T cells
     roh_L = 5.22e-7; %expression of PD-L1 on T cells
     eps = 0.01; %expression PD-L1 on tumor cells (realtive to T cells)
     d_t = 0.191; %death rate T cells
     mu_PA = 2.1e5; %depletion of anti-PD-1 through PD-1
155  d_A = 0.027; %decay of anti-PD-1

     %ODE system
     dydt = zeros(4,1);
     dydt(1) = lambda_c * y(1) * (1 - y(1)/C_M) - eta * y(1) * y(2);
160  dydt(2) = (lambda_T_I12 * T_0 * (I_12/(K_I12 + I_12)) + lambda_T_I2 * ...
         ↪ y(2) * (I_2/(K_I2 + I_2))) * 1/(1 + (y(4) * (roh_L * (y(2) + ...
         ↪ eps * y(1))))/K_TQhat) - d_t * y(2);
     dydt(3) = - mu_PA * y(3) * y(4) - d_A * y(3);
     dydt(4) = roh_P * (lambda_T_I12 * T_0 * (I_12/(K_I12 + I_12)) + ...
         ↪ lambda_T_I2 * y(2) * (I_2/(K_I2 + I_2))) * 1/(1 + (y(4) * ...
         ↪ (roh_L * (y(2) + eps * y(1))))/K_TQhat) - d_t * y(4) - mu_PA * ...
         ↪ y(3) * y(4);
     end

165
     end
```

## Listing 3

Simple script to plot data.

```matlab
%Measurement Data in mm^3
M1 = [14 1569 474 498 1248 1759];
M2 = [14 1553 1053 418 284 587];
M3 = [0 1618 614 510 260 879];
M4 = [0 1527 658 408 290 1363];
M5 = [0 940 1198 772 1084 1149];

%Timepoints at which measurements were taken
timepoints_pic = [0 63 124 223 285 333];

%Plotting
plot(timepoints_pic,M1,'Linewidth',2)
hold on
plot(timepoints_pic,M2,'Linewidth',2)
plot(timepoints_pic,M3,'Linewidth',2)
plot(timepoints_pic,M4,'Linewidth',2)
plot(timepoints_pic,M5,'Linewidth',2)
hold off
h = legend('M1','M2','M3','M4','M5');
title('Tracking 5 Exemplary Metastases over Time (P1)')
xlabel('Time in Days')
ylabel('Volume in mm^3')
```

**Listing 4**

Implementation of Thomas Algorithm to solve a system of linear equations, when the system can be represented as a tridiagonal matrix.

```matlab
function y = thomas( a1, a2, a3, b )
%implementation of the thomas algorithm. a1 is main diagonal, a2 is ...
    ↪ first diagonal below, a3 is first diagonal above. a2 needs an ...
    ↪ additional 0 in the beginning. a3 needs and additional 0 at the ...
    ↪ end. b is the right hand side of the linear system of equations.

n = length(b);
v = zeros(n,1);
y = v;
w = a1(1);
y(1) = b(1)/w;
for i=2:n
    v(i-1) = a3(i-1)/w;
    w = a1(i) - a2(i)*v(i-1);
    y(i) = ( b(i) - a2(i)*y(i-1) )/w;
end
for j=n-1:-1:1
    y(j) = y(j) - v(j)*y(j+1);
end
end
```

**Listing 5**

Implementation of Crank-Nicolson method to simulate the system of Partial Differential Equations (7.2) - (7.8) with a certain set of parameters. Once again, in this case all of this is tailored to timeline, measurements and treatment regime of P1. It can easily be adjusted to work for other data. This type of function is used throughout the thesis in several variations, but the underlying method remains as outlined here. It can also be extended to a multiple stage simulation (as was utilized to obtain proper initial conditions for simulations in Chapter 7). We can further combine it with an appropriate function to create a similar mechanism as created through Listing 1 and Listing 2 and conduct parameter fitting.

```
     function [ output ] = P1_compare_to_data()
     %simulates PDE model and compares tumor border over time to P1 data.
     %Can beused for simple fitting by including calculation of square
     %error and set it as output, which can then be optimized.
5
     %clc;
     %clear all;

     %I. Modular
10   %Death term without vasculature (eta P T) -> check1 = 0, d
     %eath term with vasculature (eta P T V) -> check1 = 1
     check1 = 0;

     %II. Modular
15   %Exclude medicine (treatment free environment) -> check2 = 0,
     %include medicine (treatment regime of P1) -> check2 = 1
     check2 = 1;

     %III. Modular
20   %Insert medicine everywhere equally -> check3 = 0, insert
     %medicine over vasculature (increase concentration proportionally
     %to vasculature) -> check3 = 1
     check3 = 1;

25   %IV. Modular
     %Use  only p/(q) in death term for T cells (eta P T)
     %-> check4 = 0, Use f(p)/(f(q)) (eta f(P) T) -> check4 = 1
     %f(p) = p + omega*p^2, exclude first p term check5 -> 0,
     %include first p term check5 -> 1
30   check4 = 0;
     check5 = 0;
     omega  = 10;

     %VI. Modular
35   %Activated T Cells enter only via the blood stream
```

```matlab
    %-> check6 = 1, T cells enter everwhere equally -> check6 = 0
    check6 = 1; %T cells
    check7 = 1; %PD1 (same dynamic)

40  % VII. Modular
    % Different post radiation rate lambda_I12 -> check8 = 1, same rate
    % lambda_I12 all the time -> check8 = 0
    check8 = 1;

45  %Number of years simulated
    years = 1;

    %time to t=0 (first measurement)
    first_meas = 30;
50  medicine = 0.0005;

    % Parameters
    D_p = 6.3e-4;   %Diffusion P cells
    D_q = 1.7*D_p; %Diffusion Q cells
55  D_v = 0.8*D_p; %Diffusion vascular cells
    D_a = 7.85e-7; %Diffusion anti PD-1
    D_t = 8.64e-2; %Diffusion T-cells

    lambda_p = 3.15; %Proliferation rate P cells
60  C_k = 1; %Carrying capacity (volume)
    alpha_pq = 0.03;%Rate of hypoxia P cells
    alpha_qp = 0.5*alpha_pq; %Rate of reoxygenation Q cells
    alpha_qn = 0.0017; %Rate of necrosis
    delt_P = 2.4e-4; %Rate of expunging P cells
65  delt_Q = 2.4e-4; %Rate of expunging Q cells
    delt_N = 2.4e-4; %Rate of expunging N cells

    eta = 23; % Killing rate of P cells by T cells
    eta2 = 5; % Killing rate of Q cells by T cells
70  chi = 0.0013; %Chemotaxis of Vascular cells

    %from ODE model
    lambda_v = 0.6; %Proliferation rate vascular cells
    delt_v = 2.4e-4; %Rate of expunging vascular cells
75  lambda_T_I12 = 25; %Activation T cells pre radiation
    lambda_T_I12_post = 133; %Activation T cells post radiation (obsolete ...
        ↪ if check8 = 0)
    lambda_T_I2 = 0.25; %Proliferation T cells
    K_I12 = 1.5e-10; %concentration IL-12
    I_12 = 1.5e-10; %half saturation IL-12
80  K_I2 = 2.37e-11; %concentration IL-2
    I_2 = 2.37e-11; %half saturation IL-2
    T_0 = 6e-4; %concentration of naive T cells
    roh_L = 5.22e-7; %expression of PD-L1 on T cells
    eps = 0.01; %expression PD-L1 on tumor cells (realtive to T cells)
```

```matlab
85  K_TQhat = 1.365e-18; %inhibition of T cells
    d_t = 0.191; %death rate T cells
    mu_PA = 2.1e5; %depletion of anti-PD-1 through PD-1
    d_A = 0.027; %decay of anti-PD-1
    roh_P = 2.49e-7; %expression rate PD-1 of T cells
90
    %timepoints for treatment cycles
    timepoints_med = [14 35 55 88 109 129 151 172 193 213 234 255 276 297 ...
        ↪ 319];

    %create spatial mesh (r)
95  L = 2;
    N = 150;
    r_vec = linspace(0,L,N);
    dx = r_vec(2) - r_vec(1);

100 %create time mesh (t)
    dt = 1/200; %1/50
    T = years*365;
    t_vec = 0:dt:T;

105 %create empty matrics for populations
    P_mat = zeros(length(r_vec),length(t_vec));
    Q_mat = zeros(length(r_vec),length(t_vec));
    N_mat = zeros(length(r_vec),length(t_vec));
    V_mat = zeros(length(r_vec),length(t_vec));
110 A_mat = zeros(length(r_vec),length(t_vec));
    T_mat = zeros(length(r_vec),length(t_vec));
    PD_mat = zeros(length(r_vec),length(t_vec));

    %initial conditions
115
    %find border at onset of angiogenesis (radius about 0.5mm)
    ini_P = round((0.05/L)*length(r_vec));

    %set initial conditions
120 for i = 1:ini_P
    P_mat(i,1) = 0.95*C_k*(5/4);
    end

    for i = (ini_P +1):length(r_vec)
125 V_mat(i,1) = 0.05*C_k;
    end

    for i = (ini_P +1):length(r_vec)
    T_mat(i,1) = 0.0006;
130 end

    for i = (ini_P +1):length(r_vec)
    PD_mat(i,1) = roh_P*T_mat(i,1);
```

```matlab
        end
135
        for tdx = 1:length(t_vec)-1
            %switch to post radiation activation rate (careful with t mesh)
            if tdx*dt == (68+first_meas)
                lambda_T_I12 = check8*lambda_T_I12_post + (1 - ...
                    ↪ check8)*lambda_T_I12;
140         end

            %set up and solve system of linear equation for proliferating cells
            %set up A,b for system of linear equations
            P_GLS = zeros(length(r_vec)-1,length(r_vec)-1);
145         P_b = zeros(length(r_vec)-1,1);

            P_eps = (D_p)/(2*dx^2);
            P_delt = 1/dt + D_p/(dx^2);
            P_roh = (D_p)/(4*dx);
150
            %fill matrix first row
            P_GLS(1,1) = P_delt - P_eps + (2*P_roh)/(1*dx);
            P_GLS(1,2) = -P_eps - (2*P_roh)/(1*dx);
            P_b(1) = P_mat(2,tdx)/dt + P_eps*P_mat(2+1,tdx) - ...
                ↪ 2*P_eps*P_mat(2,tdx) + P_eps*P_mat(2-1,tdx) + ...
                ↪ (2/(1*dx))*(P_roh*P_mat(1+1+1,tdx) - P_roh*P_mat(1+1-1,tdx)) ...
                ↪ + lambda_p*P_mat(2,tdx)*V_mat(2,tdx)*(1 - ...
                ↪ ((4/5)*(P_mat(2,tdx) + Q_mat(2,tdx) + N_mat(2,tdx)) + ...
                ↪ V_mat(2,tdx))) + alpha_qp*Q_mat(2,tdx)*V_mat(2,tdx) - ...
                ↪ alpha_pq*P_mat(2,tdx)*(1 - V_mat(2,tdx)) - ...
                ↪ delt_P*P_mat(2,tdx) - eta*((1-check4)*P_mat(2,tdx) + ...
                ↪ check4*(check5*P_mat(2,tdx) + ...
                ↪ omega*P_mat(2,tdx)^2))*T_mat(2,tdx)*((1-check1) + ...
                ↪ (check1*V_mat(2,tdx)));
155
            %fill matrix middle rows
            for idx = 2:length(r_vec)-2
                P_GLS(idx,idx-1) = -P_eps + (2*P_roh)/(idx*dx);
                P_GLS(idx,idx)   = P_delt;
160             P_GLS(idx,idx+1) = -P_eps - (2*P_roh)/(idx*dx);

                P_b(idx) = P_mat(idx+1,tdx)/dt + P_eps*P_mat(idx+1+1,tdx) - ...
                    ↪ 2*P_eps*P_mat(idx+1,tdx) + P_eps*P_mat(idx+1-1,tdx)+ ...
                    ↪ (2/(idx*dx))*(P_roh*P_mat(idx+1+1,tdx) - ...
                    ↪ P_roh*P_mat(idx+1-1,tdx)) + ...
                    ↪ lambda_p*P_mat(idx+1,tdx)*V_mat(idx+1,tdx)*(1 - ...
                    ↪ ((4/5)*(P_mat(idx+1,tdx) + Q_mat(idx+1,tdx) + ...
                    ↪ N_mat(idx+1,tdx)) + V_mat(idx+1,tdx))) + ...
                    ↪ alpha_qp*Q_mat(idx+1,tdx)*V_mat(idx+1,tdx) - ...
                    ↪ alpha_pq*P_mat(idx+1,tdx)*(1 - V_mat(idx+1,tdx))  - ...
                    ↪ delt_P*P_mat(idx+1,tdx) - ...
                    ↪ eta*((1-check4)*P_mat(idx+1,tdx) + ...
```

```matlab
            ↪ check4*(check5*P_mat(idx+1,tdx) + ...
            ↪ omega*P_mat(idx+1,tdx)^2))*T_mat(idx+1,tdx)*((1-check1) ...
            ↪ + (check1*V_mat(idx+1,tdx)));

    end

    %fill matrix last row
    P_GLS(length(r_vec)-1,length(r_vec)-2) = -2*P_eps + ...
        ↪ (2*P_roh)/((length(r_vec)-1)*dx) - ...
        ↪ (2*P_roh)/((length(r_vec)-1)*dx);
    P_GLS(length(r_vec)-1,length(r_vec)-1) = P_delt;
    P_b(length(r_vec)-1) = P_mat(length(r_vec),tdx)/dt + ...
        ↪ P_eps*P_mat(length(r_vec)-1,tdx) - ...
        ↪ 2*P_eps*P_mat(length(r_vec),tdx) + ...
        ↪ P_eps*P_mat(length(r_vec)-1,tdx) + ...
        ↪ (2/((length(r_vec)-1)*dx))*(P_roh*P_mat(length(r_vec)-1,tdx) ...
        ↪ - P_roh*P_mat(length(r_vec)-1,tdx)) + ...
        ↪ lambda_p*P_mat(length(r_vec),tdx)*V_mat(length(r_vec),tdx)*(1 ...
        ↪ - ((4/5)*(P_mat(length(r_vec),tdx) + ...
        ↪ Q_mat(length(r_vec),tdx) + N_mat(length(r_vec),tdx)) + ...
        ↪ V_mat(length(r_vec),tdx))) + ...
        ↪ alpha_qp*Q_mat(length(r_vec),tdx)*V_mat(length(r_vec),tdx) - ...
        ↪ alpha_pq*P_mat(length(r_vec),tdx)*(1 - ...
        ↪ V_mat(length(r_vec),tdx)) - delt_P*P_mat(length(r_vec),tdx) ...
        ↪ - eta*((1-check4)*P_mat(length(r_vec),tdx) + ...
        ↪ check4*(check5*P_mat(length(r_vec),tdx) + omega * ...
        ↪ P_mat(length(r_vec),tdx)^2)) * T_mat(length(r_vec),tdx) * ...
        ↪ ((1-check1) + (check1*V_mat(length(r_vec),tdx)));

    %set up vectors for thomas algorithm
    P_a1 = zeros(length(r_vec)-1,1);
    P_a2 = zeros(length(r_vec)-1,1);
    P_a3 = zeros(length(r_vec)-1,1);

    %fill thomas algorithm vectors first entry
    P_a1(1) = P_GLS(1,1);
    P_a2(1) = 0;
    P_a3(1) = P_GLS(1,1+1);

    %fill thomas algorithm vectors middle entries
    for i = 2:length(r_vec)-2
        P_a1(i) = P_GLS(i,i);
        P_a2(i) = P_GLS(i,i-1);
        P_a3(i) = P_GLS(i,i+1);
    end

    %fill thomas algorithm vectors last entry
    P_a1(length(r_vec)-1) = P_GLS(length(r_vec)-1,length(r_vec)-1);
    P_a2(length(r_vec)-1) = P_GLS(length(r_vec)-1,length(r_vec)-2);
    P_a3(length(r_vec)-1) = 0;
```

```matlab
      %solve system of linear equations with thomas algorithm
      P_solve_tr = thomas(P_a1,P_a2,P_a3,P_b);
195
      %add value at r=0
      P_solve = [P_solve_tr(1); P_solve_tr];
      P_mat(:,tdx+1) = P_solve;

200   %set up and solve system of linear equation for quiescent cells
      %(same procedure as for proliferating cells)
      Q_GLS = zeros(length(r_vec)-1,length(r_vec)-1);
      Q_b = zeros(length(r_vec)-1,1);

205   Q_eps = (D_q)/(2*dx^2);
      Q_delt = 1/dt + D_q/(dx^2);
      Q_roh = (D_q)/(4*dx);

      Q_GLS(1,1) = Q_delt - Q_eps + (2*Q_roh)/(1*dx);
210   Q_GLS(1,2) = - Q_eps - (2*Q_roh)/(1*dx);
      Q_b(1) = Q_mat(2,tdx)/dt + Q_eps*Q_mat(2+1,tdx) - ...
          ↪ 2*Q_eps*Q_mat(2,tdx) + Q_eps*Q_mat(2-1,tdx) + ...
          ↪ (2/(1*dx))*(Q_roh*Q_mat(1+1+1,tdx) - Q_roh*Q_mat(1+1-1,tdx)) ...
          ↪ - alpha_qp*Q_mat(2,tdx)*V_mat(2,tdx) + ...
          ↪ alpha_pq*P_mat(2,tdx)*(1 - V_mat(2,tdx))  - ...
          ↪ alpha_qn*Q_mat(2,tdx) - delt_Q*Q_mat(2,tdx) - ...
          ↪ eta2*Q_mat(2,tdx)*T_mat(2,tdx)*((1-check1) + ...
          ↪ (check1*V_mat(2,tdx)));

      for idx = 2:length(r_vec)-2
          Q_GLS(idx,idx-1) = -Q_eps + (2*Q_roh)/(idx*dx);
215       Q_GLS(idx,idx)   = Q_delt;
          Q_GLS(idx,idx+1) = -Q_eps - (2*Q_roh)/(idx*dx);

          Q_b(idx) = Q_mat(idx+1,tdx)/dt + Q_eps*Q_mat(idx+1+1,tdx) - ...
              ↪ 2*Q_eps*Q_mat(idx+1,tdx) + Q_eps*Q_mat(idx+1-1,tdx) + ...
              ↪ (2/(idx*dx))*(Q_roh*Q_mat(idx+1+1,tdx) - ...
              ↪ Q_roh*Q_mat(idx+1-1,tdx)) - ...
              ↪ alpha_qp*Q_mat(idx+1,tdx)*V_mat(idx+1,tdx) + ...
              ↪ alpha_pq*P_mat(idx+1,tdx)*(1 - V_mat(idx+1,tdx)) - ...
              ↪ alpha_qn*Q_mat(idx+1,tdx) - delt_Q*Q_mat(idx+1,tdx) - ...
              ↪ eta2*Q_mat(idx+1,tdx)*T_mat(idx+1,tdx) * ((1-check1) + ...
              ↪ (check1*V_mat(idx+1,tdx)));
      end
220
      Q_GLS(length(r_vec)-1,length(r_vec)-2) = -2*Q_eps + ...
          ↪ (2*Q_roh)/((length(r_vec)-1)*dx) - ...
          ↪ (2*Q_roh)/((length(r_vec)-1)*dx);
      Q_GLS(length(r_vec)-1,length(r_vec)-1) = Q_delt;
      Q_b(length(r_vec)-1) = Q_mat(length(r_vec),tdx)/dt + ...
          ↪ Q_eps*Q_mat(length(r_vec)-1,tdx) - ...
```

```
         ↪ 2*Q_eps*Q_mat(length(r_vec),tdx) + ...
         ↪ Q_eps*Q_mat(length(r_vec)-1,tdx) + ...
         ↪ (2/((length(r_vec)-1)*dx))*(Q_roh*Q_mat(length(r_vec)-1,tdx) ...
         ↪ - Q_roh*Q_mat(length(r_vec)-1,tdx)) - ...
         ↪ alpha_qp*Q_mat(length(r_vec),tdx)*V_mat(length(r_vec),tdx) + ...
         ↪ alpha_pq*P_mat(length(r_vec),tdx)*(1 - ...
         ↪ V_mat(length(r_vec),tdx)) - ...
         ↪ alpha_qn*Q_mat(length(r_vec),tdx) - ...
         ↪ delt_Q*Q_mat(length(r_vec),tdx) - ...
         ↪ eta2*Q_mat(length(r_vec),tdx) * T_mat(length(r_vec),tdx) * ...
         ↪ ((1-check1) + (check1*V_mat(length(r_vec),tdx)));

225      Q_a1 = zeros(length(r_vec)-1,1);
         Q_a2 = zeros(length(r_vec)-1,1);
         Q_a3 = zeros(length(r_vec)-1,1);

         Q_a1(1) = Q_GLS(1,1);
230      Q_a2(1) = 0;
         Q_a3(1) = Q_GLS(1,1+1);

         for i = 2:length(r_vec)-2
             Q_a1(i) = Q_GLS(i,i);
235          Q_a2(i) = Q_GLS(i,i-1);
             Q_a3(i) = Q_GLS(i,i+1);
         end

         Q_a1(length(r_vec)-1) = Q_GLS(length(r_vec)-1,length(r_vec)-1);
240      Q_a2(length(r_vec)-1) = Q_GLS(length(r_vec)-1,length(r_vec)-2);
         Q_a3(length(r_vec)-1) = 0;

         Q_solve_tr = thomas(Q_a1,Q_a2,Q_a3,Q_b);
         Q_solve = [Q_solve_tr(1); Q_solve_tr];
245      Q_mat(:,tdx+1) = Q_solve;

         %set up and solve system of linear equation for vascular cells
         %(same procedure as for proliferating cells)
         V_GLS = zeros(length(r_vec)-1,length(r_vec)-1);
250      V_b = zeros(length(r_vec)-1,1);

         V_eps = (D_v)/(2*dx^2);
         V_delt = 1/dt + D_v/(dx^2);
         V_roh = (D_v)/(4*dx);
255
         V_GLS(1,1) = V_delt - V_eps + (2*V_roh)/(1*dx) + ...
             ↪ (chi/(4*dx))*((Q_mat(1+1+1,tdx+1) - Q_mat(1,tdx+1) + ...
             ↪ Q_mat(1+1+1,tdx) - Q_mat(1,tdx))/(4*dx));
         V_GLS(1,2) = -V_eps - (2*V_roh)/(1*dx) - ...
             ↪ (chi/(4*dx))*((Q_mat(1+1+1,tdx+1) - Q_mat(1,tdx+1) + ...
             ↪ Q_mat(1+1+1,tdx) - Q_mat(1,tdx))/(4*dx));
         V_b(1) =  V_mat(2,tdx)/dt + V_eps*V_mat(2+1,tdx) - ...
```

119

```
      ↪ 2*V_eps*V_mat(2,tdx) + V_eps*V_mat(2-1,tdx) + ...
      ↪ (2/(1*dx))*(V_roh*V_mat(1+1+1,tdx) - V_roh*V_mat(1+1-1,tdx)) ...
      ↪ + chi*V_mat(2,tdx)*(((1/(2*dx^2))*Q_mat(2+1,tdx) - ...
      ↪ 2*(1/(2*dx^2))*Q_mat(2,tdx) + (1/(2*dx^2))*Q_mat(2-1,tdx)) + ...
      ↪ ((1/(2*dx^2))*Q_mat(2+1,tdx+1) - ...
      ↪ 2*(1/(2*dx^2))*Q_mat(2,tdx+1) + ...
      ↪ (1/(2*dx^2))*Q_mat(2-1,tdx+1))) + ...
      ↪ ((2*chi*V_mat(2,tdx))/(1*dx))*((Q_mat(1+1+1,tdx+1) - ...
      ↪ Q_mat(1+1-1,tdx+1) + Q_mat(1+1+1,tdx) - ...
      ↪ Q_mat(1+1-1,tdx))/(4*dx)) + chi*(V_mat(2+1,tdx)/(4*dx) - ...
      ↪ V_mat(2-1,tdx)/(4*dx))*((Q_mat(2+1,tdx+1) - Q_mat(2-1,tdx+1) ...
      ↪ + Q_mat(2+1,tdx) - Q_mat(2-1,tdx))/(4*dx)) + ...
      ↪ lambda_v*V_mat(2,tdx)*Q_mat(2,tdx)*(1 - ((4/5)*(P_mat(2,tdx) ...
      ↪ + Q_mat(2,tdx) + N_mat(2,tdx)) + V_mat(2,tdx))) - ...
      ↪ delt_v*V_mat(2,tdx);

260   for idx = 2:length(r_vec)-2
          V_GLS(idx,idx-1) = -V_eps + (2*V_roh)/(idx*dx) + ...
              ↪ (chi/(4*dx))*((Q_mat(idx+1+1,tdx+1) - ...
              ↪ Q_mat(idx+1-1,tdx+1) + Q_mat(idx+1+1,tdx) - ...
              ↪ Q_mat(idx+1-1,tdx))/(4*dx));
          V_GLS(idx,idx)   = V_delt;
          V_GLS(idx,idx+1) = -V_eps - (2*V_roh)/(idx*dx) - ...
              ↪ (chi/(4*dx))*((Q_mat(idx+1+1,tdx+1) - ...
              ↪ Q_mat(idx+1-1,tdx+1) + Q_mat(idx+1+1,tdx) - ...
              ↪ Q_mat(idx+1-1,tdx))/(4*dx));

265       V_b(idx) =  V_mat(idx+1,tdx)/dt + V_eps*V_mat(idx+1+1,tdx) - ...
              ↪ 2*V_eps*V_mat(idx+1,tdx) + V_eps*V_mat(idx+1-1,tdx) + ...
              ↪ (2/(idx*dx))*(V_roh*V_mat(idx+1+1,tdx) - ...
              ↪ V_roh*V_mat(idx+1-1,tdx)) + ...
              ↪ chi*V_mat(idx+1,tdx)*(((1/(2*dx^2))*Q_mat(idx+1+1,tdx+1) ...
              ↪ - 2*(1/(2*dx^2))*Q_mat(idx+1,tdx+1) + ...
              ↪ (1/(2*dx^2))*Q_mat(idx+1-1,tdx+1)) + ...
              ↪ ((1/(2*dx^2))*Q_mat(idx+1+1,tdx) - ...
              ↪ 2*(1/(2*dx^2))*Q_mat(idx+1,tdx) + ...
              ↪ (1/(2*dx^2))*Q_mat(idx+1-1,tdx))) + ...
              ↪ ((2*chi*V_mat(idx+1,tdx))/(idx*dx)) * ...
              ↪ ((Q_mat(idx+1+1,tdx+1) - Q_mat(idx+1-1,tdx+1) + ...
              ↪ Q_mat(idx+1+1,tdx) - Q_mat(idx+1-1,tdx))/(4*dx)) + ...
              ↪ chi*(V_mat(idx+1+1,tdx)/(4*dx) - ...
              ↪ V_mat(idx+1-1,tdx)/(4*dx))*((Q_mat(idx+1+1,tdx+1) - ...
              ↪ Q_mat(idx+1-1,tdx+1) + Q_mat(idx+1+1,tdx) - ...
              ↪ Q_mat(idx+1-1,tdx))/(4*dx)) + ...
              ↪ lambda_v*V_mat(idx+1,tdx)*Q_mat(idx+1,tdx)*(1 - ...
              ↪ ((4/5)*(P_mat(idx+1,tdx) + Q_mat(idx+1,tdx) + ...
              ↪ N_mat(idx+1,tdx)) + V_mat(idx+1,tdx))) - ...
              ↪ delt_v*V_mat(idx+1,tdx);
      end
```

```matlab
        V_GLS(length(r_vec)-1,length(r_vec)-2) = -V_eps + ...
            ↪ (2*V_roh)/((length(r_vec)-1)*dx) - ...
            ↪ (2*V_roh)/((length(r_vec)-1)*dx) - ...
            ↪ (chi/(4*dx))*((Q_mat(length(r_vec)-1,tdx+1) - ...
            ↪ Q_mat(length(r_vec)-1,tdx+1) + Q_mat(length(r_vec)-1,tdx) - ...
            ↪ Q_mat(length(r_vec)-1,tdx))/(4*dx)) + ...
            ↪ (chi/(4*dx))*((Q_mat(length(r_vec)-1,tdx+1) - ...
            ↪ Q_mat(length(r_vec)-1,tdx+1) + Q_mat(length(r_vec)-1,tdx) - ...
            ↪ Q_mat(length(r_vec)-1,tdx))/(4*dx));
        V_GLS(length(r_vec)-1,length(r_vec)-1) = V_delt;

        V_b(length(r_vec)-1) =  V_mat(length(r_vec),tdx)/dt + ...
            ↪ V_eps*V_mat(length(r_vec)-1,tdx) - ...
            ↪ 2*V_eps*V_mat(length(r_vec),tdx) + ...
            ↪ V_eps*V_mat(length(r_vec)-1,tdx) + ...
            ↪ (2/((length(r_vec)-1)*dx)) * ...
            ↪ (V_roh*V_mat(length(r_vec)-1,tdx) - ...
            ↪ V_roh*V_mat(length(r_vec)-1,tdx)) + ...
            ↪ chi*V_mat(length(r_vec),tdx) * ...
            ↪ (((1/(2*dx^2))*Q_mat(length(r_vec)-1,tdx) - ...
            ↪ 2*(1/(2*dx^2))*Q_mat(length(r_vec),tdx) + ...
            ↪ (1/(2*dx^2))*Q_mat(length(r_vec)-1,tdx)) + ...
            ↪ ((1/(2*dx^2))*Q_mat(length(r_vec)-1,tdx) - ...
            ↪ 2*(1/(2*dx^2))*Q_mat(length(r_vec),tdx) + ...
            ↪ (1/(2*dx^2))*Q_mat(length(r_vec)-1,tdx))) + ...
            ↪ ((2*chi*V_mat(length(r_vec),tdx))/((length(r_vec)-1)*dx)) * ...
            ↪ ((Q_mat(length(r_vec)-1,tdx+1) - ...
            ↪ Q_mat(length(r_vec)-1,tdx+1) + Q_mat(length(r_vec)-1,tdx) - ...
            ↪ Q_mat(length(r_vec)-1,tdx))/(4*dx)) + ...
            ↪ chi*(V_mat(length(r_vec)-1,tdx)/(4*dx) - ...
            ↪ V_mat(length(r_vec)-1,tdx)/(4*dx)) * ...
            ↪ ((Q_mat(length(r_vec)-1,tdx+1) - ...
            ↪ Q_mat(length(r_vec)-1,tdx+1) + Q_mat(length(r_vec)-1,tdx) - ...
            ↪ Q_mat(length(r_vec)-1,tdx))/(4*dx)) + ...
            ↪ lambda_v*V_mat(length(r_vec),tdx)*Q_mat(length(r_vec),tdx)*(1 ...
            ↪ - ((4/5)*(P_mat(length(r_vec),tdx) + ...
            ↪ Q_mat(length(r_vec),tdx) + N_mat(length(r_vec),tdx)) + ...
            ↪ V_mat(length(r_vec),tdx))) - delt_v*V_mat(length(r_vec),tdx);

        V_a1 = zeros(length(r_vec)-1,1);
        V_a2 = zeros(length(r_vec)-1,1);
        V_a3 = zeros(length(r_vec)-1,1);

        V_a1(1) = V_GLS(1,1);
        V_a2(1) = 0;
        V_a3(1) = V_GLS(1,1+1);

        for i = 2:length(r_vec)-2
            V_a1(i) = V_GLS(i,i);
            V_a2(i) = V_GLS(i,i-1);
```

```
            V_a3(i) = V_GLS(i,i+1);
285     end

        V_a1(length(r_vec)-1) = V_GLS(length(r_vec)-1,length(r_vec)-1);
        V_a2(length(r_vec)-1) = V_GLS(length(r_vec)-1,length(r_vec)-2);
        V_a3(length(r_vec)-1) = 0;
290
        V_solve_tr = thomas(V_a1,V_a2,V_a3,V_b);

        V_solve = [V_solve_tr(1); V_solve_tr];
        V_mat(:,tdx+1) = V_solve;
295
        %set up and solve system of linear equation for anti-PD-1
        %(same procedure as for proliferating cells)
        if check2 ==1
            A_GLS = zeros(length(r_vec)-1,length(r_vec)-1);
300         A_b = zeros(length(r_vec)-1,1);

            A_eps = (D_a)/(2*dx^2);
            A_delt = 1/dt + D_a/(dx^2);
            A_roh = (D_a)/(4*dx);
305
            A_GLS(1,1) = A_delt - A_eps + (2*A_roh)/(1*dx);
            A_GLS(1,2) = - A_eps - (2*A_roh)/(1*dx);
            A_b(1)     =  A_mat(2,tdx)/dt + A_eps*A_mat(2+1,tdx) - ...
                ↪ 2*A_eps*A_mat(2,tdx) + A_eps*A_mat(2-1,tdx) + ...
                ↪ (2/(1*dx))*(A_roh*A_mat(1+1+1,tdx) - ...
                ↪ A_roh*A_mat(1+1-1,tdx)) - ...
                ↪ mu_PA*PD_mat(2,tdx)*A_mat(2,tdx) - d_A*A_mat(2,tdx);

310         for idx = 2:length(r_vec)-2
                A_GLS(idx,idx-1) = -A_eps + (2*A_roh)/(idx*dx);
                A_GLS(idx,idx)   = A_delt;
                A_GLS(idx,idx+1) = -A_eps - (2*A_roh)/(idx*dx);

315             A_b(idx) = A_mat(idx+1,tdx)/dt + A_eps*A_mat(idx+1+1,tdx) ...
                    ↪ - 2*A_eps*A_mat(idx+1,tdx) + ...
                    ↪ A_eps*A_mat(idx+1-1,tdx) + ...
                    ↪ (2/(idx*dx))*(A_roh*A_mat(idx+1+1,tdx) - ...
                    ↪ A_roh*A_mat(idx+1-1,tdx)) - ...
                    ↪ mu_PA*PD_mat(idx+1,tdx)*A_mat(idx+1,tdx) - ...
                    ↪ d_A*A_mat(idx+1,tdx);
            end

            A_GLS(length(r_vec)-1,length(r_vec)-2) = -2*A_eps + ...
                ↪ (2*A_roh)/((length(r_vec)-1)*dx) - ...
                ↪ (2*A_roh)/((length(r_vec)-1)*dx);
            A_GLS(length(r_vec)-1,length(r_vec)-1) = A_delt;
320         A_b(length(r_vec)-1) = A_mat(length(r_vec),tdx)/dt + ...
                ↪ A_eps*A_mat(length(r_vec)-1,tdx) - ...
```

```
                   ↪ 2*A_eps*A_mat(length(r_vec),tdx) + ...
                   ↪ A_eps*A_mat(length(r_vec)-1,tdx) + ...
                   ↪ (2/((length(r_vec)-1)*dx)) * ...
                   ↪ (A_roh*A_mat(length(r_vec)-1,tdx) - ...
                   ↪ A_roh*A_mat(length(r_vec)-1,tdx)) - ...
                   ↪ mu_PA*PD_mat(length(r_vec),tdx)*A_mat(length(r_vec),tdx) ...
                   ↪ - d_A*A_mat(length(r_vec),tdx);

             A_a1 = zeros(length(r_vec)-1,1);
             A_a2 = zeros(length(r_vec)-1,1);
             A_a3 = zeros(length(r_vec)-1,1);
325
             A_a1(1) = A_GLS(1,1);
             A_a2(1) = 0;
             A_a3(1) = A_GLS(1,1+1);

330          for i = 2:length(r_vec)-2
                 A_a1(i) = A_GLS(i,i);
                 A_a2(i) = A_GLS(i,i-1);
                 A_a3(i) = A_GLS(i,i+1);
             end
335
             A_a1(length(r_vec)-1) = A_GLS(length(r_vec)-1,length(r_vec)-1);
             A_a2(length(r_vec)-1) = A_GLS(length(r_vec)-1,length(r_vec)-2);
             A_a3(length(r_vec)-1) = 0;

340          A_solve_tr = thomas(A_a1,A_a2,A_a3,A_b);
             A_solve = [A_solve_tr(1); A_solve_tr];
             A_mat(:,tdx+1) = A_solve;


345
          % add anti-PD-1 at treatment dates
             if tdx*dt ==  44 || tdx*dt == 65 || tdx*dt == 85 || tdx*dt == ...
                 ↪ 118 || tdx*dt == 139 || tdx*dt == 159 || tdx*dt == 181 ...
                 ↪ || tdx*dt == 202 || tdx*dt == 223 || tdx*dt == 243 || ...
                 ↪ tdx*dt == 264 || tdx*dt == 285 || tdx*dt == 306 || ...
                 ↪ tdx*dt == 327 || tdx*dt == 349
                 A_mat(:,tdx+1) = A_mat(:,tdx+1) + medicine*((1-check3) + ...
                     ↪ check3*V_mat(:,tdx+1));
             end
350
      else
             A_mat(:,tdx+1) = 0;
      end

355   %set up and solve system of linear equation for T cells
      %(same procedure as for proliferating cells)
      T_GLS = zeros(length(r_vec)-1,length(r_vec)-1);
      T_b = zeros(length(r_vec)-1,1);
```

```matlab
360     T_eps = (D_t)/(2*dx^2);
        T_delt = 1/dt + D_t/(dx^2);
        T_roh = (D_t)/(4*dx);

        T_GLS(1,1) = T_delt - T_eps + (2*T_roh)/(1*dx);
365     T_GLS(1,2) = - T_eps - (2*T_roh)/(1*dx);
        T_b(1) = T_mat(2,tdx)/dt + T_eps*T_mat(2+1,tdx) - ...
            ↪ 2*T_eps*T_mat(2,tdx) + T_eps*T_mat(2-1,tdx) + ...
            ↪ (2/(1*dx))*(T_roh*T_mat(1+1+1,tdx) - T_roh*T_mat(1+1-1,tdx)) ...
            ↪ + ((check6*V_mat(2,tdx) + (1-check6))*lambda_T_I12 * T_0 * ...
            ↪ (I_12/(K_I12 + I_12)) + lambda_T_I2 * T_mat(2,tdx) * ...
            ↪ (I_2/(K_I2 + I_2))) * 1/(1 + (PD_mat(2,tdx) * (roh_L * ...
            ↪ (T_mat(2,tdx) + eps * (P_mat(2,tdx) + ...
            ↪ Q_mat(2,tdx)))))/K_TQhat) - d_t*T_mat(2,tdx);

        for idx = 2:length(r_vec)-2
            T_GLS(idx,idx-1) = -T_eps + (2*T_roh)/(idx*dx);
370         T_GLS(idx,idx)   = T_delt;
            T_GLS(idx,idx+1) = -T_eps - (2*T_roh)/(idx*dx);

            T_b(idx) = T_mat(idx+1,tdx)/dt + T_eps*T_mat(idx+1+1,tdx) - ...
                ↪ 2*T_eps*T_mat(idx+1,tdx) + T_eps*T_mat(idx+1-1,tdx) + ...
                ↪ (2/(idx*dx))*(T_roh*T_mat(idx+1+1,tdx) - ...
                ↪ T_roh*T_mat(idx+1-1,tdx)) + ((check6*V_mat(idx+1,tdx) + ...
                ↪ (1-check6))*lambda_T_I12 * T_0 * (I_12/(K_I12 + I_12)) + ...
                ↪ lambda_T_I2 * T_mat(idx+1,tdx) * (I_2/(K_I2 + I_2)) * ...
                ↪ 1/(1 + (PD_mat(idx+1,tdx) * (roh_L * (T_mat(idx+1,tdx) + ...
                ↪ eps * (P_mat(idx+1,tdx) + Q_mat(idx+1,tdx)))))/K_TQhat) ...
                ↪ - d_t*T_mat(idx+1,tdx);
        end
375
        T_GLS(length(r_vec)-1,length(r_vec)-2) = -2*T_eps + ...
            ↪ (2*T_roh)/((length(r_vec)-1)*dx) - ...
            ↪ (2*T_roh)/((length(r_vec)-1)*dx);
        T_GLS(length(r_vec)-1,length(r_vec)-1) = T_delt;
        T_b(length(r_vec)-1) = T_mat(length(r_vec)+1-1,tdx)/dt + ...
            ↪ T_eps*T_mat(length(r_vec)-1,tdx) - ...
            ↪ 2*T_eps*T_mat(length(r_vec),tdx) + ...
            ↪ T_eps*T_mat(length(r_vec)-1,tdx) + ...
            ↪ (2/((length(r_vec)-1)*dx))*(T_roh*T_mat(length(r_vec)-1,tdx) ...
            ↪ - T_roh*T_mat(length(r_vec)-1,tdx)) + ...
            ↪ ((check6*V_mat(length(r_vec),tdx) + (1-check6))*lambda_T_I12 ...
            ↪ * T_0 * (I_12/(K_I12 + I_12)) + lambda_T_I2 * ...
            ↪ T_mat(length(r_vec),tdx) * (I_2/(K_I2 + I_2)) * 1/(1 + ...
            ↪ (PD_mat(length(r_vec),tdx) * (roh_L * ...
            ↪ (T_mat(length(r_vec),tdx) + eps * (P_mat(length(r_vec),tdx) ...
            ↪ + Q_mat(length(r_vec),tdx)))))/K_TQhat) - ...
            ↪ d_t*T_mat(length(r_vec),tdx);
```

```matlab
T_a1 = zeros(length(r_vec)-1,1);
T_a2 = zeros(length(r_vec)-1,1);
T_a3 = zeros(length(r_vec)-1,1);


T_a1(1) = T_GLS(1,1);
T_a2(1) = 0;
T_a3(1) = T_GLS(1,1+1);


for i = 2:length(r_vec)-2
    T_a1(i) = T_GLS(i,i);
    T_a2(i) = T_GLS(i,i-1);
    T_a3(i) = T_GLS(i,i+1);
end


T_a1(length(r_vec)-1) = T_GLS(length(r_vec)-1,length(r_vec)-1);
T_a2(length(r_vec)-1) = T_GLS(length(r_vec)-1,length(r_vec)-2);
T_a3(length(r_vec)-1) = 0;


T_solve_tr = thomas(T_a1,T_a2,T_a3,T_b);


T_solve = [T_solve_tr(1); T_solve_tr];
T_mat(:,tdx+1) = T_solve;


%set up and solve system of linear equation for PD-1
%(same procedure as for proliferating cells)
PD_GLS = zeros(length(r_vec)-1,length(r_vec)-1);
PD_b = zeros(length(r_vec)-1,1);


PD_eps = (D_t)/(2*dx^2);
PD_delt = 1/dt + D_t/(dx^2);
PD_roh = (D_t)/(4*dx);


PD_GLS(1,1) = PD_delt - PD_eps + (2*PD_roh)/(1*dx);
PD_GLS(1,2) = - PD_eps - (2*PD_roh)/(1*dx);
PD_b(1) = PD_mat(2,tdx)/dt + PD_eps*PD_mat(2+1,tdx) - ...
    ↪ 2*PD_eps*PD_mat(2,tdx) + PD_eps*PD_mat(2-1,tdx) + ...
    ↪ (2/(1*dx))*(PD_roh*PD_mat(1+1+1,tdx) - ...
    ↪ PD_roh*PD_mat(1+1-1,tdx)) + roh_P*((check7*V_mat(2,tdx) + ...
    ↪ (1-check7))*lambda_T_I12 * T_0 * (I_12/(K_I12 + I_12)) + ...
    ↪ lambda_T_I2 * T_mat(2,tdx) * (I_2/(K_I2 + I_2))) * 1/(1 + ...
    ↪ (PD_mat(2,tdx) * (roh_L * (T_mat(2,tdx) + eps * ...
    ↪ (P_mat(2,tdx) + Q_mat(2,tdx)))))/K_TQhat) - ...
    ↪ mu_PA*PD_mat(2,tdx)*A_mat(2,tdx) -d_t*PD_mat(2,tdx);


for idx = 2:length(r_vec)-2
    PD_GLS(idx,idx-1) = -PD_eps + (2*PD_roh)/(idx*dx);
    PD_GLS(idx,idx)   = PD_delt;
    PD_GLS(idx,idx+1) = -PD_eps - (2*PD_roh)/(idx*dx);


    PD_b(idx) = PD_mat(idx+1,tdx)/dt + PD_eps*PD_mat(idx+1+1,tdx) - ...
```

```
                    ↪ 2*PD_eps*PD_mat(idx+1,tdx) + PD_eps*PD_mat(idx+1-1,tdx) ...
                    ↪ + (2/(idx*dx))*(PD_roh*PD_mat(idx+1+1,tdx) - ...
                    ↪ PD_roh*PD_mat(idx+1-1,tdx)) + ...
                    ↪ roh_P*((check7*V_mat(idx+1,tdx) + ...
                    ↪ (1-check7))*lambda_T_I12 * T_0 * (I_12/(K_I12 + I_12)) + ...
                    ↪ lambda_T_I2 * T_mat(idx+1,tdx) * (I_2/(K_I2 + I_2))) * ...
                    ↪ 1/(1 + (PD_mat(idx+1,tdx) * (roh_L * (T_mat(idx+1,tdx) + ...
                    ↪ eps * (P_mat(idx+1,tdx) + Q_mat(idx+1,tdx)))))/K_TQhat) ...
                    ↪ - mu_PA*PD_mat(idx+1,tdx)*A_mat(idx+1,tdx) ...
                    ↪ -d_t*PD_mat(idx+1,tdx);
            end

            PD_GLS(length(r_vec)-1,length(r_vec)-2) = -2*PD_eps + ...
                ↪ (2*PD_roh)/((length(r_vec)-1)*dx) - ...
                ↪ (2*PD_roh)/((length(r_vec)-1)*dx);
425         PD_GLS(length(r_vec)-1,length(r_vec)-1) = PD_delt;
            PD_b(length(r_vec)-1) = PD_mat(length(r_vec)-1+1,tdx)/dt + ...
                ↪ PD_eps*PD_mat(length(r_vec)-1,tdx) - ...
                ↪ 2*PD_eps*PD_mat(length(r_vec)-1+1,tdx) + ...
                ↪ PD_eps*PD_mat(length(r_vec)-1+1-1,tdx) + ...
                ↪ (2/((length(r_vec)-1)*dx)) * ...
                ↪ (PD_roh*PD_mat(length(r_vec)-1,tdx) - ...
                ↪ PD_roh*PD_mat(length(r_vec)-1,tdx)) + ...
                ↪ roh_P*((check7*V_mat(length(r_vec),tdx) + ...
                ↪ (1-check7))*lambda_T_I12 * T_0 * (I_12/(K_I12 + I_12)) + ...
                ↪ lambda_T_I2 * T_mat(length(r_vec)-1+1,tdx) * (I_2/(K_I2 + ...
                ↪ I_2))) * 1/(1 + (PD_mat(length(r_vec)-1+1,tdx) * (roh_L * ...
                ↪ (T_mat(length(r_vec)-1+1,tdx) + eps * ...
                ↪ (P_mat(length(r_vec)-1+1,tdx) + ...
                ↪ Q_mat(length(r_vec)-1+1,tdx)))))/K_TQhat) - ...
                ↪ mu_PA*PD_mat(length(r_vec)-1+1,tdx) * ...
                ↪ A_mat(length(r_vec)-1+1,tdx) -d_t*PD_mat(length(r_vec)-1+1,tdx);

            PD_a1 = zeros(length(r_vec)-1,1);
            PD_a2 = zeros(length(r_vec)-1,1);
430         PD_a3 = zeros(length(r_vec)-1,1);

            PD_a1(1) = PD_GLS(1,1);
            PD_a2(1) = 0;
            PD_a3(1) = PD_GLS(1,1+1);
435
            for i = 2:length(r_vec)-2
                PD_a1(i) = PD_GLS(i,i);
                PD_a2(i) = PD_GLS(i,i-1);
                PD_a3(i) = PD_GLS(i,i+1);
440         end

            PD_a1(length(r_vec)-1) = PD_GLS(length(r_vec)-1,length(r_vec)-1);
            PD_a2(length(r_vec)-1) = PD_GLS(length(r_vec)-1,length(r_vec)-2);
            PD_a3(length(r_vec)-1) = 0;
```

```matlab
        PD_solve_tr = thomas(PD_a1,PD_a2,PD_a3,PD_b);

        PD_solve = [PD_solve_tr(1); PD_solve_tr];
        PD_mat(:,tdx+1) = PD_solve;



        %update necrotic cells (pure reaction and therefore no system of linear
        %equations needed)
        for idx = 1:length(r_vec)-1
        N_mat(idx,tdx+1) = N_mat(idx,tdx) + dt*(alpha_qn*Q_mat(idx,tdx) - ...
            ↪ delt_N*N_mat(idx,tdx));
        end
        N_mat(length(r_vec),tdx+1) = N_mat(length(r_vec)-1,tdx) + ...
            ↪ dt*(alpha_qn*Q_mat(length(r_vec),tdx) - ...
            ↪ delt_N*N_mat(length(r_vec),tdx));
    end

    %may be needed for plots, not used here
    G_mat = P_mat+Q_mat+N_mat+V_mat;
    Tumor_mat = P_mat+Q_mat+N_mat;

%%% Plotting begins here.
%%% A selection of useful plot examples is given, but
%%% more interesting figures can be extracted from the results

    timepoint_day = 100;
    timepoint_mat = round(timepoint_day/dx) + 1;

    subplot(2,3,1)
    plot(r_vec,P_mat(:,timepoint_mat))
    hold on
    plot(r_vec,Q_mat(:,timepoint_mat),'red')
    hold on
    plot(r_vec,N_mat(:,timepoint_mat),'green')
    title('P cells(blue), Q cells(red), N cells(green)')
    subplot(2,3,2)
    plot(r_vec,V_mat(:,timepoint_mat))
    title('Vasculature')
    subplot(2,3,3)
    plot(r_vec,T_mat(:,timepoint_mat))
    title('T cells')
    subplot(2,3,4)
    plot(r_vec,PD_mat(:,timepoint_mat))
    title('Free PD-1')
    subplot(2,3,5)
    plot(r_vec,A_mat(:,timepoint_mat),'magenta')
    title('Anti-PD-1')
```

```matlab
    %calculate average densities of populations
    average_p = (1/N).*sum(P_mat);
    average_q = (1/N).*sum(Q_mat);
495 average_n = (1/N).*sum(N_mat);
    average_v = (1/N).*sum(V_mat);
    average_t = (1/N).*sum(T_mat);
    average_a = (1/N).*sum(A_mat);
    average_tumor = average_p + average_q + average_n;
500
    %plot average densities
    figure
    subplot(3,2,1)
    plot(t_vec,average_p)
505 title('P Cells Average')
    subplot(3,2,2)
    plot(t_vec,average_q)
    title('Q Cells Average')
    subplot(3,2,3)
510 plot(t_vec,average_n)
    title('N Cells Average')
    subplot(3,2,4)
    plot(t_vec,average_tumor)
    title('All Tumor Cells Average')
515 subplot(3,2,5)
    plot(t_vec,average_t)
    title('Average T cells')
    subplot(3,2,6)
    plot(t_vec,average_v)
520 title('Average vascular cells')
    hold on
    %plot treatments in same figure
    for i = 1:length(timepoints_med)
        line([timepoints_med(i)+first_meas timepoints_med(i)+first_meas], ...
            ↪ [0 0.09], 'LineWidth',2,'Color',[223/255 255/255 ...
            ↪ 0/255],'LineStyle',':')
525 end
    line([68+first_meas 68+first_meas], [0 0.09], ...
        ↪ 'LineWidth',2,'Color',[175/255 238/255 238/255],'LineStyle',':')
    hold off

    %set up vector for border of tumor
530 border = zeros(1,length(t_vec));
    t_cell_tumor_conc = zeros(1,length(t_vec));

    %find border in each timepoint
    for idt = 1:length(t_vec)
535     local_poss_bor = find([P_mat(:,idt); 0] ≤ 0.02);
        border(idt) = (local_poss_bor(1)-1)*dx;

        %calculate average T cell concentration inside tumor border
```

```matlab
        onlytumor_tcells = T_mat(1:(local_poss_bor(1)-1),idt);
540     t_cell_tumor_conc(idt) = ...
          ↪ (1/length(onlytumor_tcells)).*sum(onlytumor_tcells);
    end

    meas_times = [0 63 124 223 285 333] + first_meas;

545 %radii of M1-M5 calculated from volume assuming perfect sphere
    M1 = [1.5 7.2 4.8 4.9 6.7 7.5];
    M2 = [1.5 7.0 6.3 4.7 4.2 5.2];
    M3 = [0   7.3 5.3 5.0 4.0 5.9];
    M4 = [0   7.1 5.4 4.6 4.1 6.9];
550 M5 = [0   6.1 6.6 5.7 6.4 6.5];

    %calculate average of M1-M5
    avg_M = (1/5).*(M1+M2+M3+M4+M5);
    avg_M(1) = 1.5;
555
    %plot tumor border and compare to single metastases M1-M5
    %and average of M1-M5
    figure
    subplot(1,2,1)
560 plot(t_vec,border)
    title('Tumor Radius over Time (Response)')
    hold on
    scatter(meas_times,avg_M/10,'LineWidth',2)
    for i = 1:length(timepoints_med)
565 line([timepoints_med(i)+first_meas timepoints_med(i)+first_meas], [0 ...
        ↪ 1.5], 'LineWidth',2,'Color',[223/255 255/255 ...
        ↪ 0/255],'LineStyle',':')
    end
    line([68+first_meas 68+first_meas], [0 1.5], ...
        ↪ 'LineWidth',2,'Color',[175/255 238/255 238/255],'LineStyle',':')
    hold off
    xlabel('Time in Days')
570 ylabel('Tumor Radius in cm')
    axis([0 365 0 1.5])
    subplot(1,2,2)
    p1=plot(t_vec,border);
    title('Tumor Radius over Time')
575 hold on
    p2=scatter(meas_times,M1/10,'LineWidth',2);
    p3=scatter(meas_times,M2/10,'LineWidth',2);
    p4=scatter(meas_times,M3/10,'LineWidth',2);
    p5=scatter(meas_times,M4/10,'LineWidth',2);
580 p6=scatter(meas_times,M5/10,'LineWidth',2);
    for i = 1:length(timepoints_med)
    line([timepoints_med(i)+first_meas timepoints_med(i)+first_meas], [0 ...
        ↪ 0.9], 'LineWidth',2,'Color',[223/255 255/255 ...
        ↪ 0/255],'LineStyle',':')
```

```matlab
    end
    line([68+first_meas 68+first_meas], [0 0.9], ...
        ↪ 'LineWidth',2,'Color',[175/255 238/255 238/255],'LineStyle',':')
585 hold off
    xlabel('Time in Days')
    ylabel('Tumor Radius in cm')
    axis([0 365 0 0.9])
    h = legend([p2 p3 p4 p5 p6], 'M1','M2','M3','M4','M5');
590
    %plot average T cell concentration inside tummor border over time
    figure
    plot(t_vec,t_cell_tumor_conc)
    title('T cell concetration inside tumor border')
595 hold on
    for i = 1:length(timepoints_med)
    line([timepoints_med(i)+first_meas timepoints_med(i)+first_meas], [0 ...
        ↪ 0.02], 'LineWidth',2,'Color',[223/255 255/255 ...
        ↪ 0/255],'LineStyle',':')
    end
    line([68+first_meas 68+first_meas], [0 0.02], ...
        ↪ 'LineWidth',2,'Color',[175/255 238/255 238/255],'LineStyle',':')
600 hold off

    end
```

# List of Figures

# List of Tables

# Bibliography

[1] *3D Slicer.* Website. `https://www.slicer.org/` (2018); last accessed on November 1, 2018.

[2] J. K. Adam, B. Odhav, and K. Bhoola. "Immune responses in cancer". In: *Pharmacology & therapeutics* 99(1) (2003).

[3] *AJCC (American Joint Committee on Cancer) - What is Cancer Staging?* Website. `https://cancerstaging.org/references-tools/Pages/What-is-Cancer-Staging.aspx` (2018); last accessed on November 1, 2018.

[4] H. O. Alsaab, S. Sau, R. Alzhrani, et al. "PD-1 and PD-L1 Checkpoint Signaling Inhibition for Cancer Immunotherapy: Mechanism, Combinations, and Clinical Outcome". In: *Frontiers in Pharmacology* 8 (2017).

[5] K. Alsmeier. *Mathematical Modeling of Tumor Growth under Immunotherapy.* Master's Thesis, Technische Universität München, Department of Mathematics. 2017.

[6] B. Anderson, J. Jackson, and M. Sitharam. "Descartes' Rule of Signs Revisited". In: *The American Mathematical Monthly* 105(5) (1998).

[7] C. M. Anderson, J. Tabacof, and S. S. Legha. "Malignant Melanoma: Biology, Diagnosis, and Management". In: *Oncology, Melanoma* 19 (2005).

[8] J. Awrejcewicz. *Ordinary Differential Equations and Mechanical Systems.* Springer International Publishing, 2014.

[9] V. Bahrambeigi, N. Ahmadi, R. Salehi, et al. "Genetically Modified Murine Adipose-Derived Mesenchymal Stem Cells Producing Interleukin-2 Favor B16F10 Melanoma Cell Proliferation". In: *Immunological investigations* 44(3) (2015).

[10] R. Baskar, J. Dai, N. Wenlong, et al. "Biological response of cancer cells to radiation treatment". In: *Frontiers in Molecular Biosciences* 1(34) (2014).

[11] C. Benz and E. Liu. *Oncogenes and Tumor Suppressor Genes in Human Malignancies.* Cancer Treatment and Research. Springer US, 2012.

[12] D. Bleecker and G. Csordas. *Basic Partial Differential Equations.* Taylor & Francis, 1992.

[13] P. Boasberg. *BRAF Targeted Therapy - Where Do We Go From Here.* Lecture. `https://www.youtube.com/watch?v=3zPGBtXJyOg` (2013); last accessed on November 1, 2018.

[14] H. Bougherara, A. Mansuet-Lupo, M. Alifano, et al. "Real-Time Imaging of Resident T Cells in Human Lung and Ovarian Carcinomas Reveals How Different Tumor Microenvironments Control T Lymphocyte Migration". In: *Frontiers in Immunology* 500(6) (2015).

[15] G. Capaccio. *Cancer Treatments.* Advances in Medicine. Marshall Cavendish Benchmark, 2013.

[16] J. A. Carlson. "Tumor Doubling Time of Cutaneous Melanoma and its Metastasis". In: *Immunological investigations - The American Journal of Dermatopathology* 25(4) (2003).

[17] D. D. Chaplin. "Overview of the Immune Response". In: *The Journal of Allergy and Clinical Immunology* 125(2 sup2) (2010).

[18] C. Chicone. *Ordinary Differential Equations with Applications.* Texts in Applied Mathematics. Springer New York, 2006.

[19] M. J. Cipolla. *The Cerebral Circulation.* Colloquium Series on Integrated Systems Physiology: From Molecule to Function. Biota Publishing, 2016.

[20] A. Coddington and N. Levinson. *Theory of Ordinary Differential Equations.* International series in pure and applied mathematics. McGraw-Hill, 1955.

[21] D. Colton. *Partial Differential Equations: An Introduction.* Dover Books on Mathematics. Dover Publications, 2012.

[22] C. M. Croce. "Oncogenes and Cancer". In: *New England Journal of Medicine* 358(5) (2008).

[23] R. Daneman and A. Prat. "The Blood–Brain Barrier". In: *Cold Spring Harbor Perspectives in Biology* 7(1) (2015).

[24] S. Däster, N. Amatruda, D. Calabrese, et al. "Induction of hypoxia and necrosis in multicellular tumor spheroids is associated with resistance to chemotherapy treatment". In: *Oncotarget* 8(1) (2017).

[25] K. P. Davy and D. R. Seals. "Total blood volume in healthy young and older men". In: *Journal of Applied Physiology* 76(5) (1994).

[26] *Definition of targeted therapy - NCI Dictionary of Cancer Terms - National Cancer Institute.* Website. https://www.cancer.gov/publications/dictionaries/cancer-terms/def/targeted-therapy?redirect=true (2018); last accessed on November 1, 2018.

[27] A. DeFranco, R. Locksley, and M. Robertson. *Immunity: The Immune Response in Infectious and Inflammatory Disease.* Primers in Biology. OUP Oxford, 2007.

[28] R. Descartes. *Discours de la méthode pour bien conduire sa raison et chercher la vérité dans les sciences , plus la dioptrique, les météores et la géométrie qui sont des essais de cette méthode.* 1637.

[29] P. V. Dickson and J. Gershenwald. "Staging and Prognosis of Cutaneous Melanoma". In: *Surgical oncology clinics of North America* 20 (2011).

[30] R. Dummer, M. Pittelkow, K. Iwatsuki, et al. *Skin Cancer - A World-Wide Perspective*. Springer Berlin Heidelberg, 2011.

[31] H. Dvorak. "How Tumors Make Bad Blood Vessels and Stroma". In: *American Journal of Pathology* 162 (2003).

[32] L. Edelstein-Keshet. *Mathematical Models in Biology*. Classics in Applied Mathematics. Society for Industrial and Applied Mathematics, 1988.

[33] A. Eladdadi, P. Kim, and D. Mallet. *Mathematical Models of Tumor-Immune System Dynamics*. Springer Proceedings in Mathematics & Statistics. Springer New York, 2014.

[34] L. Falto-Aizpurua, R. Griffith, B. Simmons, et al. "The history of skin cancer". In: *Journal of the American Academy of Dermatology* 72(5) (2015).

[35] *FastStats - Leading Causes of Deaths (Centers of Disease Control and Prevention)*. Website. https://www.cdc.gov/nchs/fastats/leading-causes-of-death.htm (2017); last accessed on November 1, 2018.

[36] *FDA Full Prescribing Information: Keytruda (Pembrolizumab)*. Website. https://www.accessdata.fda.gov/drugsatfda_docs/label/2016/125514s012lbl.pdf (2016); last accessed on November 1, 2018.

[37] P. Fessas, H. Lee, S. Ikemizu, et al. "A molecular and preclinical comparison of the PD-1–targeted T-cell checkpoint inhibitors nivolumab and pembrolizumab". In: *Seminars in Oncology* 44(2) (2017).

[38] J. C. Forster, W. M. Harriss-Phillips, M. J. Douglass, et al. "A review of the development of tumor vasculature and its effects on the tumor microenvironment". In: *Hypoxia (Auckl)* 5 (2017).

[39] J. P. Freyer. "Role of necrosis in regulating the growth saturation of multicellular spheroids". In: *Cancer Research* 48(9) (1988).

[40] A. Friedman and W. Hao. "The Role of Exosomes in Pancreatic Cancer Microenvironment". In: *Bulletin of Mathematical Biology* 80(5) (2018).

[41] J. Gallaher, A. Babu, S. Plevritis, et al. "Bridging Population and Tissue Scale Tumor Dynamics: A New Paradigm for Understanding Differences in Tumor Growth and Metastatic Disease". In: *Cancer Research* 74(2) (2014).

[42] T. C. Gangadhar, W. J. Hwu, M. A. Postow, et al. "Efficacy and Safety of Pembrolizumab in Patients Enrolled in KEYNOTE-030 in the United States: An Expanded Access Program". In: *Journal of Immunotherapy* 40(9) (2017).

[43] C. Goldsmith. *Skin Cancer*. USA TODAY Health Reports: Diseases and Disorders Series. Twenty-First Century Books, 2010.

[44] J. Gong, A. Chehrazi-Raffle, S. Reddi, et al. "Development of PD-1 and PD-L1 inhibitors as a form of cancer immunotherapy: a comprehensive review of registration trials and future considerations". In: *Journal for ImmunoTherapy of Cancer* 6(1) (2018).

[45] *Guide to Keytruda (Pembrolizumab): Information for dosing, administration ...* Website. `https://www.keytruda.com/static/pdf/guide-for-keytruda.pdf` (2018); last accessed on November 1, 2018.

[46] S. A. Hendry, R. H. Farnsworth, B. Solomon, et al. "The Role of the Tumor Vasculature in the Host Immune Response: Implications for Therapeutic Strategies Targeting the Tumor Microenvironment". In: *Frontiers in Immunology* 621(7) (2016).

[47] T. Hillen and K. J. Painter. "A user's guide to PDE models for chemotaxis". In: *Journal of Mathematical Biology* 58(1) (2008).

[48] J. C. Holland and R. Zittoun. *Psychosocial Aspects of Oncology.* ESO Monographs. Springer Berlin Heidelberg, 2012.

[49] *Institut Curie. "How T Cells Attack Tumors". ScienceDaily.* Website. `https://www.sciencedaily.com/releases/2007/02/070221111538.htm` (2007); last accessed on November 1, 2018.

[50] F. Ito and M. Ernstoff. *Immune Checkpoint Inhibitors in Cancer.* Elsevier Health Sciences, 2018.

[51] H. Ito, I. Kanno, H. Iida, et al. "Arterial fraction of cerebral blood volume in humans measured by positron emission tomography". In: *Annals of Nuclear Medicine* 15(2) (2001).

[52] R. W. Jenkins, D. A. Barbie, and K. T. Flaherty. "Mechanisms of resistance to immune checkpoint inhibitors". In: *British Journal of Cancer* 118(1) (2018).

[53] F. Khan. *The Physics of Radiation Therapy.* Wolters Kluwer Health, 2012.

[54] D. Kirschner and J. C. Panetta. "Modeling immunotherapy of the tumor - Immune interaction". In: *Journal of mathematical biology* 37 (1998).

[55] K. Königsberger. *Analysis 1.* Springer-Lehrbuch. Springer Berlin Heidelberg, 2003.

[56] G. Kramer, K. Capello, B. Bearss, et al. "Linear dimensions and volumes of human lungs obtained from CT images". In: *Health physics* 102(4) (2012).

[57] G. Kumar, K. Narayan, and B. Reddy. "Dynamics of an sis epidemic model with a saturated incidence rate under time delay and stochastic influence". In: *International Journal of Pure and Apllied Mathematics* 112 (2017).

[58] C. Kuttler. *Advanced Mathematical Biology, SS 2017.* Lecture Script from Technische Universität München. 2017.

[59] C. Kuttler. *Reaction-Diffusion equations with applications.* Lecture Script from Technische Universität München. 2016.

[60] X. Lai and A. Friedman. "Combination therapy of cancer with cancer vaccine and immune checkpoint inhibitors: A mathematical model." In: *PLoS ONE* 12(5) (2017).

[61] R. Lakhtakia. "A Brief History of Breast Cancer: Part I: Surgical Domination Reinvented." In: *Sultan Qaboos University Medical Journal* 14.2 (2014).

[62] L. Lapidus and G. Pinder. *Numerical Solution of Partial Differential Equations in Science and Engineering.* Wiley, 1982.

[63] R. Larson. *Brief Calculus: An Applied Approach.* Cengage Learning, 2007.

[64] I. Lasley. *21st Century Cancer Treatment.* Createspace Independent Pub, 2011.

[65] S. Y. Lee, C.-N. Qian, A. S. Ooi, et al. "Changes in specialized blood vessels in lymph nodes and their role in cancer metastasis". In: *Journal of Translational Medicine* 10(1) (2012).

[66] R. LeVeque. *Finite Difference Methods for Ordinary and Partial Differential Equations: Steady-State and Time-Dependent Problems.* Other Titles in Applied Mathematics. Society for Industrial and Applied Mathematics, 2007.

[67] M. L. Lewis, J. Gnoj, V. J. Fisher, et al. "Determinants of pulmonary blood volume". In: *The Journal of Clinical Investigation* 49(1) (1970).

[68] L. Li, S. Mori, M. Kodama, et al. "Enhanced Sonographic Imaging to Diagnose Lymph Node Metastasis: Importance of Blood Vessel Volume and Density". In: *Cancer Research* 73(7) (2013).

[69] K.-L. Liao, X.-F. Bai, and A. Friedman. "Mathematical Modeling of Interleukin-27 Induction of Anti-Tumor T Cells Response". In: *PLoS ONE* 9 (2014).

[70] D. Liu, R. W. Jenkins, and R. J. Sullivan. "Mechanisms of Resistance to Immune Checkpoint Blockade". In: *American Journal of Clinical Dermatology* (2018).

[71] I. Lugowska, P. Teterycz, and P. Rutkowski. "Immunotherapy of melanoma". In: *Contemporary Oncology* 1 (2018).

[72] F. R. Macfarlane, T. Lorenzi, and M. A. J. Chaplain. "Modelling the Immune Response to Cancer: An Individual-Based Approach Accounting for the Difference in Movement Between Inactive and Activated T Cells". In: *Bulletin of Mathematical Biology* 80(6) (2018).

[73] R. MacKie. *Skin Cancer, Second Edition.* Taylor & Francis, 1996.

[74] K. M. Mahoney, P. D. Rennert, and G. J. Freeman. "Combination cancer immunotherapy and new immunomodulatory targets". In: *Nature Reviews Drug Discovery* 14 (2015).

[75]  A. Mathai and H. Haubold. *Linear Algebra: A Course for Physicists and Engineers.* De Gruyter Textbook. De Gruyter, 2017.

[76]  R. L. Maute, S. R. Gordon, A. T. Mayer, et al. "Engineering high-affinity PD-1 variants for optimized immunotherapy and immuno-PET imaging". In: *Proceedings of the National Academy of Sciences* 112(47) (2015).

[77]  J. E. McKenney. "Finding the Volume of an Ellipsoid Using Cross-Sectional Slices". In: *Mathematics Magazine* 64(1) (1991).

[78]  F. Miller, A. Vandome, and J. McBrewster. *Fick's Law of Diffusion.* VDM Publishing, 2009.

[79]  J. L. Milton and W. P. Goss. "Stability criteria for explicit finite difference solutions of the parabolic diffusion equation with non-linear boundary conditions". In: *Numerical Methods in Engineering* 7(1) (1973).

[80]  S. Mukherjee. *The Emperor of All Maladies: A Biography of Cancer.* Scribner, 2011.

[81]  J. Müller and C. Kuttler. *Methods and Models in Mathematical Biology: Deterministic and Stochastic Approaches.* Lecture Notes on Mathematical Modelling in the Life Sciences. Springer Berlin Heidelberg, 2015.

[82]  H. Murphy, H. Jaafari, and H. M. Dobrovolny. "Differences in predictions of ODE models of tumor growth: a cautionary example". In: *BMC Cancer* 163(16) (2016).

[83]  *National Cancer Institute - Cancer Classification - SEER Training.* Website. `https://training.seer.cancer.gov/disease/categories/classification.html` (2018); last accessed on November 1, 2018.

[84]  *Neoplasms and Cancer: Basicmedical Key.* Website. `https://basicmedicalkey.com/neoplasms-and-cancer/` (2018); last accessed on November 1, 2018.

[85]  E. Nikolopoulou, L. R. Johnson, D. Harris, et al. "Tumour-immune dynamics with an immune checkpoint inhibitor". In: *Letters in Biomathematics* 5(sup1) (2018).

[86]  M. Nowak. *Evolutionary Dynamics.* Harvard University Press, 2006.

[87]  H. Oberkampf, S. Zillner, J. A. Overton, et al. "Semantic representation of reported measurements in radiology". In: *BMC Medical Informatics and Decision Making* 16(5) (2015).

[88]  K. Ogungbenro, A. Patel, R. Duncombe, et al. "Dose Rationalization of Pembrolizumab and Nivolumab Using Pharmacokinetic Modeling and Simulation and Cost Analysis". In: *Clinical Pharmacology & Therapeutics* 103(4) (2018).

[89]  M. Özisik, H. Orlande, M. Colaço, et al. *Finite Difference Methods in Heat Transfer, Second Edition.* Heat Transfer. CRC Press, 2017.

[90]  V. Padma. "An overview of targeted cancer therapy". In: *BioMedicine* 5 (2015).

[91]  A. Patnaik, S. Kang, D. Rasco, et al. "Phase I Study of Pembrolizumab (MK-3475; Anti-PD-1 Monoclonal Antibody) in Patients with Advanced Solid Tumors". In: *Clinical Cancer Research* 21(19) (2015).

[92]  E. Peranzoni, J. Lemoine, L. Vimeux, et al. "Macrophages impede CD8 T cells from reaching tumor cells and limit the efficacy of anti–PD-1 treatment". In: *Proceedings of the National Academy of Sciences* (2018).

[93]  L. Perko. *Differential Equations and Dynamical Systems.* Texts in Applied Mathematics. Springer New York, 2013.

[94]  P. Price, K. Sikora, and T. Illidge. *Treatment of Cancer Fifth Edition.* A Hodder Arnold Publication. Taylor & Francis, 2008.

[95]  A. I. Riker, N. Zea, and T. Trinh. "The Epidemiology, Prevention, and Detection of Melanoma". In: *The Ochsner journal* 10 (2010).

[96]  A. Rotte and M. Bhandaru. *Immunotherapy of Melanoma.* Springer International Publishing, 2016.

[97]  E. A. Sarapata. *A Comparison and Catalog of Intrinsic Tumor Growth Models.* HMC Senior Theses. Paper 52. `http://scholarship.claremont.edu/hmc_theses/52`. 2013.

[98]  J. Schachter, A. Ribas, G. V. Long, et al. "Pembrolizumab versus ipilimumab for advanced melanoma: final overall survival results of a multicentre, randomised, open-label phase 3 study (KEYNOTE-006)". In: *The Lancet* 390(10105) (2017).

[99]  P. Schlicke. *Mathematical investigation of tumour growth and metastasis under the effect of vascularization and chemotherapy.* Master's Thesis, Technische Universität München, Department of Mathematics. 2017.

[100]  L. H. Schwartz, S. Litière, E. de Vries, et al. "RECIST 1.1—Update and clarification: From the RECIST committee". In: *European Journal of Cancer* 62 (2016).

[101]  A. Shete, M. Thakar, P. R. Abraham, et al. "A review on peripheral blood CD4+ T lymphocyte counts in healthy adult Indians". In: *The Indian Journal of Medical Research* 132(6) (2010).

[102]  A. Silverstein, V. Silverstein, and L. Nunn. *Cancer: Conquering a Deadly Disease.* Twenty-first century medical library. Twenty-First Century Books, 2006.

[103]  A. Sudhakar. "History of Cancer, Ancient and Modern Treatment Methods". In: *Journal of Cancer Science and Therapy* 1(2) (2009).

[104]  R. Sullivan. *BRAF Targets in Melanoma: Biological Mechanisms, Resistance, and Drug Discovery.* Cancer Drug Discovery and Development. Springer New York, 2014.

[105]  *T Cells - Ask A Biologist.* Website. `https://askabiologist.asu.edu/t-cell` (2018); last accessed on November 1, 2018.

[106]  G. Teschl. *Ordinary Differential Equations and Dynamical Systems.* Graduate studies in mathematics. American Mathematical Society, 2012.

[107]  *The Nobel Prize in Physiology or Medicine 2018.* Website. `https://www.nobelprize.org/prizes/medicine/2018/summary/` (2018); last accessed on November 1, 2018.

[108]  J. Thompson, R. Scolyer, and R. Kefford. "Melanoma: A management guide for GPs". In: *Australian Family Physician* 41(7) (2012).

[109]  *Timothy - Tissue Modelling Framework (Examples).* Website. `https://timothy.icm.edu.pl/examples.html` (2018); last accessed on November 1, 2018.

[110]  *User gernot - TeX - LaTeX Stack Exchange.* Website. `https://tex.stackexchange.com/users/110998/gernot` (2017); last accessed on November 1, 2018.

[111]  E. J. Van Limbergen, D. K. De Ruysscher, V. Olivo Pimentel, et al. "Combining radiotherapy with immunotherapy: the past, the present and the future". In: *The British Journal of Radiology* 90(1076) (2017).

[112]  D. I. Wallace and X. Guo. "Properties of Tumor Spheroid Growth Exhibited by Simple Mathematical Models". In: *Frontiers in Oncology* 3(51) (2018).

[113]  H. K. Weir, R. N. Anderson, S. M. Coleman King, et al. "Heart Disease and Cancer Deaths — Trends and Projections in the United States 1969–2020". In: *Preventing Chronic Disease* 13(157) (2016).

[114]  I. Wilhelm, J. Molnár, C. Fazakas, et al. "Role of the Blood-Brain Barrier in the Formation of Brain Metastases". In: *International Journal of Molecular Sciences* 14(1) (2013).

[115]  J. S. Wilmott, H. Rizos, R. A. Scolyer, et al. "The "Tricky Business" of Identifying Mechanisms of Resistance to Anti–PD-1". In: *Clinical Cancer Research* 23(12) (2017).

[116]  R. M. Young, A. Jamshidi, G. Davis, et al. "Current trends in the surgical management and treatment of adult glioblastoma". In: *Annals of Translational Medicine* 3(9) (2015).

[117]  E. Zauderer. *Partial Differential Equations of Applied Mathematics.* Pure and Applied Mathematics: A Wiley Series of Texts, Monographs and Tracts. Wiley, 2011.

[118]  M. Zhang, G. Li, Y. J. Wang, et al. "PD-L1 expression in lung cancer and its correlation with driver mutations: a meta-analysis". In: *Scientific Reports* 7(10255) (2017).

[119]   A. Zupnick. "Supplement: Cancer Immunotherapies Development Barriers". In: *GEN: Genetic Engineering & Biotechnology News* 38(7) (2018).